Synthesis and Solid-State Photochemical [2+2] Cycloaddition Reaction of MOFs Containing 4,4′-bipyridyl-ethylene

BY

Hasan Ali Al-Mohsin

A Thesis Presented to the

DEANSHIP OF GRADUATE STUDIES

KING FAHD UNIVERSITY OF PETROLEUM & MINERALS

DHAHRAN, SAUDI ARABIA

In Partial Fulfillment of the
Requirements for the Degree of

MASTER OF SCIENCE

In

Chemistry

May 2018

KING FAHD UNIVERSITY OF PETROLEUM & MINERALS

DHAHRAN, SAUDI ARABIA

DEANSHIP OF GRADUATE STUDIES

This thesis, written by Hasan Ali Al-Mohsin under the direction of his advisor and approved by his thesis committee, has been presented to and accepted by the Dean of Graduate Studies, in partial fulfillment of the requirements for the degree of **MASTER OF SCIENCE** in **CHEMISTRY**

Thesis Committee

Dr. Abdulmalik P. Peedikakkal

Dr. Mohammed B. Fettouhi

Dr. Sulayman A. Oladepo

9/5/2018

Dr. Abdulaziz A. Al-Saadi

Chemistry Department Chairman

14/5/18

Dr. Salam A. Zummo

Dean of Graduate Studies

Dedication

I dedicate this work to all the people who helped and encouraged me in my journey, specially my wife and kid who endured difficult circumstances for me. I also dedicate this work to my parents who keep supporting me all the way, to my mother for her continuous encouragement and prayer, and my father for sacrificing all he has for me.

ACKNOWLEDGEMENT

First of all, I thank Allah for all his gifts, guidance and giving me the strength and ability to successfully complete my MS degree. This work would not have been possible without the help and support of many people. I specially thank my family for their love, patience and support.

I owe my thesis advisor, Dr. Abdulmalik Puthan Peedikakkal, a great debt for all the knowledge I received from him, I sincerely cannot thank him enough for all he has done for me. I also specially thank my thesis committee members Dr. Mohammed B. Fettouhi for his great help and support, and Dr. Sulayman Adeyemi Oladepo for his great support.

I would like to express my deepest gratitude to Dr. Altaf and Dr. Adam for lending me their expertise in the laboratory during my thesis research. I'm also very grateful to the department of chemistry staff for their continuous support.

I also would like to thank the chairman of department of chemistry, Dr. Abdulaziz Al-Saadi, as well as Dr. Bassam El Ali for their continuous help and support during my MS program.

I acknowledge King Fahd University of Petroleum and Minerals (KFUPM) for giving me the opportunity to pursue my master's degree.

Table of Contents

List of Tables

List of Figures

List of Schemes

List of Abbreviations

MOFs	**:**	Metal-Organic Frameworks
bpe	**:**	4,4’-bipyridylethylene
ox	**:**	Oxalic Acid
fum	**:**	Fumaric Acid
tpcb	**:**	tetrakis(4-pyridyl)cyclobutane
DMF	**:**	Dimethylformamide
UV	**:**	Ultraviolet
EtOH	**:**	Ethanol
NMR	**:**	Nuclear Magnetic Resonance
PXRD	**:**	Powder X-ray Diffraction
TGA	**:**	Thermogravimetric Analysis
FT-IR	**:**	Fourier-Transform Infrared Spectroscopy
^{0}C	**:**	Celsius
h	**:**	Hour
RT	**:**	Room Temperature
a.u.	**:**	Arbitrary Unit
Å	**:**	Angstrom

Thesis Abstract

Name : Hasan A. Al-Mohsin

Title : Metal-Organic Frameworks for Photochemical [2+2] Cycloaddition Reaction in the Solid-State

Major : Chemistry

Several Metal-Organic Frameworks (MOFs) were designed and synthesized to stack a pair of olefinic C=C bonds in a parallel manner with less than 4.2 Å distance in crystal lattice for solid-state photochemical [2+2] cycloaddition reaction using 4,4'-bipyridylethylene (bpe), fumaric acid (fum**)** and oxalic acid (ox) as spacer ligands with several metals ion nodes, such as Zn(II), Pb(II) and Cd(II). The synthesized compounds; $\{(Hbpe)_2[Zn_2(ox)_3]\}_n \cdot (H_2O) \cdot 2.2(DMF)$ **(1)**, $[Pb_4(ox)_3(bpe)_4(H_2O)_4]_n \cdot (NO_3)_2$ **(2)** and $[Pb(bpe)(fum)]_n \cdot 0.25(H_2O)$ **(3)**, were characterized *by* FT-IR and ^{1}H-NMR spectroscopies, powder X-ray diffraction (PXRD), Elemental Analysis (CHN) and thermogravimetric Analysis (TGA). The photochemical [2+2] cycloaddition reaction of these compounds was monitored by ^{1}H-NMR spectroscopy. The ^{1}H-NMR studies were carried out on the compounds before and after *UV* irradiation for a variety of time durations (5, 10, 15, 30, and 50 hours). Higher % of conversions (90-100%) were achieved after 50 hours of UV irradiation for **1** and **2**, and 5 hours for **3**.

A reported dinuclear triple-strands-like 1D ladder Cd(II)-based MOF, $[Cd(bpe)_{1.5}(NO_3)_2(H_2O)]_n$ **(4)**, was synthesized and its photoreactivity has been studied. It has shown photoreaction with 100% yield by initiation of mechanically induced large internal molecular motion through grinding. The study was conducted through *UV* irradiation before and after grinding, while monitoring conversion *via* ^{1}H-NMR spectroscopy. Thermogravimetric Analysis (TGA) was used to study the behavior of solvent loss due to grinding within the lattice structure.

Thesis Abstract (Arabic)

ملخص الرسالة

الاسم : حسن علي آل محسن

العنوان : تصميم وتحضير هياكل معدنية عضوية لتفاعلات الإضافة الحلقية [٢+٢] الكيميائية الضوئية في الحالة الصلبة

التخصص : كيمياء

تم تصميم العديد من الهياكل المعدنية العضوية (Metal-Organic Frameworks) تحتوي على أزواج من الروابط الكربونية المزدوجة تمت محاذاتها بطريقة متوازية مع مسافة تقل عن ٤,٢ أنغستروم داخل البنية البلورية بحيث تكون فيها القابلية لتتفاعل عن طريق الضوء (الكيمياء الضوئية) بتفاعل الإضافة الحلقية [٢+٢] في الحالة الصلبة. ومن ثم تم تحضير هذه المركبات باستخدام ٤،٤- ثنائي بيريديل الإيثيلين **(bpe)**، حمض الفوماريك **(fum)** وحمض الأكساليك **(ox)** كربيطات عضوية موصلة مع العديد من أيونات أو عقد المعادن، مثل ثنائي الزنك Zn(II)، ثنائي الرصاص Pb(II) وثنائي الكادميوم Cd(II). تمت دراسة المركبات المحضرة $\{(Hbpe)_2[Zn_2(ox)_3]\}_n\bullet(H_2O)\bullet 2.2(DMF)$ **(١)**، $[Pb_4(ox)_3(bpe)_4(H_2O)_4]_n\bullet(NO_3)_2$ **(٢)** و $[Pb(bpe)(fum)]_n\bullet 0.25(H_2O)$ **(٣)** باستخدام مطيافية الأشعة تحت الحمراء (FT-IR)، طيف الرنين النووي المغناطيسي للبروتون (^{1}H-NMR)، حيود الأشعة السينية للمسحوق (PXRD)، التحليل العنصري (CHN) و التحليل الوزني الحراري (TGA). تمت مراقبة التفاعلات الكيميائية الضوئية عن طريق طيف الرنين المغناطيسي للبروتون (^{1}H-NMR). كما أن القياسات الطيفية للمركبات أخذت قبل وبعد التعرض للأشعة فوق البنفسجية (*UV*) لفترات متفاوتة (٥، ١٠، ١٥، ٣٠ و٥٠ ساعة). تم الحصول على محصول بنسبة تحويل عالية، ٩٠% بعد التعرض لـ ٥٠ ساعة من الأشعة فوق البنفسجية للمركبين ١ و٢، ونسبة ١٠٠% بعد التعرض لخمس ساعات من الأشعة فوق البنفسجية للمركب ٣.

تمت زيادة التفاعلية الضوئية للهيكل المعدني العضوي أحادي البعد $[Cd(bpe)_{1.5}(NO_3)_2(H_2O)]_n$ **(٤)** والحصول على محصول بنسبة تحويل ١٠٠% من خلال تفعيل الحركة الكبيرة للجزيئات الداخلية المستحثة ميكانيكيا من خلال الطحن. تمت مراقبة التفاعل عن طريق طيف الرنين المغناطيسي للبروتون (^{1}H-NMR) بعد التعرض للأشعة فوق البنفسجية قبل وبعد الطحن. كما تم استخدام التحليل الوزني الحراري (TGA) لدراسة سلوك جزيئات الماء داخل البنية البلورية.

CHAPTER 1
INTRODUCTION

1.1 Metal-Organic Frameworks

Metal-Organic Frameworks (MOFs) are unique class of hybrid materials, with uniform and infinite structural network.[1] These materials have emerged within the last two decades, and they are rapidly developing and attracting chemists and researchers around the globe due to their interesting properties, as well as potential applications.[1,2]

MOFs are well defined crystalline materials that consist of metal ions or metal ion clusters (known as nodes) bridged by organic ligands (known as linkers or spacers) **(Figure 1)**.[3–5]

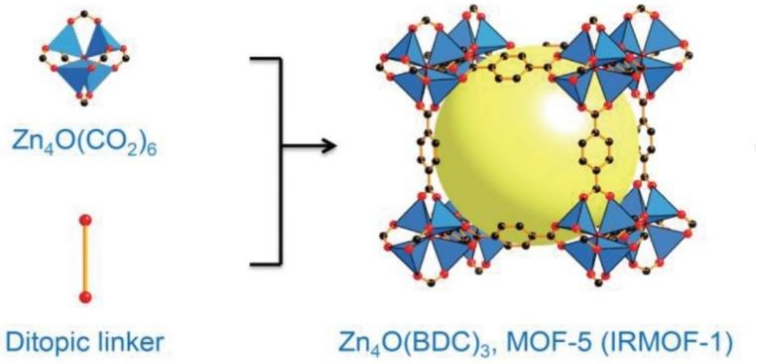

Figure 1: An example shows both the metal ion cluster and organic linker in MOF-5.[6]

The vast variety of building blocks of MOFs, metal ions or metal clusters and organic linkers, leads to infinite chemical and topological structures. This would allow fine tuning of MOFs properties.[1,2] The structural topology can be designed or predicted by selecting the type and nature of metal ions and linkers **(Figure 2)**.[7] A linear linker, for instance, and octahedral nodes will produce primitive cubic unit (PCU) topology **(Figure 1 and 2)**.[6,7] More than 20,000 MOFs

have been reported in the literature and many topologies have been reported and studied in variety of applications.[2] Linkers are critical part of MOFs design and can have linear, angular, trigonal, tetrahedral and other types of geometries **(Figure 3).**[8] The combination of each type will produce a predicted geometry suitable for a specific type of applications.

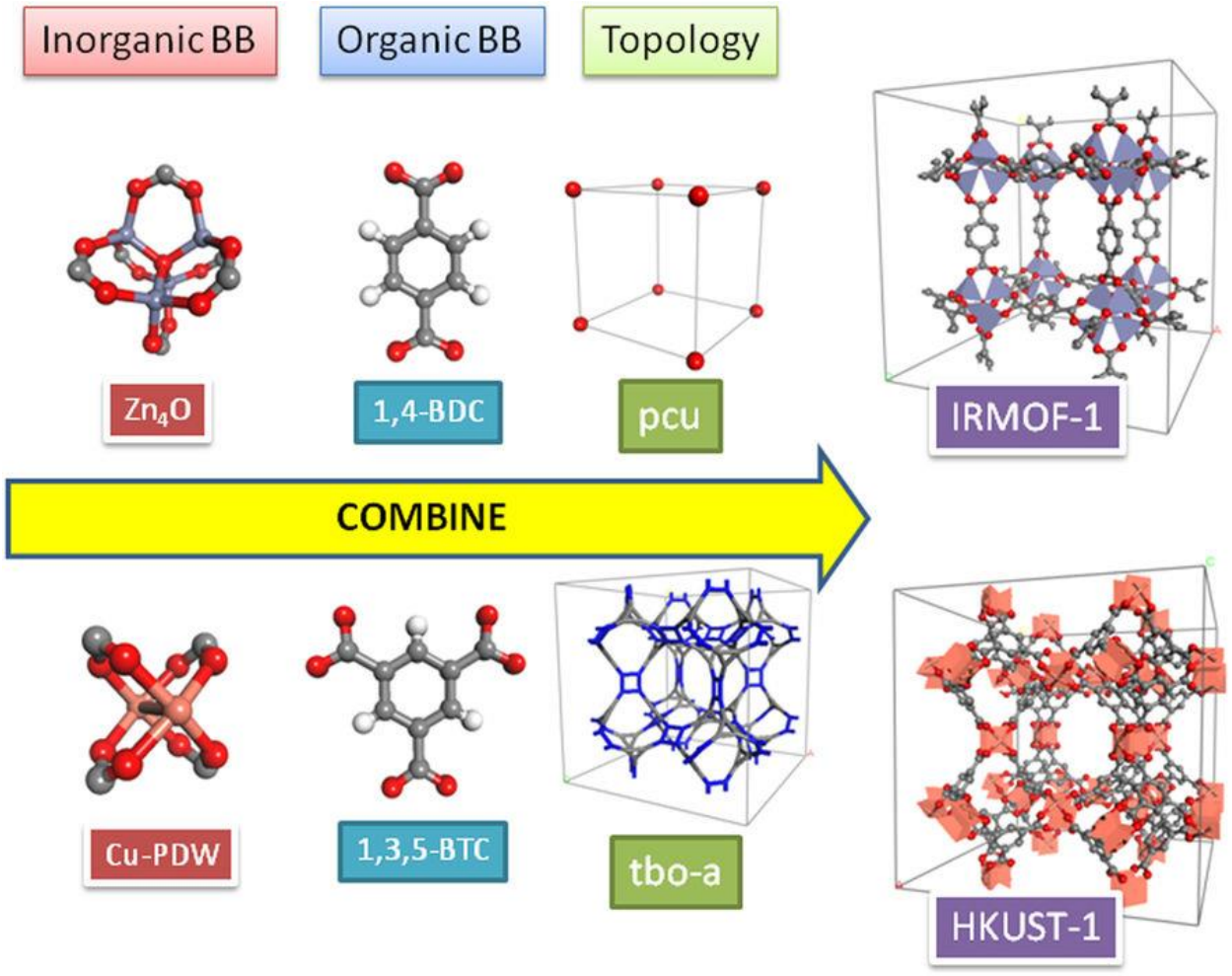

Figure 2: MOFs design and prediction of topology.[7]

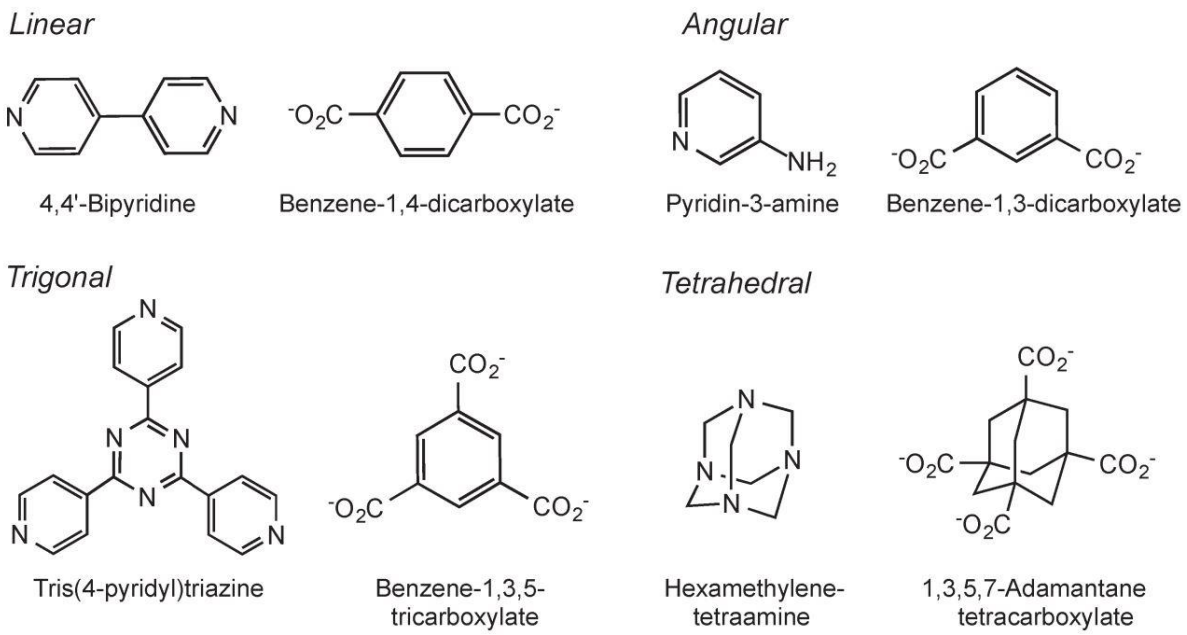

Figure 3: Types of linker geometries that can be used in MOFs design and prediction of topology.[8]

MOFs properties have led to enormously important potential applications in a variety of fields related to both research and industry, such as sensors and other applications.[5,2] However, the performance of MOFs in each of these applications is affected greatly by the chemical structure of the organic linkers, thus the functionalities of the material. Therefore, many methods have been developed to change the structure of the organic linkers.[2,5,9–13] However, the most essential method to change the structure of the organic linkers is by replacing them at the start of the synthesis process.[14] However, linkers can be modified after the synthesis of MOFs through post-synthesis modification (PSM) methods. It is an alternative and simple route and it has been widely used recently for tuning the functionalities of the material.[9]

Post-synthesis modification (PSM) is an effective tool that can be used to functionalize a reactive component in MOFs structure.[9–13] It is a valid way to incorporate organic linkers or other moieties into MOFs without affecting the topological structure that are otherwise incompatible with conventional solvothermal synthesis and usually can complicate or prevent the formation of

MOF.[9,10,15] Moreover, some organic linkers may be very difficult to synthesize, but can be easily formed within the MOF structure by PSM method,[15] such as cyclobutane derivatives. PSM has been an active area in the past few years, and rapidly developing in both methods and applications.[10–13] Variety of methods have been reported for use as PSM, such as covalent PSM, dative PSM and inorganic PSM[11] **(Figure 4).**[12,13]

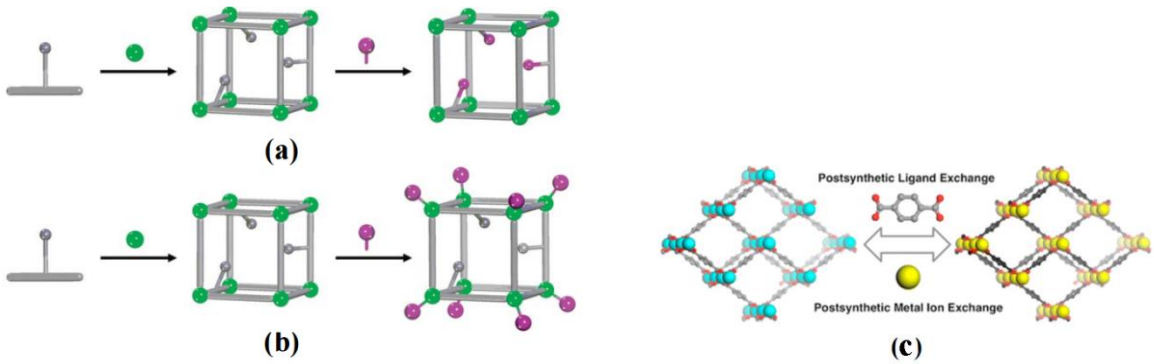

Figure 4: (a) covalent PSM, (b) Dative PSM,[12] and (c) Inorganic PSM.[13]

Covalent PSM is the most studied method among PSM methods. It occurs through modifying a covalent bond of linker ligands. It can be carried out by adding a reagent through thermal, photochemical or electrochemical treatment.[11] Solid-state photochemical [2+2] cycloaddition reaction can be considered as one type of covalent PSM.[16] It is a typical method to produce cyclobutane derivatives.[15] It can be used also for the modification of properties of photoreactive MOFs.[17]

1.2 Cycloaddition reactions

Cycloaddition reactions are concerted pericyclic reactions that involve the combination of two molecules with two or more π systems to form new ring.[18] These reactions are important tools to construct cyclic structures.[19] Diels-Alder reaction [4+2] is a familiar example of these type of reactions, which is used to construct 6-membered rings. Another well-known example is 1,3-dipolar cycloaddition [3+2] reactions, which are used to construct 5-membered rings.[19] Other less familiar cycloaddition reactions are 4-membered rings (cyclobutane derivatives) [2+2], 8-membered rings [4+4], 10-membered rings [4+6] and 12-membered rings [6+6] **(Figure 5)**.[20] However, although the cycloaddition reactions require heat, the [2+2] cycloaddition reaction is an exception to that rule. It is one of the most difficult and less common due to its orbital symmetry requirements **(Figure 6)**.[21]

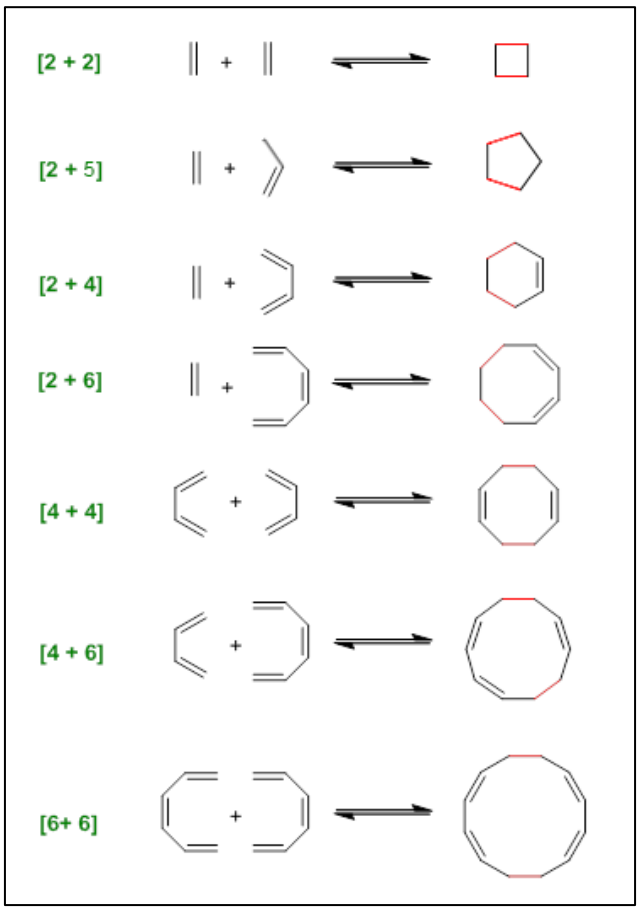

Figure 5: Types of cycloaddition reactions.[20]

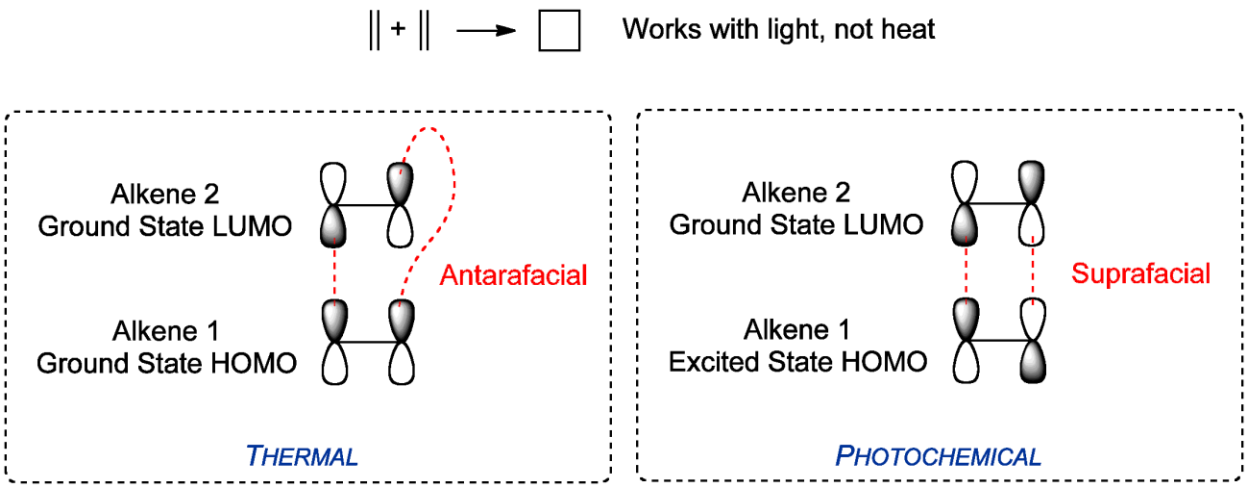

Figure 6: [2+2] cycloaddition reaction orbital symmetry with heat (a) and light (b).[21]

1.3 Schmidt Postulate and Solid-State Reactions

The [2+2] cycloaddition reaction of disubstituted alkene can produce several isomers in solution, but depending on the arrangement of the solid-state, specific isomer can be targeted. The photochemical reaction [2+2] cycloaddition in the solid-state can only occur if Schmidt geometry criteria are met.[22] Schmidt topochemical postulate suggests that a pair of parallel aligned C=C olefinic bonds in the solid-state can undergo [2+2] cycloaddition reaction only if they are separated by a distance of 4.2 Å or less **(Figure 7)**.[15,17,22] Hence, based on this postulate, many

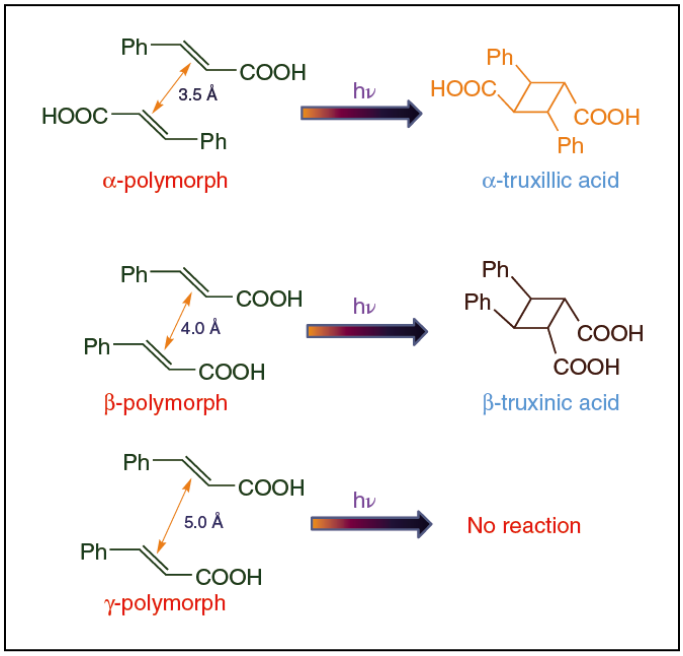

Figure 7: Demonstration of Schmidt Postulate.[17]

studies have been conducted in attempts to control the packing and alignment of the C=C olefinic bonds, and several methods have been tested with a variety of success levels.[10]

The % conversion of the photochemical reaction in the solid state depends on the structure of the compound whether all olefinic C=C double bonds are in the right alignment or free ones are present within the lattice structure.[15] For instance, triple-stranded one-dimensional ladder-like MOF can achieve 67% of conversion.[23] However, the photochemical [2+2] cycloaddition reaction can yield four possible regioisomers. These regioisomers are *rctt*, *rtct*, *rcct* and *rccc* (**Figure 8**), where the c stands for *cis*- while the t stands for *trans*-. The description of the isomer geometry starts with a substituted group in clockwise manner.[15]

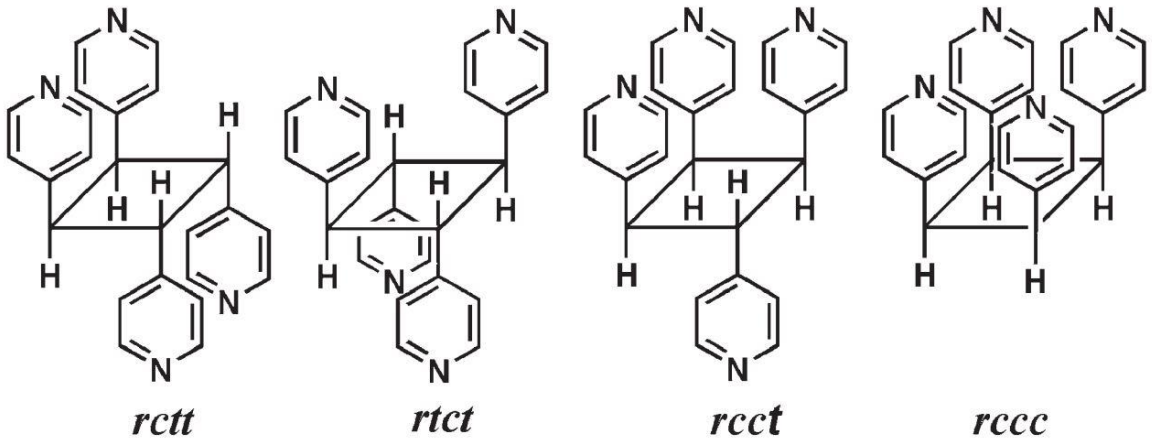

Figure 8: tetrakis(4-pyridyl)cyclobutane (tpcb) isomers.[15]

Although the geometric criteria for the photochemical [2+2] cycloaddition reaction in the solid-state have been well studied, it is a huge challenge to stack a pair of C=C olefinic bonds by design in MOFs. This requires an appropriate selection of ligands and co-ligands as templates.

1.4 Applications of photoreactive MOFs

The alignment of C=C olefinic bonds in a photoreactive MOF is considered a very attractive way for the synthesis of cyclic organic linkers,[15] as well as the modification of MOFs properties in the solid-state.[17] The photochemical [2+2] cycloaddition reaction in MOFs is a well-established method that can be used to synthesize stereospecific cyclobutane ligands that are otherwise difficult to synthesize in solution.[17] It has also been employed in pore modification[17] for photo-switching properties[24] and enhanced adsorption of guest molecules **(Figure 9)**.[25]

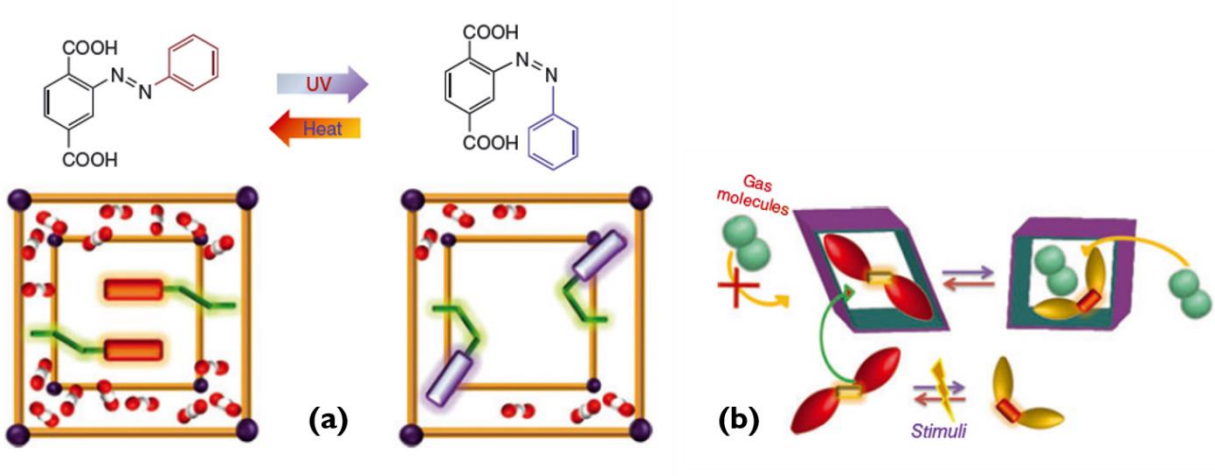

Figure 9: Pore modification for photo-switching properties **(a)**[24] and enhanced adsorption of guest molecules **(b)**.[25]

The photo-switching property was employed to gain access to the pores volume, as well as to lock guest molecules.[24] On the other hand, the enhanced adsorption of guest molecules has freed inaccessible internal volume by isomerization from *trans* to *cis* configuration of the azobenzene occupying the pores space.[25]

MOFs are constructed in one-step by self-assembly method. The photochemical [2+2] cycloaddition reaction within MOFs *via* post-synthesis modification (PSM) allows modification of MOFs for tuning the properties. It has been used to increase the dimensionality of MOFs, such as converting one-dimensional coordination polymer to two-dimensional one, then the latter one

to three-dimensional MOF, which allows to achieve full synthetic control on MOFs structure **(Figure 10)**.[17]

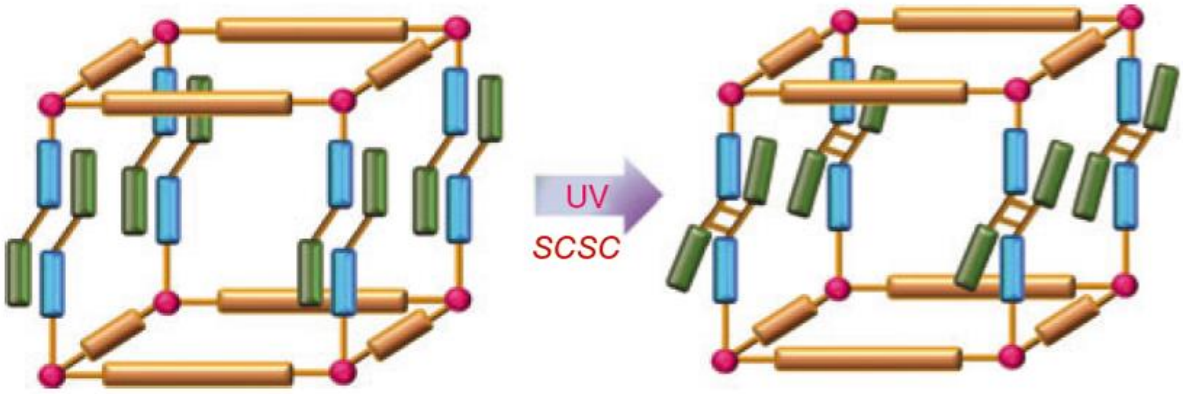

Figure 10: Step-wise synthesis of 3D-MOF using the photochemical [2+2] cycloaddition reaction as PSM method.[17]

Furthermore, such PSM has numerous advantages. It is a green process because it does not require any solvent and does not produce any by-product (regio-selective), in addition to its ability to achieve 100% conversion.[15] The photosensitive MOFs may also find applications in optical storage and sensing.[17]

1.5 Statement of Problem

Although the photochemical reaction [2+2] cycloaddition in the solid-state has been well established, it is still a challenge to stack a pair of C=C bonds in the crystal lattice by design. The aim of the research is to synthesize photoreactive MOFs that can stack a pair of C=C olefinic bonds of 4,4'-bipyridylethylene (**bpe**) with less than 4.2 Å distance in crystal lattice for solid-state photochemical [2+2] cycloaddition reaction, while using fumaric acid (**fum**) and oxalic acid (**ox**) as co-linkers (**Figure 11**) and Cd(II), Pb(II) and Zn(II) as metal ion nodes.

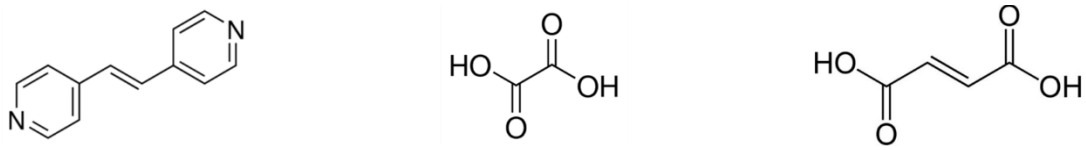

4,4'-bipyridyl ethylene
(Bpe)

Oxalic Acid
(Ox)

Fumaric Acid
(Fum)

Figure 11: Three ligands will be used in the synthesis of photoreactive MOFs**.**

The photoreactivity of the synthesized photoreactive MOFs will be studied. The photodimerization reactions will be carried out in different time intervals to determine the yield with % conversion, as well as the stereoselectivity of cyclobutane conversion.

1.6 Objectives

The objective of the study is to synthesize photoreactive MOFs *via* parallel alignment of the C=C double bonds of 4,4'-bipyridylethylene **(bpe) (Figure 11)**, while using fumaric acid **(fum)** and oxalic acid **(ox)** as co-linkers **(Figure 11)**, with Cd(II), Zn(II) and Pb(II) as metal ions. The specific objectives are as follows:

- To design appropriate MOFs using a judicious choice of linkers based on CCDC database.
- To synthesize photoreactive MOFs based on **bpe**, **ox** and **fum** as spacer ligands with Cd(II), Pb(II) and Zn(II) as metal ion nodes.
- To characterize the synthesized MOFs using various techniques, such as FT-IR, ^{1}H-NMR, powder XRD, elemental analysis and TGA.
- To conduct photoirradiation of MOFs in crystal and monitored it by ^{1}H-NMR spectroscopy.
- To gain an insight into the photoreaction of these systems in order to develop future specific light sensitive materials.

CHAPTER 2
LITERATURE REVIEW

2.1 Templating Methods

Large advancement has been made in the field of solid-state photochemical reactions, and a number of reviews has been written on this topic.[15,17] Extensive studies has been conducted on bpe and many reports have been published on aligning the C=C olefinic bonds of bpe by design.

The alignment of a pair of C=C olefinic bonds has been achieved by several types of templates, in which the substituents are able to stabilize the packing by a number of non-covalent interactions, such has hydrogen bonding, charge transfer, halogen-halogen and π-π interactions **(Figure 12)**.[10,15]

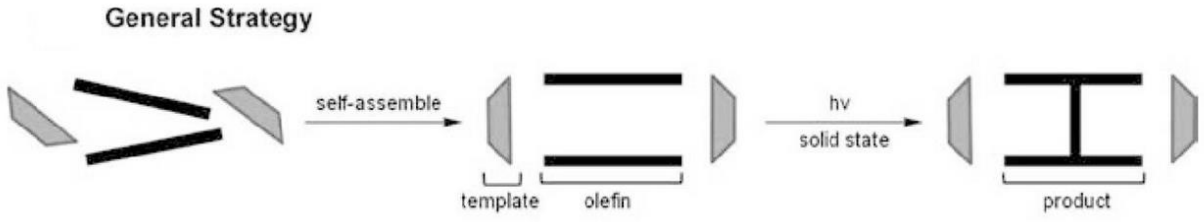

Figure 12: Using a template to align two ligands that contains C=C olefinic bonds.[10]

Theses templates can be organic, metal complexes **(Figure 13)**[10] or MOFs **(Figure 9** and **10)**.[15,24,25] However, most of the documented reports on stacking C=C bonds have been concerned with discrete compounds containing organic template or coordination complexes, and less work has been focused on infinite structures such as MOFs.[15] Nevertheless, there are some article reviews in the literature that focus on photochemical reactivity of MOFs.[17]

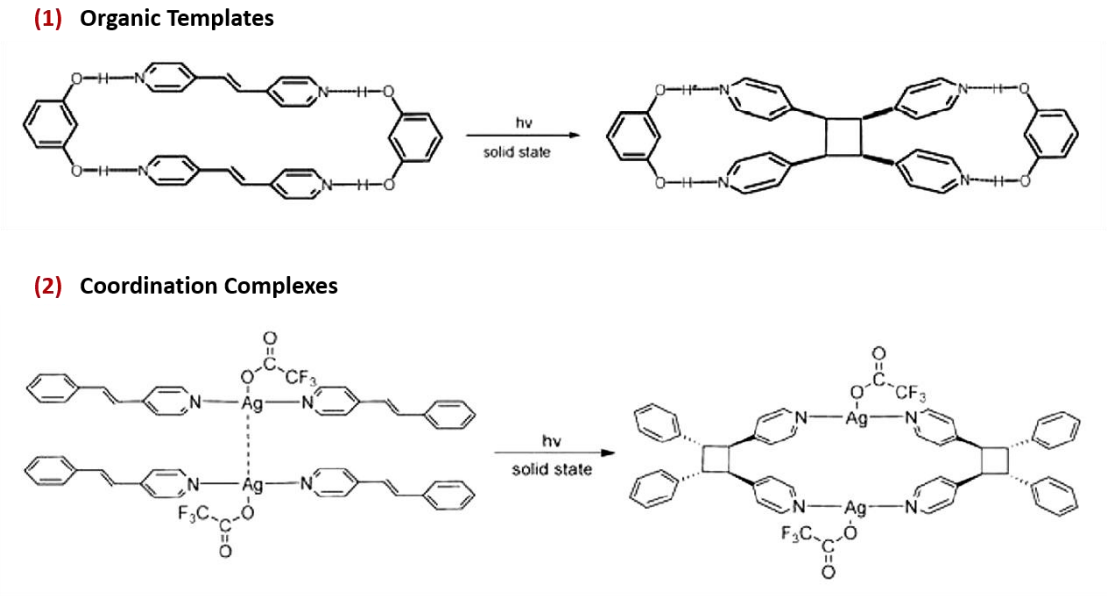

Figure 13: Templating methods used to align two C=C olefinic bonds other than MOFs.[10]

2.2 Double Bonds Alignment

Chemists and crystals engineers have set their eyes on aligning C=C olefinic bonds since the photochemical postulation of Schmidt.[22,23] Supramolecular interactions have been employed for such goal, such as hydrogen bonding and other non-covalent interactions.[26] Although Schmidt postulation stated that only parallelly aligned C=C double bonds can undergo photochemical [2+2] cycloaddition reaction,[17,22] over a long period of extensive researches many studies have reported that Schmidt rules are not always followed.[15] A criss-cross alignment of a pair of C=C double bonds were not expected but found to undergo photodimerization.[17] However, it was suggested that this occurs through pedal-like motion in the crystal lattice. This case has given an insight into a small part of internal molecular motion in the solid-state **(Figure 14)**.[15]

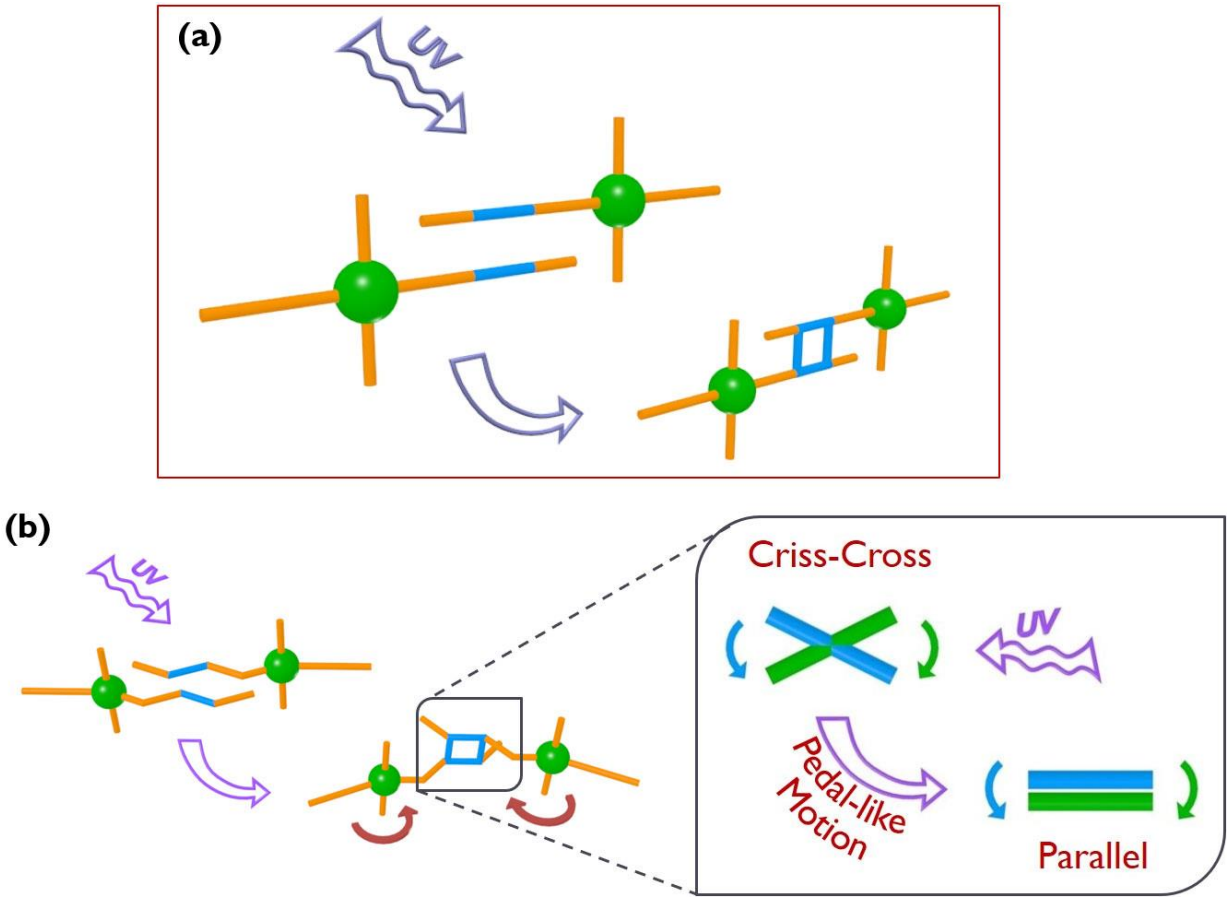

Figure 14: Photodimerization of perfectly aligned pair of C=C double bonds within the lattice structure **(a)** and criss-cross alignment **(b)** which has to go through pedal-like motion.

Furthermore, based on Schmidt's postulate, the photochemical [2 + 2] cycloaddition reaction in solid-state should take place if a pair of C=C olefinic bonds are aligned in a parallel manner with distance less than 4.2 Å, but it has been reported otherwise in some cases where the center of two double bonds are separated by more than 4.2 Å, yet the photochemical reaction still took a place.[15] Kaupp suggested that the photodimerization only took place after the molecules rearrange themselves somehow in the solid-state.[15] According to Schmidt criteria, it requires minimal internal movement in order for the photochemical [2+2] cycloaddition reaction to occur. On the other hand, large internal molecular movements also have been reported to be possible

and allow the photodimerization process to take place.[27] Therefore, the photoreactivity can be used as a powerful tool to study internal molecular motions in the solid-state.[27]

A triple-stranded ladder MOF, $[Pb_3(bpe)_3(O_2CCF_3)_4(O_2CCH_3)_2]_n$, was studied and found to be 100% photodimerized after a long period of *UV* irradiation, although it was supposed to stop at around 67% conversion based on its lattice structure.[23] The quantitative conversion was explained through large internal molecular motion **(Figure 15)**.[23]

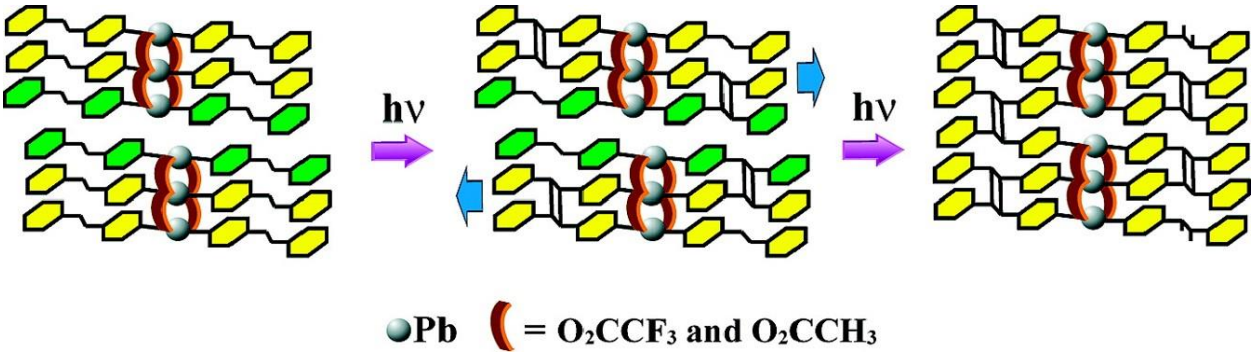

Figure 15: Large internal molecular movements of 1D-Ladder Pb(II) MOF.[23]

The alignment greatly affects the % conversion of the photochemical process as shown in the 1D-ladder MOF example **(Figure 15)**,[15,23] and the stereospecificity of the products as mentioned previously. It can also affect both as observed specially in the criss-cross alignment.[15] In fact, % conversion has not reached 100% in some cases, even where the geometrical criteria are fully satisfied.[10,17] However, further investigation showed that the yield depends on the number of aligned C=C olefinic bonds that are available to each other. This phenomenon most commonly appears on infinite structures where all double bonds are not available for photodimerization in the solid-state. The theoretical yield of infinite packing structures has been calculated to be 82-87%.[17]

2.3 Related Studies

Many photoreactive MOFs have been investigated extensively within the last few decades. A survey of the literature has been made to take a closer look at similar studies. Several studies have been found to use similar systems, namely bpe, ox and fum linkers with a range of metal sources.

A variety of metal ions have been used in these reported MOFs with aligned bpe for solid-state photochemical studies, such as Zn(II) in $[\{(H_3CCO_2)(\mu\text{-}O_2CCH_3)Zn\}_2(\mu\text{-bpe})_2]_n$,[28] Pb(II) in $[Pb(bpe\text{-}H)_2(CF_3CO_2)_4]_n$,[29] Ag(I) in $[Ag_2(bpe)_2(TFA)_2]_n$ (where TFA = Trifluoroacetate),[30] Cd(II) in $[Cd(bpe\text{-}H)_2(H_2O)(S_2O_3)_2]_n$,[31] Cu(II) in $[Cu(O_2CCF_3)_2(\mu\text{-bpe})(DMF)]_n$,[32] and Mn(II) in $[Mn(1,2\text{-chdc})(bpe)_2(H_2O)_2]\cdot H_2O$ (where 1,2-chdc = *trans*-1,2-cyclohexanedicarboxylate).[33]

No photochemical studies have been done on mixed systems with bpe-ox linkers, but the synthesis of several coordination polymers of such system has been reported.[34] Castillo and co-workers have reported five MOFs using bpe and ox as linkers with several metal ions, such as Zn(II), Ni(II), Co(II), Fe(II) and Cu(II), which has the formula [M(II)(μ-ox)(μ-bpe)]n.[34] The reported MOFs were two-dimensional rectangular grid-type frameworks **(Figure 16)**.[34] However, next to the fact that the alignment is criss-cross, the distance between the C=C olefinic bonds is more than 5.377 Å, which renders these MOFs photochemically inactive.[34] This study is targeting the design and synthesis of a photoreactive MOF of mixed system with bpe-ox.

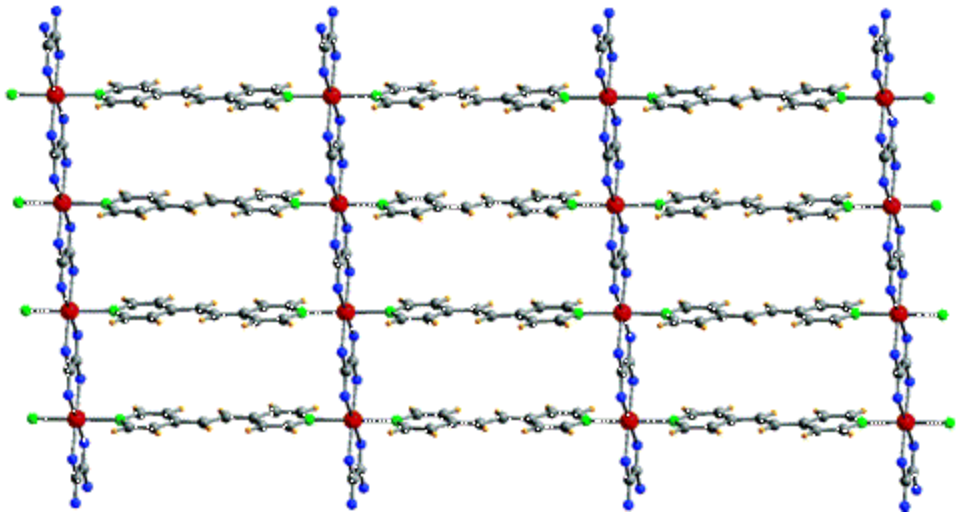

Figure 16: 2D rectangular grid-type photochemically inactive MOF structure for the mixed system with bpe-ox linkers and several metal ions, such as Zn(II), Ni(II), Co(II), Fe(II) and Cu(II).[34]

Several structures were reported for a family of bpe-ox Mn-based MOFs.[35] Although most of them are photochemically inactive because they do not meet Schmidt criteria of the topochemical postulate, either alignment is out of phase or there is a long distance between the olefinic bonds, there is only one structure that has the right conditions to undergo photodimerization **(Figure 17)**.[35] The reported MOF, $[Mn_2(\mu\text{-}ox)_2(\mu\text{-}bpe)(bpe)_2]_n$, has a broken ladder-like 2D sheet structure with an infinite alignment of C=C olefinic bonds within 4.2 Å range. However, it is hard to characterize photoreactivity of this compound using ^{1}H-NMR spectroscopy due to the paramagnetic metal ion. Nevertheless, this system presents a good opportunity to synthesize its analogous Zn(II) or Pb(II)-based MOF and study its photoreactivity in details.

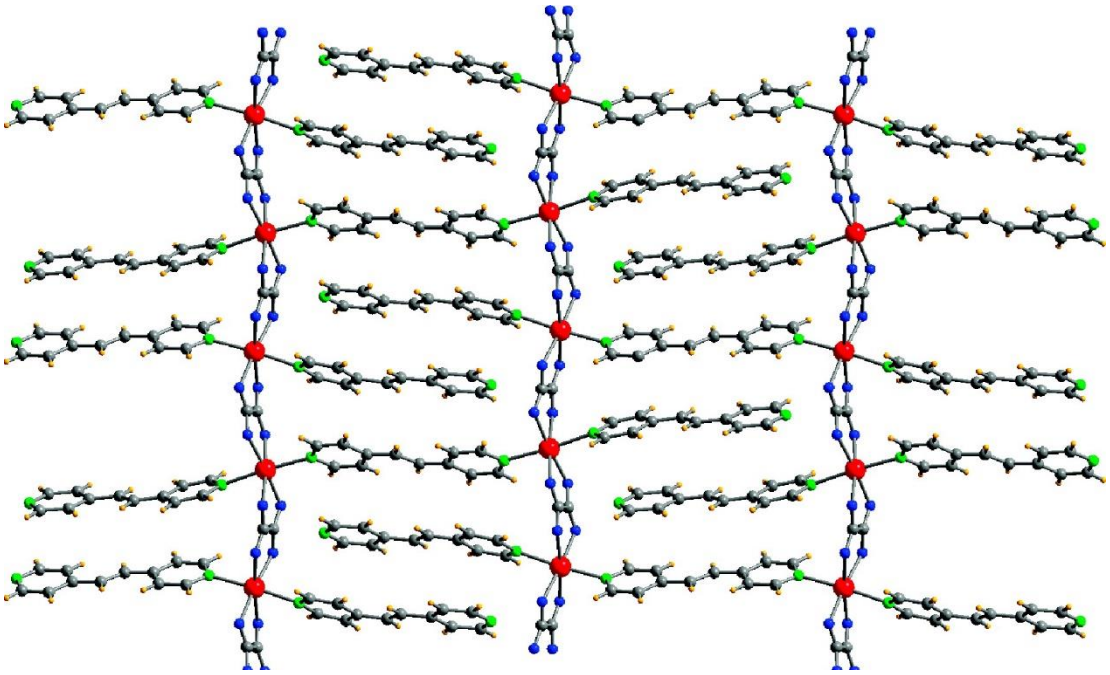

Figure 17: The structure of $[Mn_2(\mu\text{-ox})_2(\mu\text{-bpe})(bpe)_2]_n$ MOF, which has a broken ladder-like 2D sheet structure with an infinite alignment of C=C olefinic bonds within 4.2 Å range.[35]

Fumaric acid (fum) is another possible co-linker to be utilized for the alignment of bpe. Several bpe-fum based MOFs were found in the literature, but only two were found to be photochemically reactive with the alignment of olefinic C=C bonds of bpe within the right structural conditions.[36–40] The two photoactive MOFs are based on Zn(II) and Cd(II) metal ions, namely $[Cd_2(bpe)_2(fum)_2]$ and $[Zn(bpe)(fum)]\cdot 0.25H_2O$, and their photoreactivity has been reported.[36,37] It is possible to target other analogous MOFs with different metal ions and study their photoreactivity. Analogous systems of bpe-fum linkers with lead (Pb) metal ion can be targeted. Pb(II)-based photoreactive MOFs are not very common and it will be very interesting to study their photochemical behavior for making photosensitive materials. Similar behavior has been reported, in some cases, for Cd(II) and Pb(II) based photoreactive MOFs.[41] Hence, comparable results might be expected if the same structure is obtained. However, Pb(II) can maintain high coordination number which might cause different topological structure to be self-

assembled.[27] Still, considerably less number of studies has been reported about photoreactivity of fumaric acid containing MOFs,[15,17] which can be an opportunity to investigate Pb-based photoreactive MOFs containing the olefinic C=C bonds that satisfy Schmidt postulate.

Many systems of photoreactive MOFs have been explored over the past few decades, and each system has its unique characteristics.[15,17] However, when it comes to the design and synthesis of MOFs, the Zn(II) metal is the first that comes to mind due to its relative ease of control and predictable behavior. Cadmium might be also considered second in line due to its predictable geometries. With that in mind, the literature, Cambridge Structures Database (CSD), has been scanned for unstudied photoreactive cadmium-based MOF and a dinuclear triple-strands-like one-dimensional ladder photoreactive cadmium-based MOF, $[Cd(bpe)_{1.5}(NO_3)_2(H_2O)]_n$, has been found **(Figure 18)**.[41]

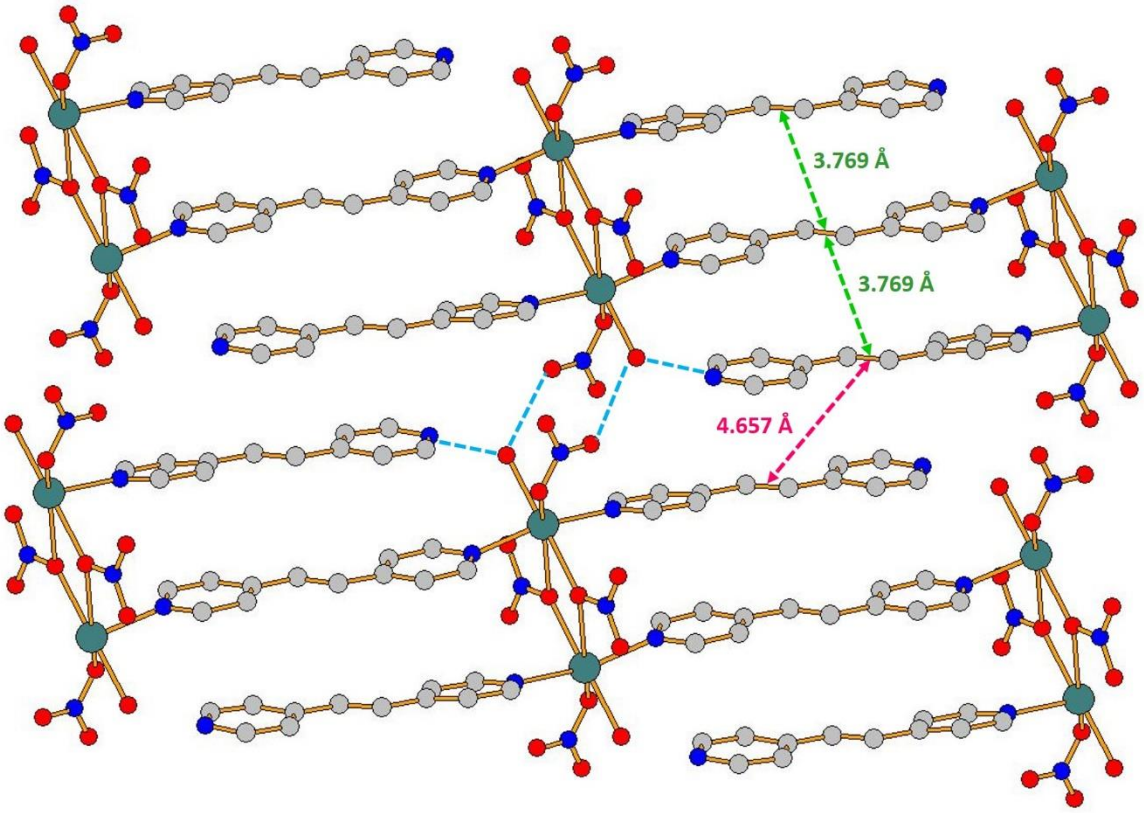

Figure 18: A dinuclear triple-strands-like one-dimensional ladder photoreactive cadmium-based MOF.[41]

The compound was reported a while ago, but no photochemical study has been conducted on it so far.[41]

Several methods have been utilized to force partially photodimerizing systems to reach 100% conversion, such as desolvation, dehydration and mechanical forces.[15] Several studies have shown that mechanical forces, such as grinding, accelerate the pedal-like motion of the system and force it to reach 100% conversion.[42] However, none has been about ladder-like structures. It will be very interesting if large internal molecular movements can be induced mechanically on this type of structures to align two ladder structures and obtain infinite number of bpe alignments.

If the two adjacent ladder structures are aligned successfully, the MOF topology will be converted to a two-dimensional sheet. The photodimerization in this type of photoreactive MOFs results in modification of the photoreactive organic linkers and leads to structural transformation. It was observed in one, two and three-dimensional MOFs.[17] The structural transformation *via* photodimerization can convert 1D→2D or 2D→3D depending on the topological structure of the MOFs.

The increase in dimensionality was reported previously,[17] such as formation of one-dimensional coordination polymer of metal complexes held together in the solid state by non-covalent bonds **(Figure 19)**,[29,31,42] the conversion of ladder-like structures to 2D sheets **(Figure 15)**[23] and 2D sheets topology to PCU topology MOFs **(Figure 10)**.[17]

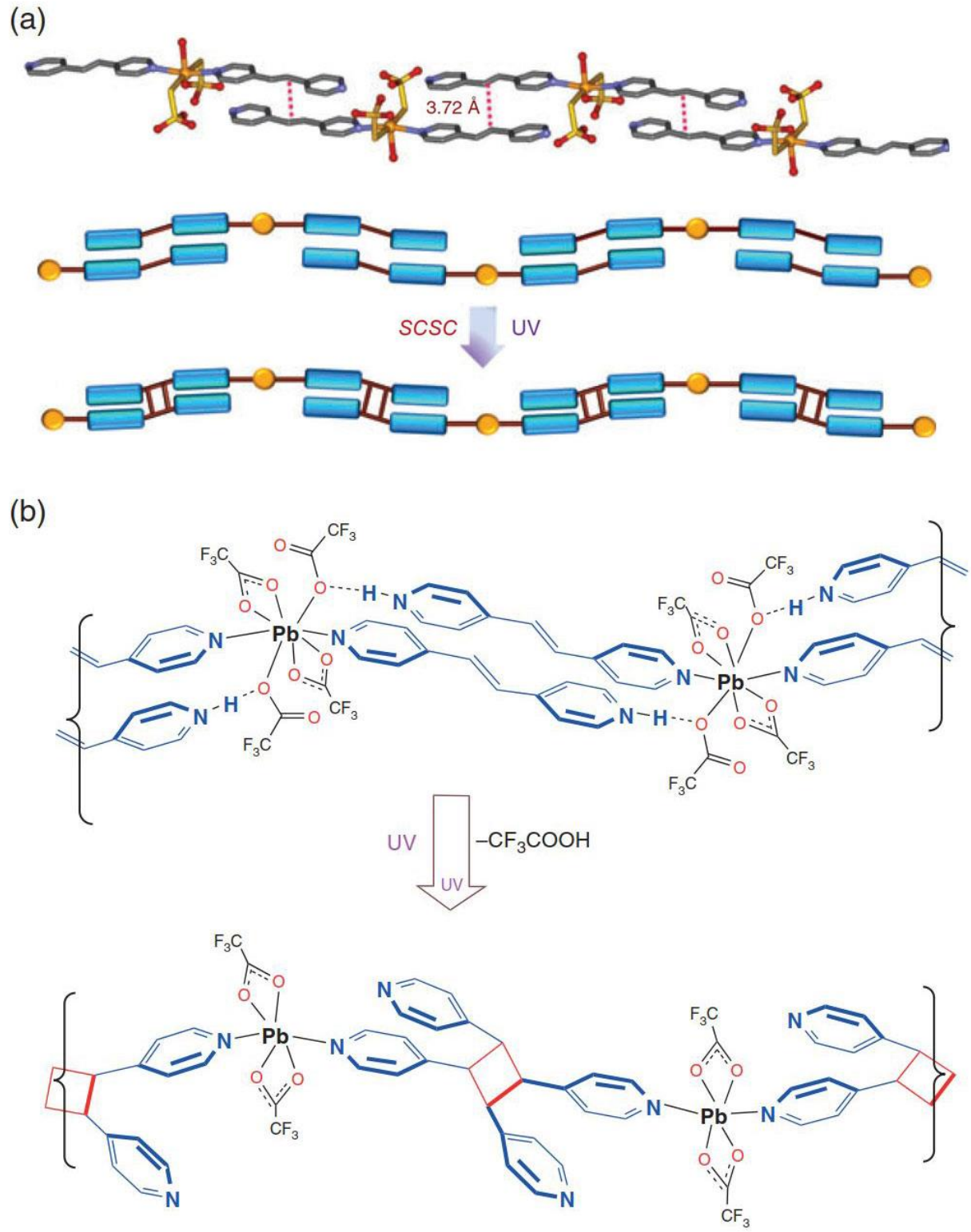

Figure 19: Photodimerization of metal complexes to form one-dimensional coordination polymers.[29,31,42]

CHAPTER 3
RESEARCH METHODOLOGY

3.1 Materials

3.1.1 Chemicals:

The used chemicals have been purchased from various commercial vendors and used as received unless otherwise stated. The 4,4'-bipyridylethylene (bpe), fumaric acid (fum) and oxalic acid (ox) were used as organic linkers for the photoreactive MOFs, while $Zn(NO_3)_2.6H_2O$ and $Pb(NO_3)_2$ were used as metal sources.

3.1.2 Solvents:

Common solvents were used for the synthesis, such as dimethylformamide (DMF), methanol and distilled water, while some other solvents were used for ^{1}H-NMR studies such as dimethyl sulfoxide (DMSO-d_6).

3.1.3 Instrumentation:

- *UV* Photoreactor
- NMR Spectrometer
- Powder X-Ray Diffractometer
- Fourier Transform-Infrared Spectrometer (FT-IR)
- CHNS Analyzer

3.2 Synthesis of Metal-Organic Frameworks

3.2.1 Synthesis of $\{(Hbpe)_2[Zn_2(ox)_3]\}_n \cdot (H_2O) \cdot 2.2(DMF)$ (1)

In a 20-mL vial, a 20 mg (0.067 mmol) of zinc(II) nitrate hexahydrate ($Zn(NO_3)_2.6H_2O$) and 36 mg (0.20 mmol) of 4,4'-bipyridylethylene (bpe) were dissolved in 2 mL of dimethylformamide (DMF). In another 20-mL vial, 12 mg (0.10 mmol) of oxalic acid dihydrate (ox) were dissolved in 1 mL of ethanol. Then, the two solutions were mixed at room temperature and an orangish white fine powder formed instantly. The vial was placed on a shaker for 1 h. The powder product was gravitationally filtered with filter paper, washed three times with DMF and three times with ethanol and left to dry over 24 h yielding 23.4 mg (90%) of MOF material **(Scheme 1)**.

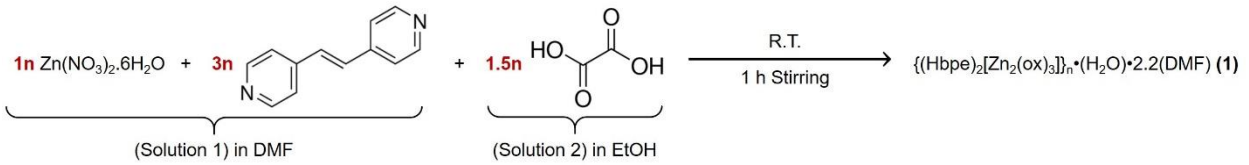

Scheme 1: Synthesis of MOF **(1)**.

3.2.2 Synthesis of $[Pb_4(ox)_3(bpe)_4(H_2O)_4]_n \cdot (NO_3)_2$ (2)

Compound **2** was synthesized in a very similar manner to **1**. In 2 mL of DMF, 20 mg (0.060 mmol) of $Pb(NO_3)_2$ and 36 mg (0.20 mmol) of bpe were dissolved. The solution was mixed at room temperature with another solution of 12 mg (0.10 mmol) of ox dissolved in 1 mL of ethanol. A pinkish white fine powder formed instantly. The mixture was placed on a shaker for 1 h. The powder product was filtered, washed three times with DMF and three times with ethanol, then left to dry over 24 h. The yield was 25.8 mg (85%) of MOF material **(Scheme 2)**.

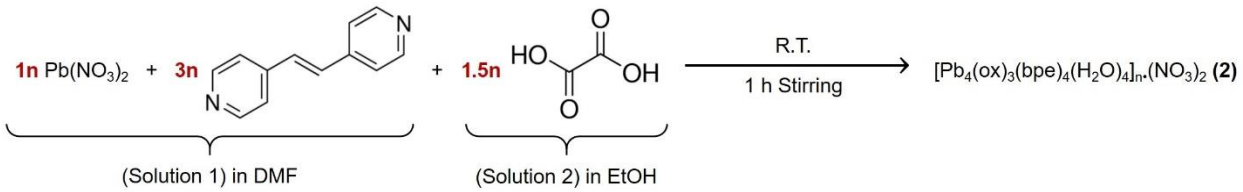

Scheme 2: Synthesis of MOF **(2)**.

3.2.3 Synthesis of $[Pb(bpe)(fum)]_n.0.25(H_2O)$ (3)

The synthesis of the third MOF was also similar to **1** and **2**. In a small vial, a 20 mg (0.060 mmol) of $Pb(NO_3)_2$ and 36 mg (0.20 mmol) of bpe were dissolved in 2 mL of dimethylformamide (DMF). In another small vial, another solution was made of 12 mg (0.10 mmol) of fumaric acid (fum) dissolved in 1 mL of ethanol. The two solutions were mixed at room temperature and a pale pink powder formed immediately. The mixture was stirred for 1 h. The product was slowly filtered, washed three times with DMF and three times with ethanol, then left to dry over 24 h. The yield of the reaction was 20.9 mg (72%) **(Scheme 3)**.

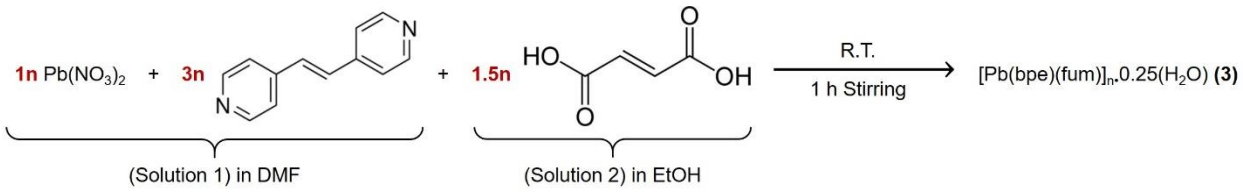

Scheme 3: Synthesis of MOF **(3)**.

The synthesis of the three MOFs can be summarized in **(Scheme 4)**.

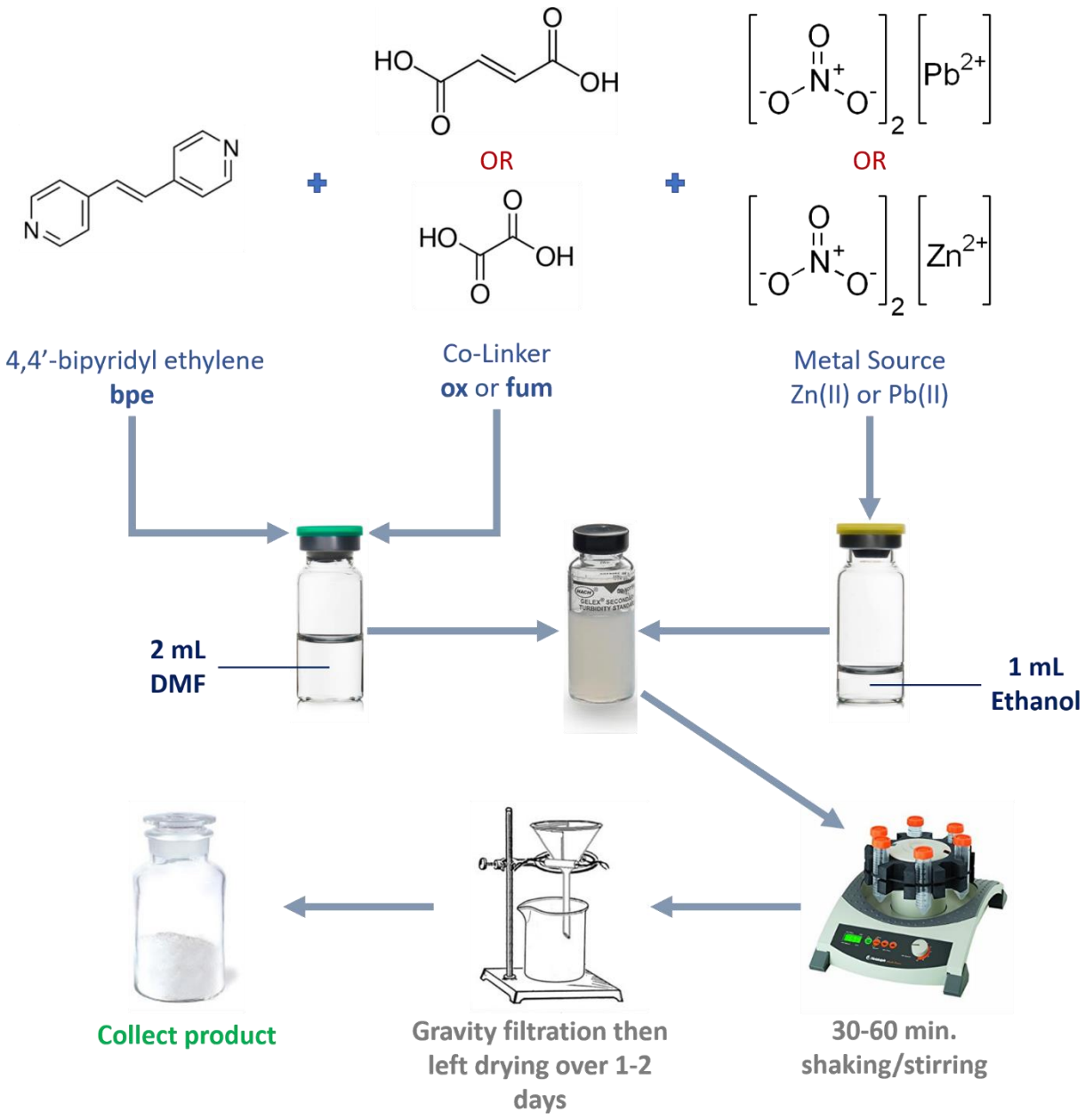

Scheme 4: Schematic diagram for general synthesis procedure for **1**, **2** and **3** MOFs.

3.2.4 Synthesis of $[Cd(bpe)_{1.5}(NO_3)_2(H_2O)]_n$ (4)

The cadmium MOF was synthesized by a layering technique based on the reported procedure with slight modification.[41] A solution of 13 mg (0.075 mmol) of bpe dissolved in 0.5 mL of ethanol was slowly layered over 0.5 mL of aqueous solution of $Cd(NO_3)_2 \cdot 4H_2O$ (15 mg, 0.050

mmol). Colorless crystals formed within few days, then the crystals were taken out, and dried in air. The yield was 18 mg (69%) **(Scheme 5)**.

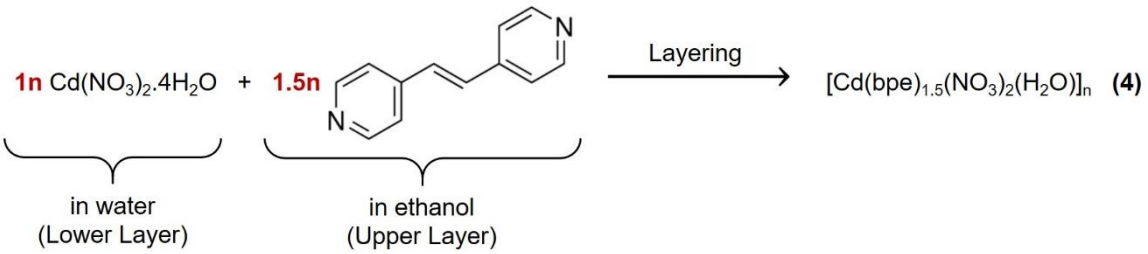

Scheme 5: Synthesis of MOF **(4)**.

3.3 Samples Characterization

3.3.1 FT-IR Spectroscopy

The FT-IR spectra were measured on a Perkin Elmer 16F PC FT-IR Spectrometer using KBr salt as filler in pellets form. The measurements were taken within the standard range of 400 - 4000 cm^{-1}. The samples were prepared by mixing 1 mg of sample with 100 mg of KBr and grounded to fine powder, which was then pressed into a pellet. The later then was mounted on a holder and inserted in the FT-IR spectrometer for measurements **(Figure 20)**.

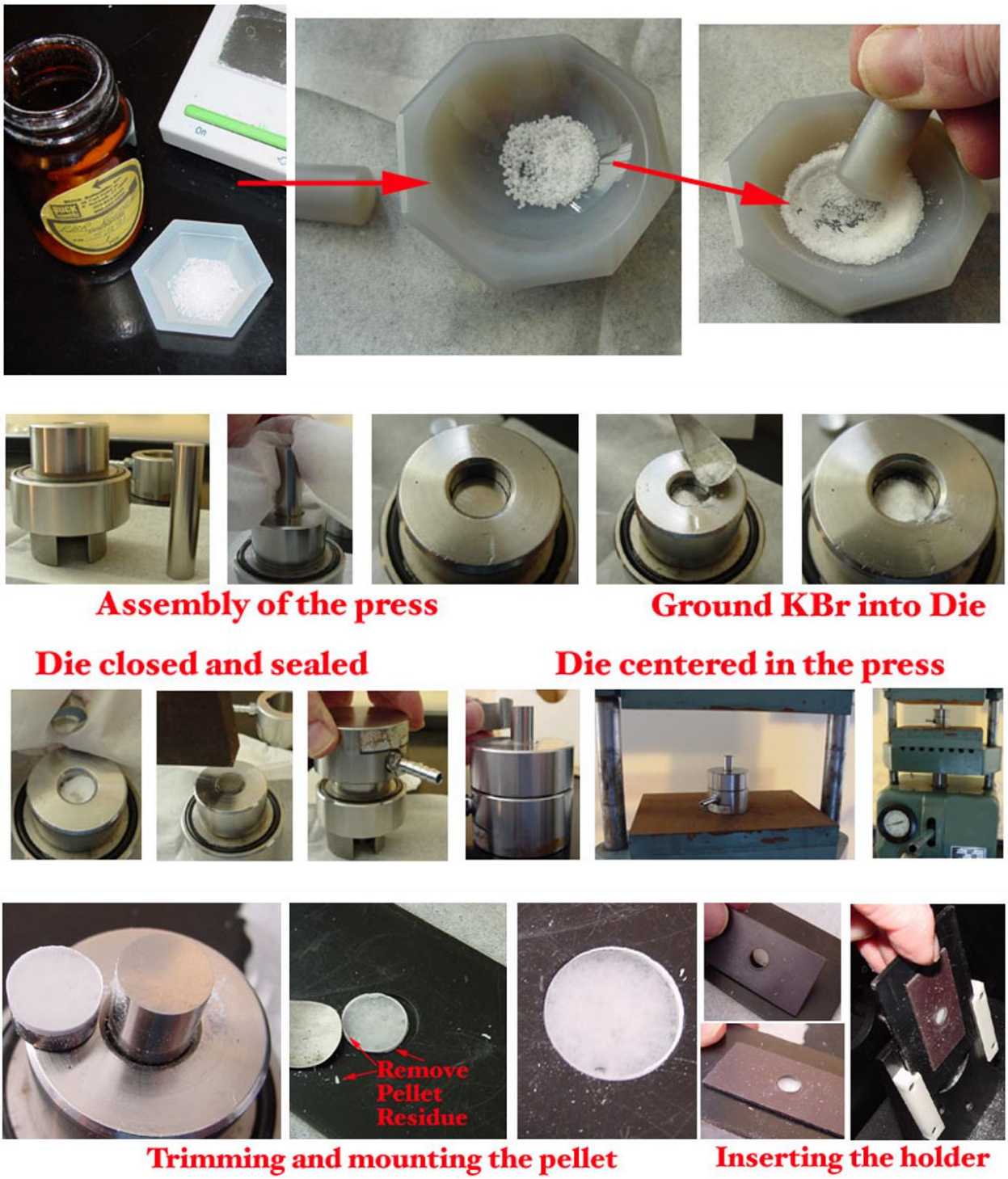

Figure 20: Sample preparation for FT-IR measurements.[43]

3.3.2 ^{1}H-NMR Spectroscopy

The Nuclear Magnetic Resonance (NMR) spectra have been obtained by a JEOL JNM-LA500 spectrometer. About 4-5 mg of each sample were placed in NMR tube. Then, 1-2 mL of deuterated dimethyl sulfoxide (DMSO-d_6) solvent was added. The samples were shaken vigorously to digest the MOF. Sonication was used to help digesting the samples. The NMR tube was placed in the NMR spectrometer and measurements were taken. All other conditions were standard conditions.

3.3.3 Powder X-Ray Diffraction (PXRD)

Powder X-ray diffraction (PXRD) patterns were obtained by a Rigaku MiniFlex II diffractometer. A monochromator of CuKα1 (1.5406 Å) was used at 30 kV and 15 mA during patterns collection. The obtained patterns were recorded in the range of 2^0 to 90^0 (2θ) with continuous scanning method. The scanning conditions were set on 1.0^0 / min. and 0.02^0 for scanning speed and step size respectively. As for sample preparation, the fine product powder was mounted into the PXRD diffractometer sample holder by back pressing.

3.3.4 Elemental Analysis (CHN)

The weight percent of carbon, hydrogen and nitrogen was determined by an elemental analyzer. The data were collected on a Perkin Elmer EA – 2400 elemental analyzer operating under CHN mode. Around 1 mg of sample was used for each measurement, and each sample was packed tightly in a small tin container that weighs 1 mg. The sample was then placed in the instrument and measurements were taken.

3.3.5 Thermogravimetric Analysis (TGA)

The thermogravimetric analysis (TGA) was done with a TA SDT 2960 thermal analyzer. The experiments conditions were set to ramp from room temperature to 600 ^{0}C at a rate of 5 ^{0}C.min^{-1} under nitrogen atmosphere at a flow rate of 50 mL/min. About 3-5 mg was used for each sample. The samples of each compound (**1-4**) were prepared right before the TGA experiment to minimize moisture exposure.

3.4 UV Irradiation

UV irradiation was performed by a Luzchem LZC-DEV photoreactor. About 4-5 mg of each sample was placed between two glass slides and placed on its side edge for irradiation. Both sides were irradiated simultaneously using the side lamps of the photoreactor. Each compound was UV irradiated for 5, 10, 15, 30 and 50 hours for NMR studies. Two more samples of each compound were UV irradiated for 50 hours for FT-IR and elemental analysis (CHN). The single crystal of compound **4** was placed on a slide of glass, then UV irradiated from the top UV lamps for 5, 20 and 50 hours for single crystals photoreactivity studies with NMR. Another batch of single crystal samples were irradiated for 50 hours for TGA. Powder samples of compound **4** were obtained by manual grinding of its single crystals for 10 minutes using a pestle and a mortar, then the powder samples were exposed to UV irradiation for 5, 10, 20, 30 and 50 hours. Another ground crystals (10 and 20 min. grinding period) samples were UV irradiated for 50 hours, then used for TGA.

3.5 NMR Studies

The ^{1}H-NMR spectra were utilized to monitor the formation of cyclobutane derivative during the course of the photochemical [2+2] cycloaddition reaction under different experimental conditions. The yield of UV irradiation experiments is reported as % conversion of bpe by integrating the relative area under the peaks of both bpe and the cyclobutane derivatives.

CHAPTER 4
RESULTS AND DISCUSSION

4.1 Photodimerization Studies

4.1.1 Compounds 1-3

In the quest for new photoreactive MOFs, it is more important to look into the photoreactivity of these compounds to check whether they are photoreactive or photostable. The photoreactivity of these compounds (**1-3**) has been studied through monitoring the photochemical [2+2] cycloaddition reaction with ^{1}H-NMR spectroscopy. Each compound was analyzed with ^{1}H-NMR spectroscopy before and after UV irradiation to determine if the compounds are photochemically active or not. The following figures (**Figures 21-26**) show ^{1}H-NMR spectra of each compound before and after UV irradiation.

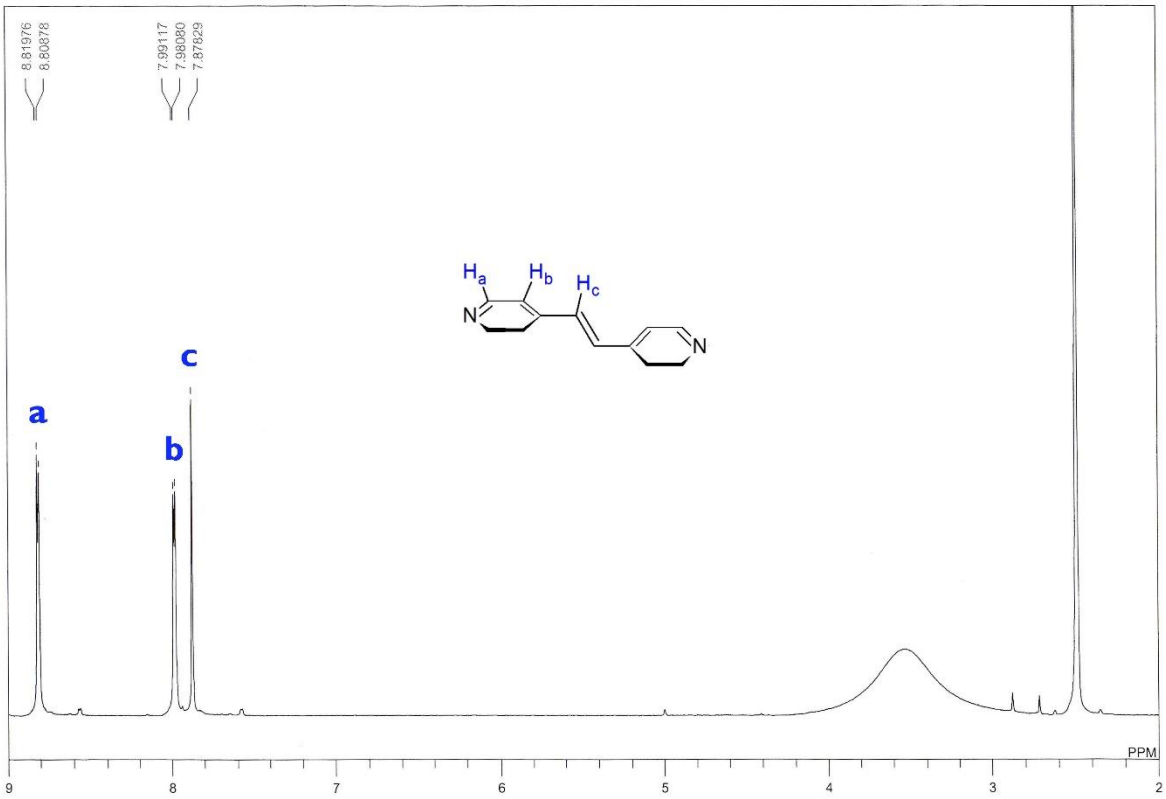

Figure 21: ^{1}H-NMR spectrum of **1** before UV irradiation (DMSO-d_6).

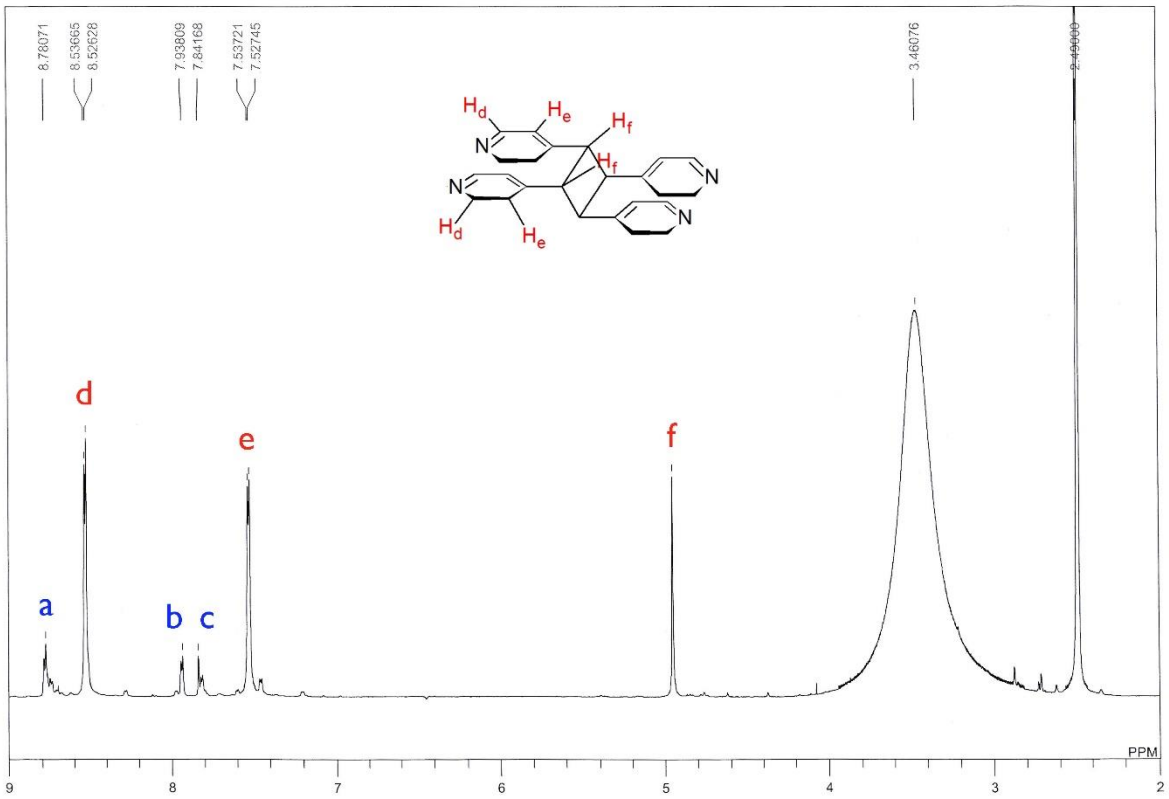

Figure 22: ^{1}H-NMR spectrum of **1** after 30 hours of UV irradiation (DMSO-d_6).

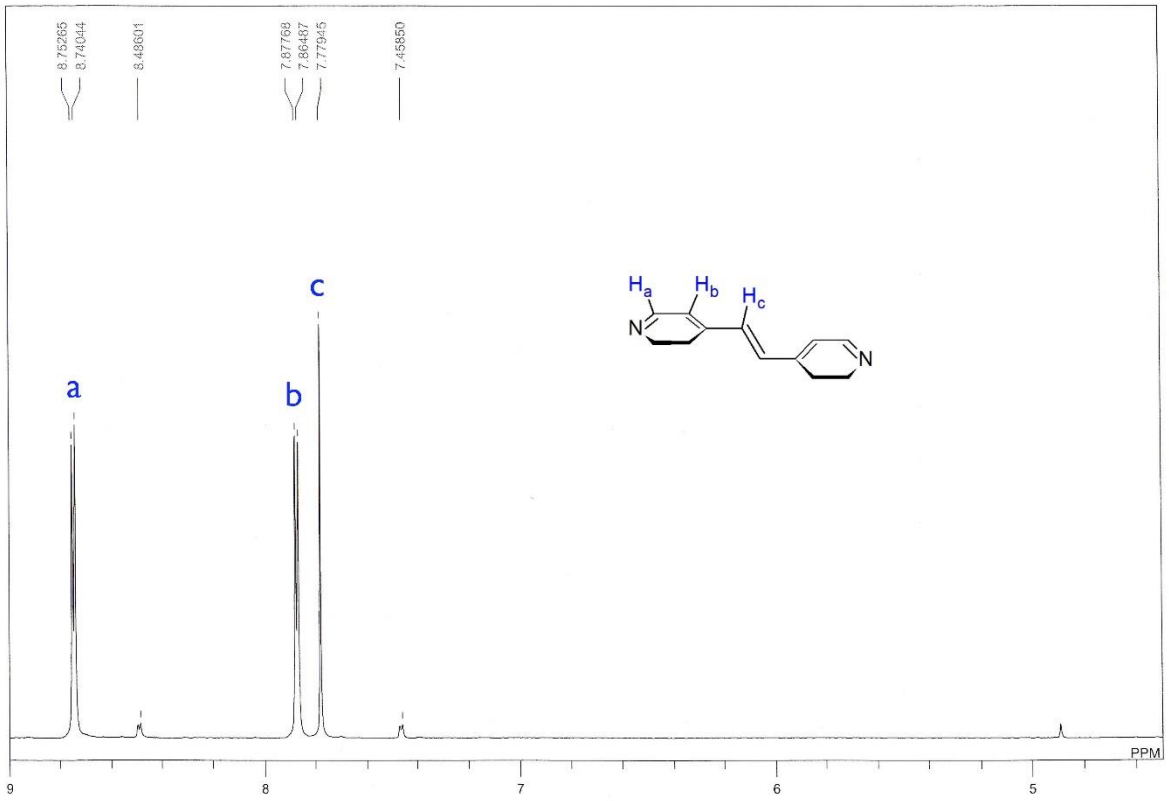

Figure 23: ^{1}H-NMR spectrum of **2** before UV irradiation (DMSO-d_6).

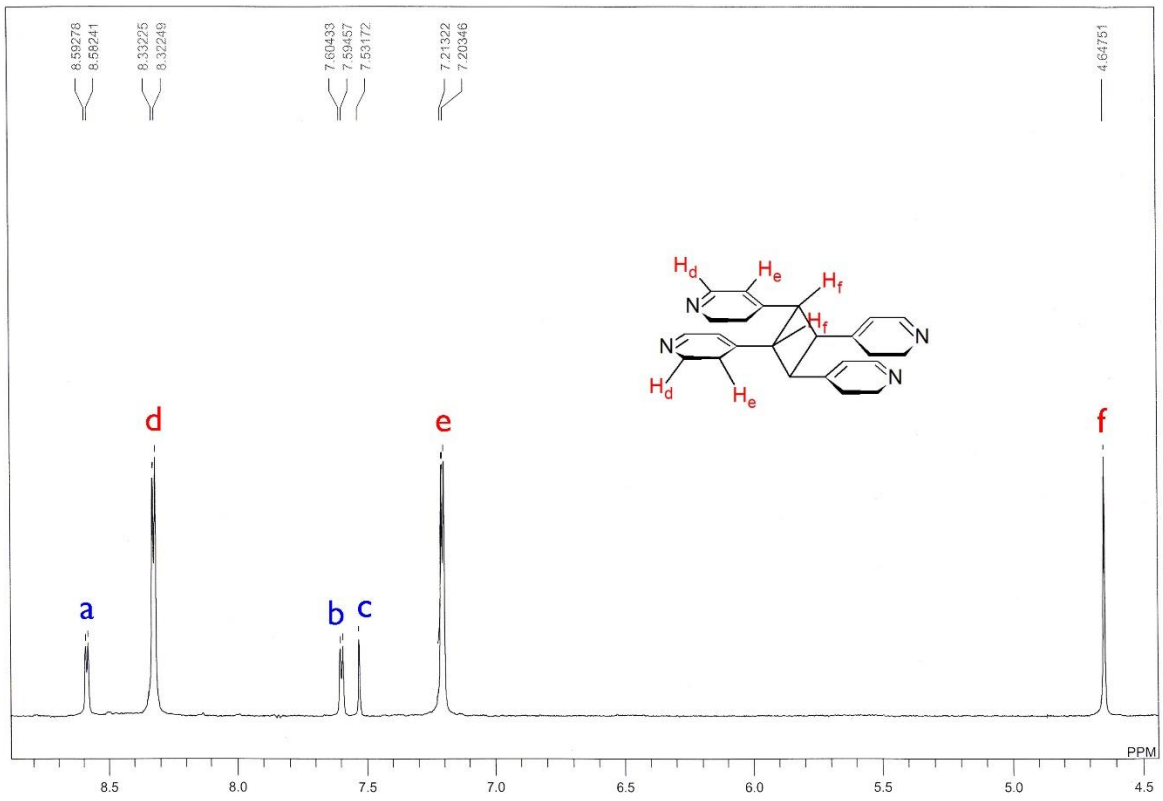

Figure 24: ^{1}H-NMR spectrum of **2** after 30 hours of UV irradiation (DMSO-d_6).

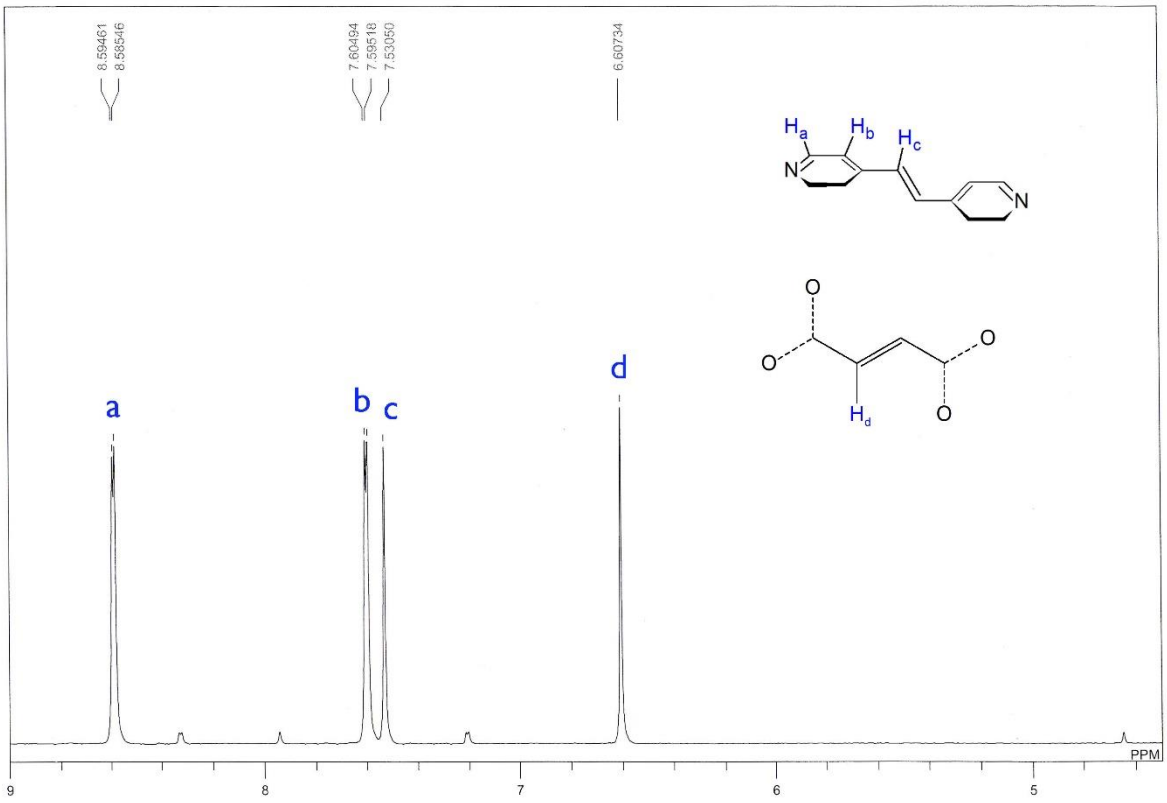

Figure 25: ^{1}H-NMR spectrum of **3** before UV irradiation (DMSO-d_6).

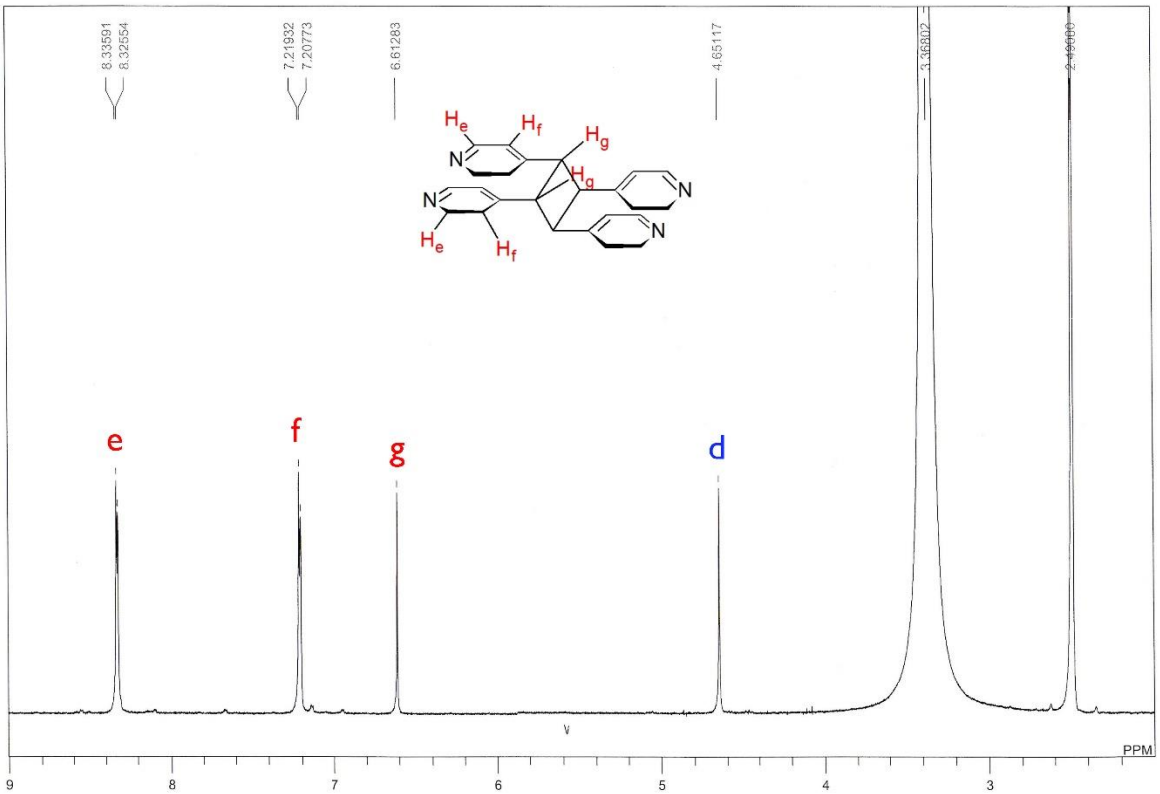

Figure 26: ^{1}H-NMR spectrum of **3** after 5 hours of UV irradiation (DMSO-d_6).

After UV irradiation ^{1}H-NMR spectra of compound **1** and **2** (**Figures 22** and **24**) show the decrease in intensity of a, b and c signals, which belong to photochemically unreacted bpe, and appearance of d, e and f signals, which belong to the product of the photochemical [2+2] cycloaddition reaction; *rctt*-tetrakis(4-pyridyl)cyclobutane (tpcb). However, in the case of compound **3**, after UV irradiation ^{1}H-NMR spectrum (**Figure 26**) has shown complete disappearance of bpe signals (a, b and c in **Figure 25**), which indicates complete conversion of bpe ligands within **3** to *rctt*-tpcb product.

It is clearly evident from ^{1}H-NMR spectra that these MOFs are photoreactive and undergo photochemical [2+2] cycloaddition reaction in the solid-state. However, it would be more appropriate to try to achieve maximum conversion of bpe. In order to do so, a deeper look into the photochemical behavior of these MOFs is required.

The two compounds (**1** and **2**) were UV irradiated for various time intervals, namely 5, 10, 15, 30 and 50 hours, then ^{1}H-NMR spectra were recorded. The following figures (**Figure 27** and **28**) show the ^{1}H-NMR spectra of each compound for 5, 10, 15, 30 and 50 hours.

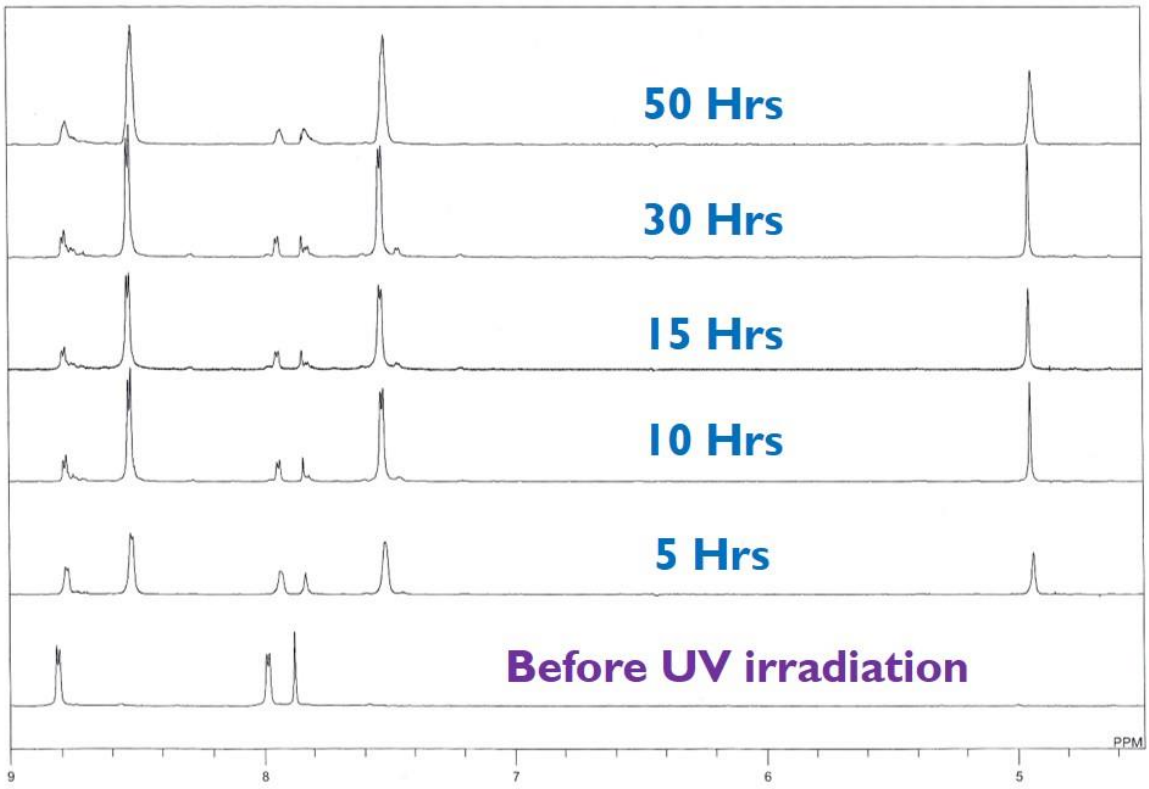

Figure 27: ^{1}H-NMR multi-spectrum of **1** after various time intervals of UV irradiation (DMSO-d_6).

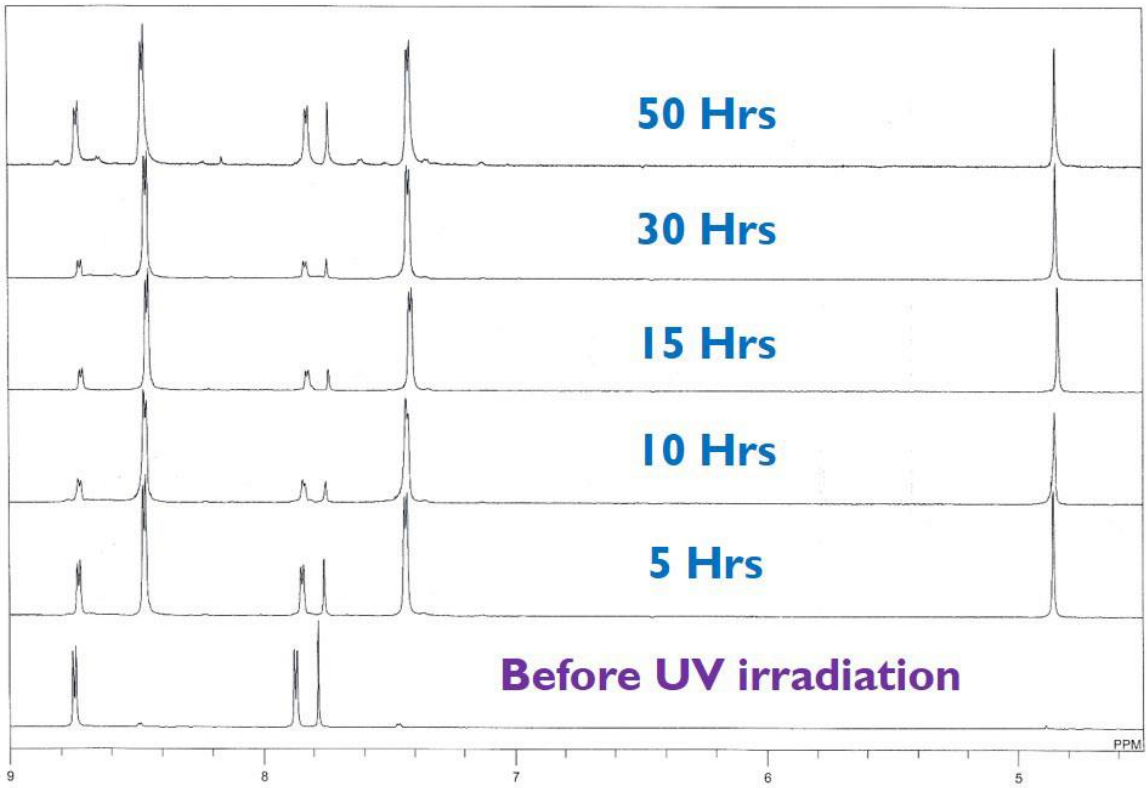

Figure 28: ^{1}H-NMR multi-spectrum of **2** after various time intervals of UV irradiation (DMSO-d_6).

The percentage conversion by UV irradiation was calculated from the obtained ^{1}H-NMR spectra of compound **1** and **2** by integrating the relative peaks areas for both bpe and *rctt*-tpcb as shown in **Figure 29-38**.

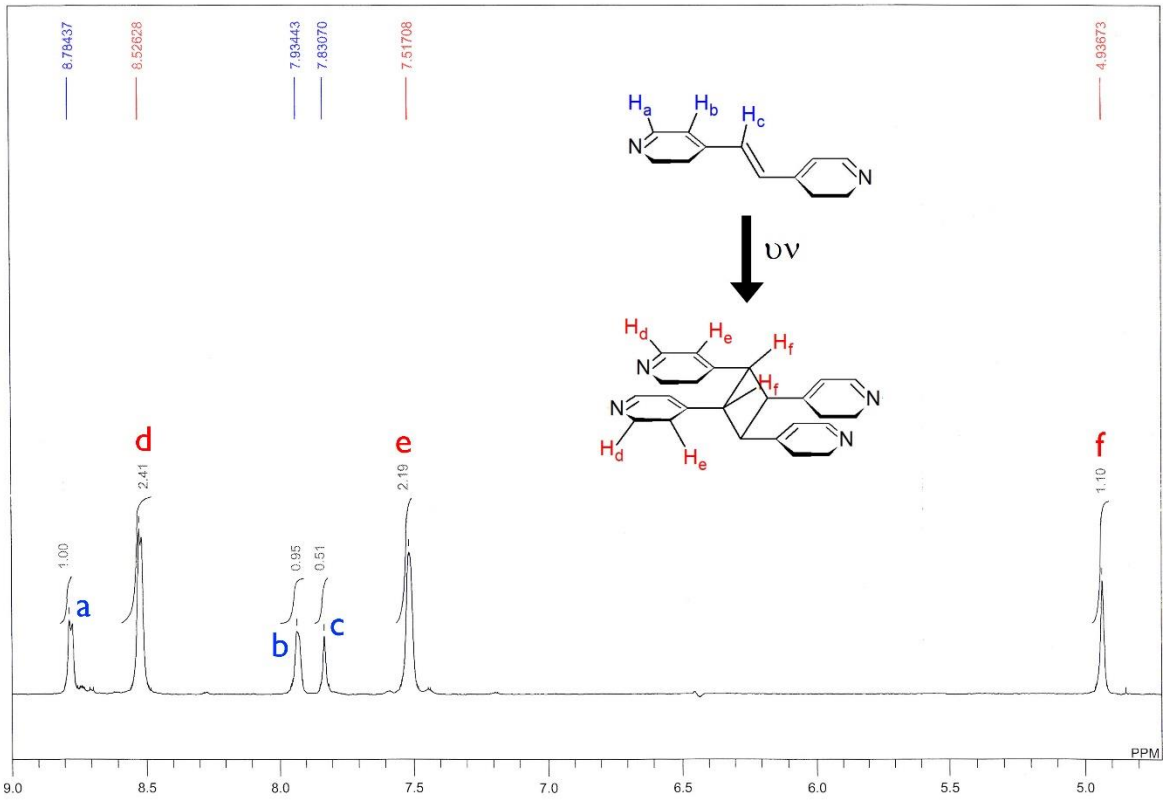

Figure 29: ^{1}H-NMR spectrum of **1** after 5 hours of UV irradiation (DMSO-d_6).

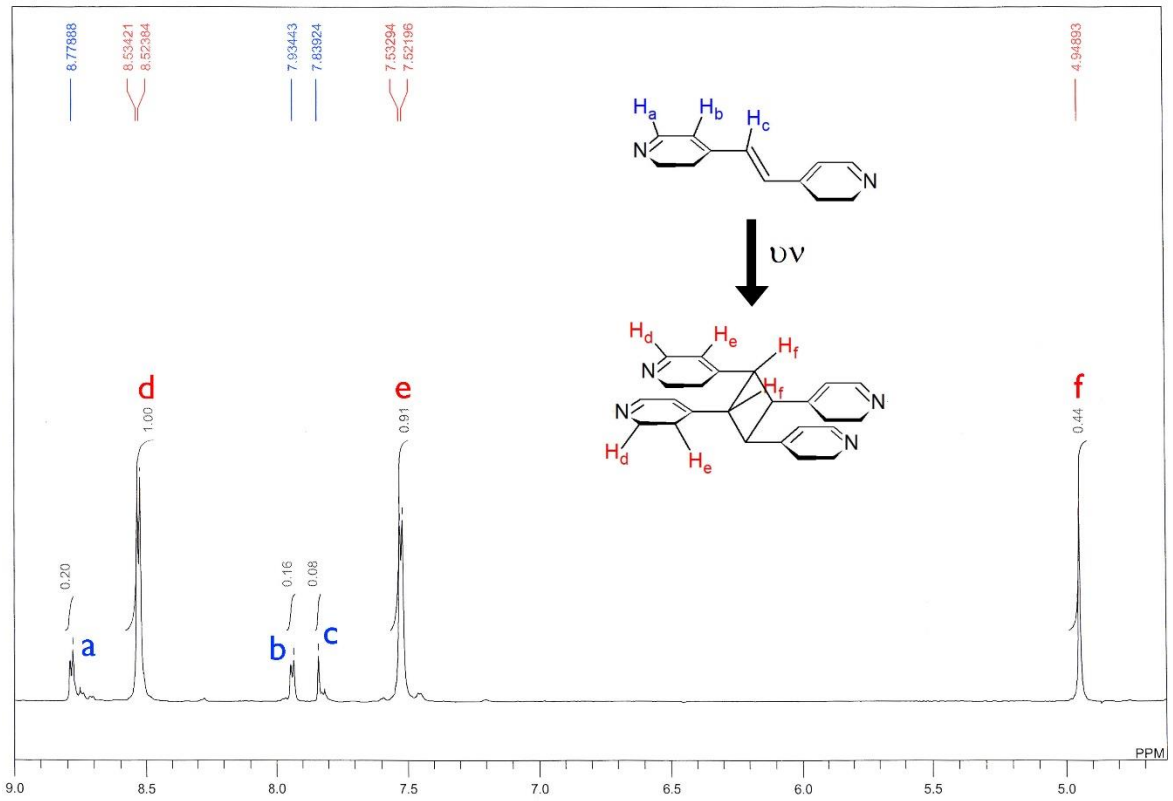

Figure 30: ^{1}H-NMR spectrum of **1** after 10 hours of UV irradiation (DMSO-d_6).

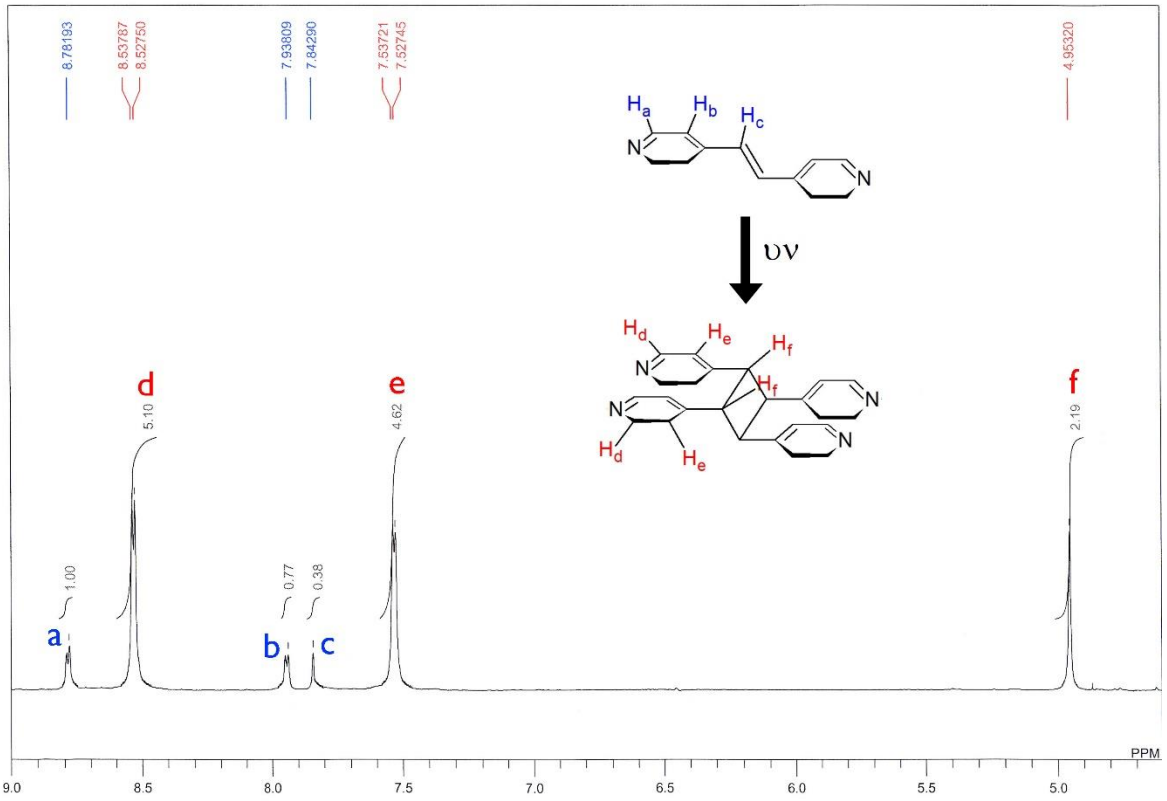

Figure 31: ^{1}H-NMR spectrum of **1** after 15 hours of UV irradiation (DMSO-d_6).

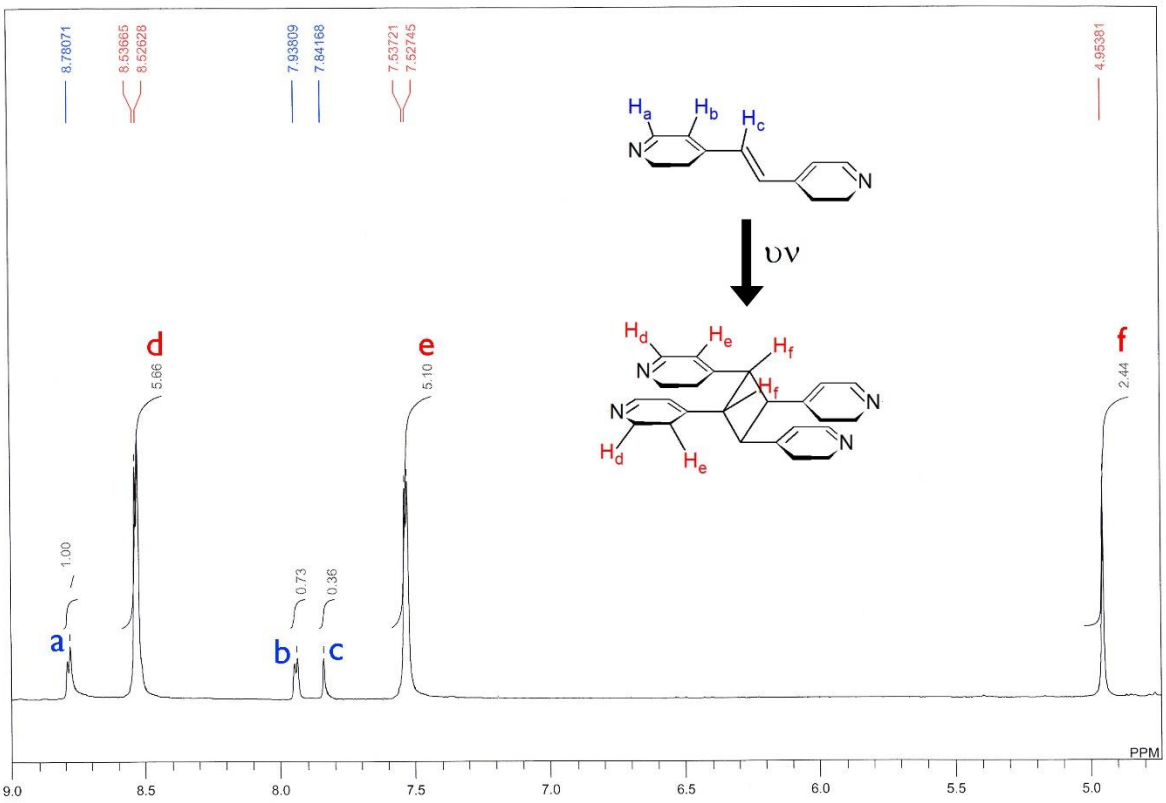

Figure 32: ^{1}H-NMR spectrum of **1** after 30 hours of UV irradiation (DMSO-d_6).

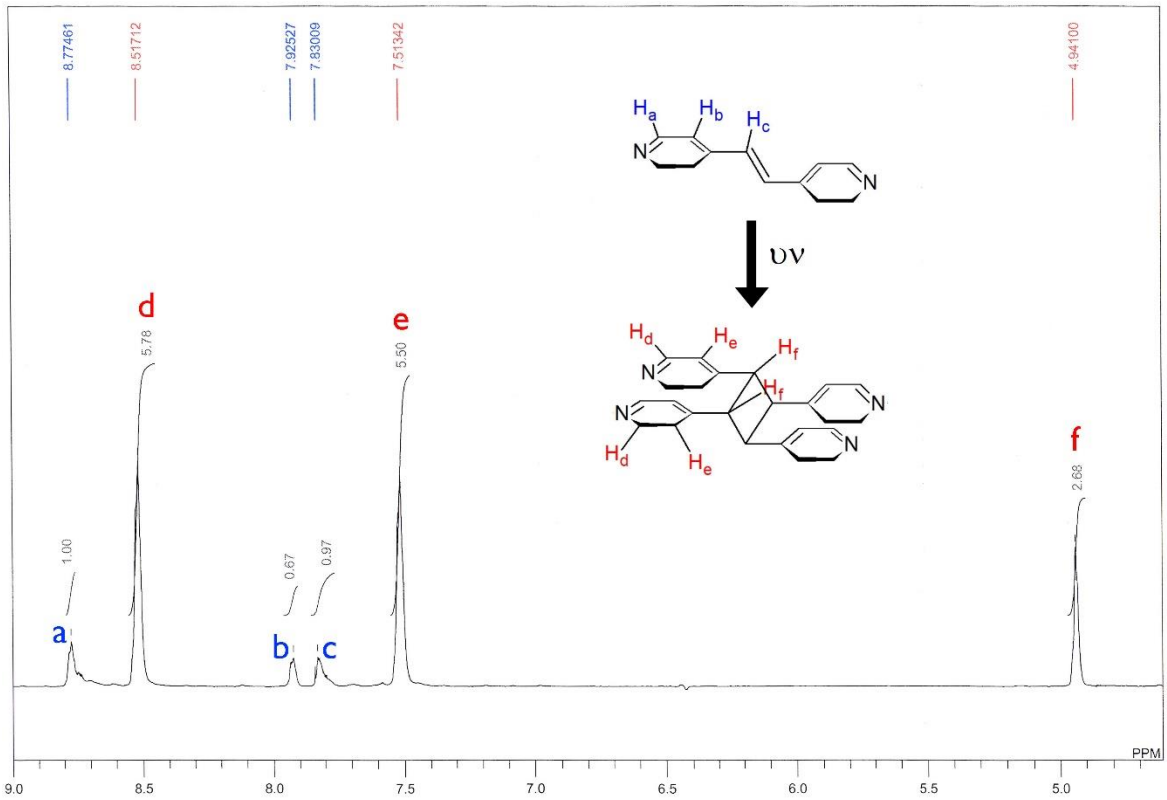

Figure 33: ^{1}H-NMR spectrum of **1** after 50 hours of UV irradiation (maximum conversion) (DMSO-d_6).

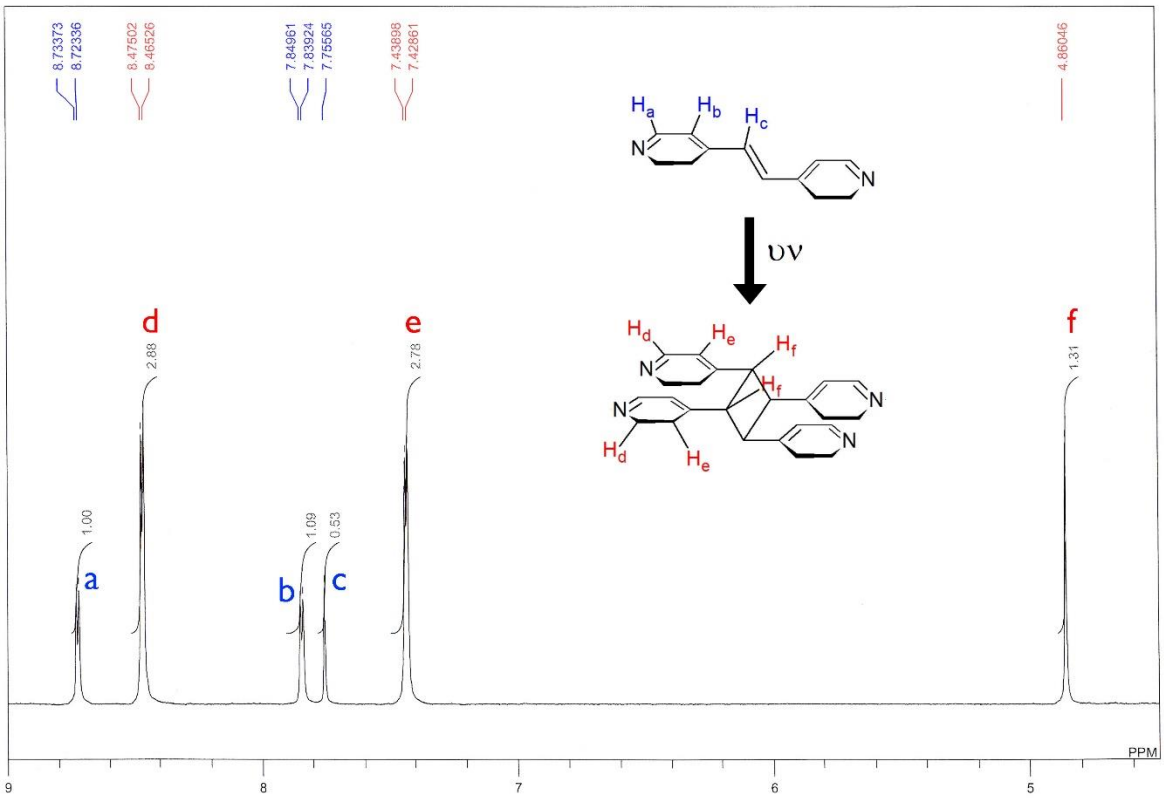

Figure 34: ^{1}H-NMR spectrum of **2** after 5 hours of UV irradiation (DMSO-d_6).

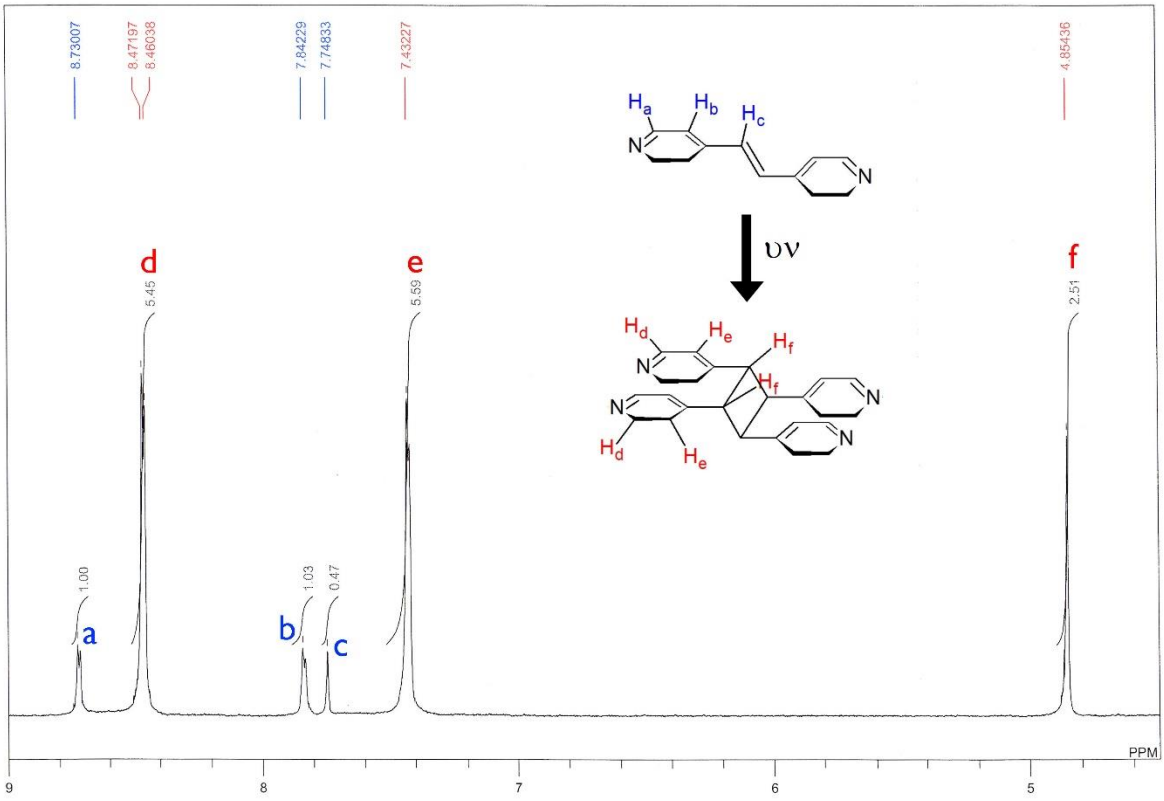

Figure 35: ^{1}H-NMR spectrum of **2** after 10 hours of UV irradiation (DMSO-d_6).

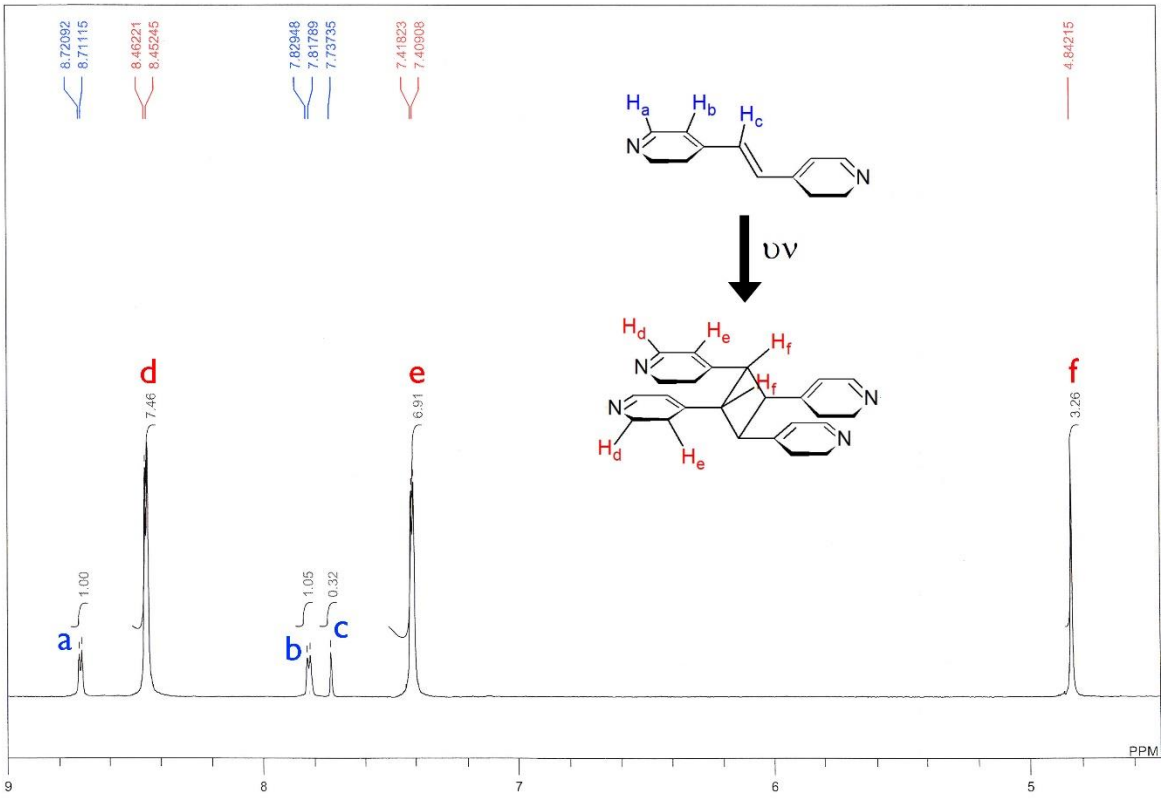

Figure 36: ^{1}H-NMR spectrum of **2** after 15 hours of UV irradiation (DMSO-d_6).

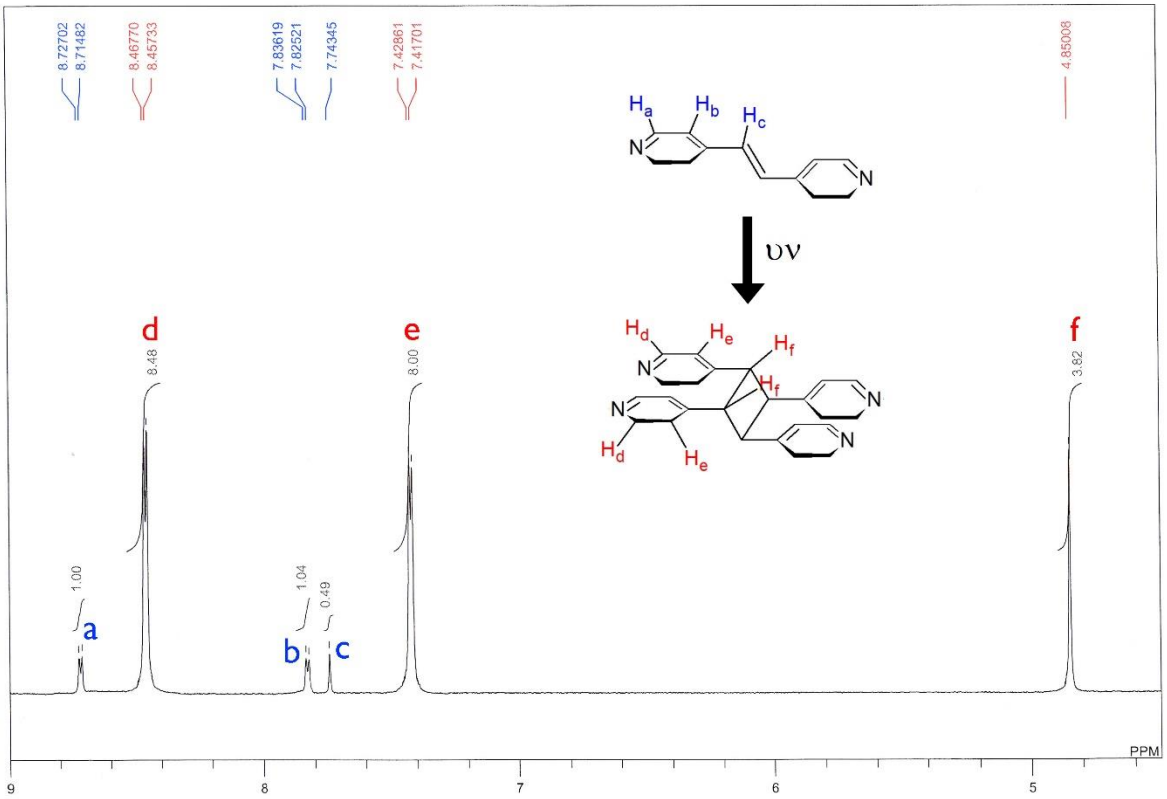

Figure 37: ^{1}H-NMR spectrum of **2** after 30 hours of UV irradiation (maximum conversion) (DMSO-d_6).

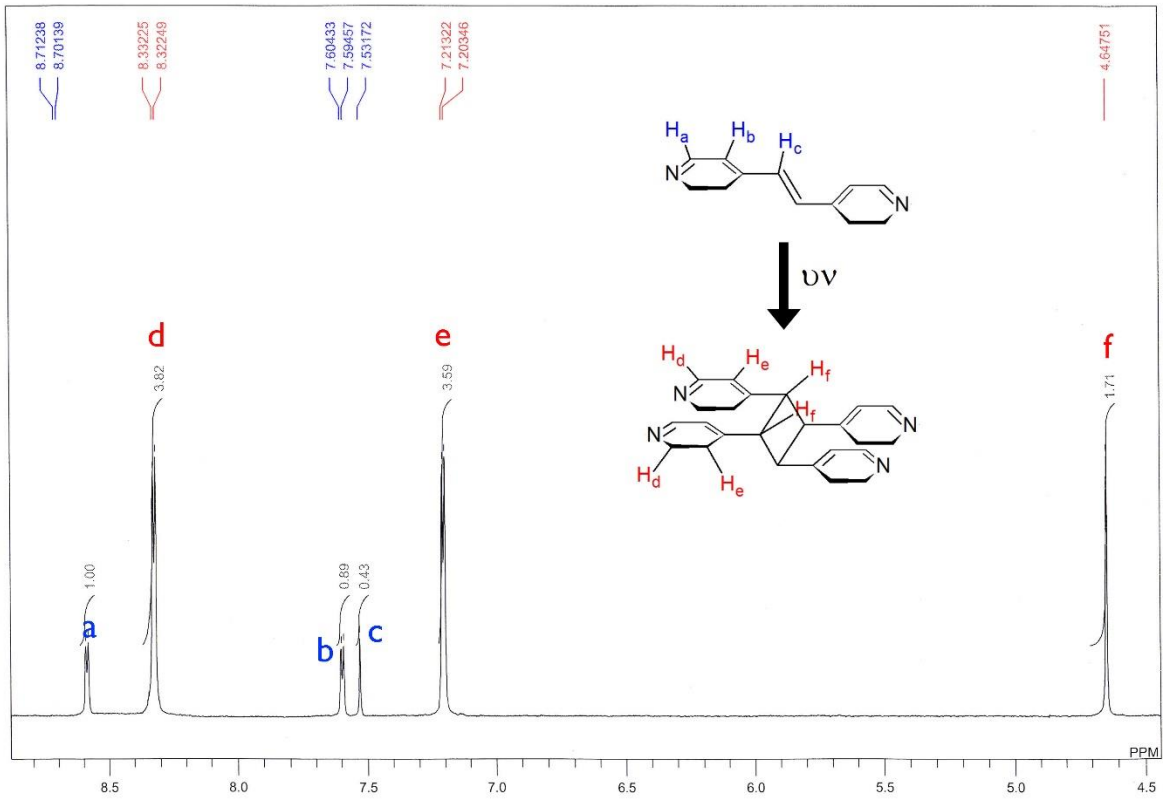

Figure 38: ^{1}H-NMR spectrum of **2** after 50 hours of UV irradiation (DMSO-d_6).

The following table (**Table 1**) summarizes the % conversion of bpe to *rctt*-tpcb in each UV irradiated sample for both compounds **1** and **2**.

Table 1. Time of exposure and calculation of % conversion for **1** and **2** based on ^{1}H-NMR spectra.

Compound Identity	Time of exposure, h	*rctt* isomer, %	Unreacted bpe, %	Bpe peaks total area	*rctt* isomer peaks total area	Total area of both
1	5	68.75	31.25	2.5	5.5	8.0
	10	83.00	17.00	0.4	2.2	2.6
	15	85.50	14.50	1.9	11.2	13.1
	30	87.14	12.86	1.8	12.2	14.0
	50	89.04	10.96	1.7	13.4	15.1
2	5	71.20	28.80	2.7	6.6	9.2
	10	84.23	15.77	2.4	12.6	14.9
	15	88.15	11.85	2.4	17.6	20.0
	30	88.43	11.57	2.5	19.1	21.6
	50	79.91	20.09	2.2	8.6	10.7

The data of **Table 1** were used to gain insight into the photochemical behavior of both compounds. A graph was made by plotting the % conversion against time (**Figure 39** and **40**).

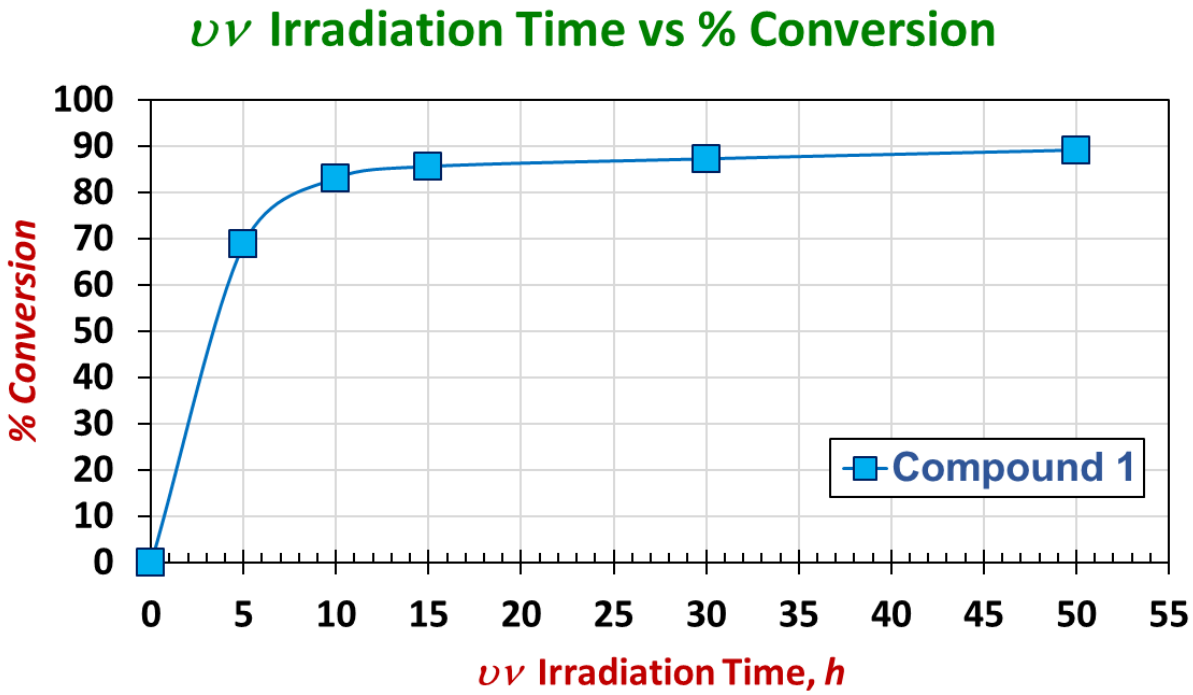

Figure 39: % conversion of bpe to *rctt*-tpcb with respect to time in **1**.

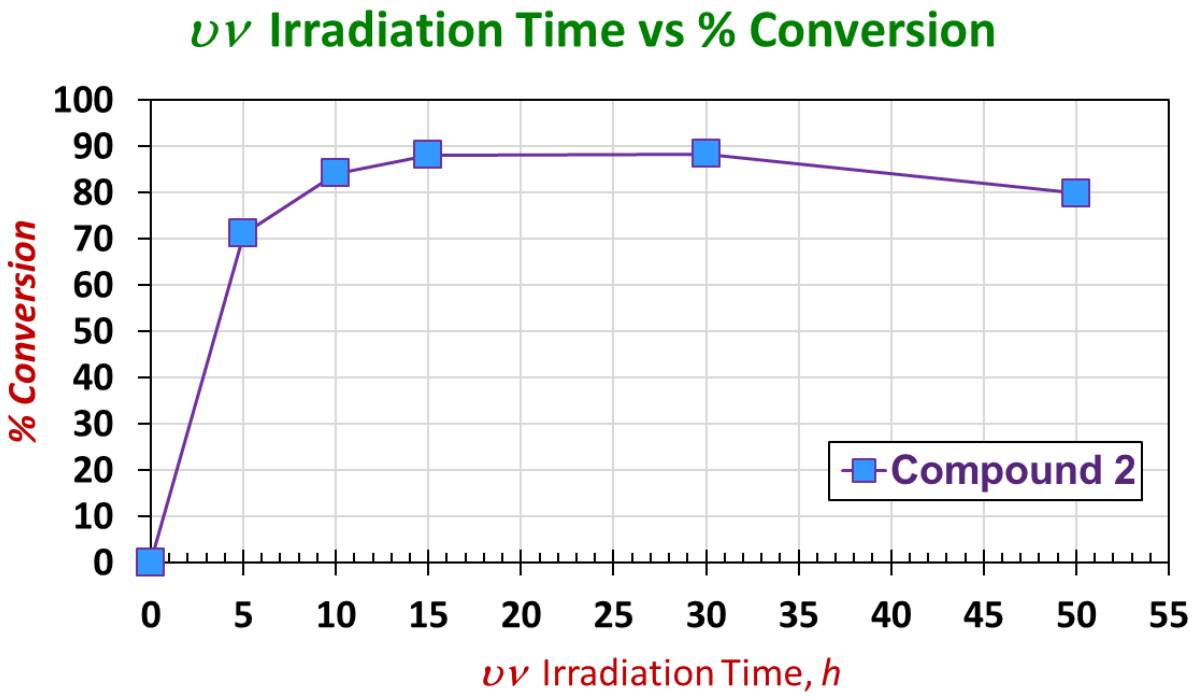

Figure 40: % conversion of bpe to *rctt*-tpcb with respect to time in **2**.

The calculated maximum % conversion for compound **1** was found to be 89% (**Table 1**) which was achieved after 50 hours of UV irradiation in the solid-state (**Figure 33**). However, it can be deduced from **Figure 39** that the maximum % conversion of **1** is not expected to go much higher as the % conversion curve is rising extremely slowly after 10 hours of UV irradiation. The difference in % conversion between 10 hours and 50 hours of UV irradiated samples is only 6% as shown in **Table 1** despite the 5 times increase in UV irradiation time.

On the other hand, 88% (maximum conversion) of bpe in compound **2** have photochemically reacted to produce *rctt*-tpcb isomer within 15 hours of UV irradiation as shown in **Table 1** and **Figure 36**. Although the maximum photochemical conversion of bpe to *rctt*-tpcb for both compounds is relatively high and very close to each other, they have different photochemical behavior. Compound **2** has achieved its maximum conversion, which is 88%, much faster than compound **1**. Fifteen hours of UV irradiation was needed for compound **2** to achieve its maximum conversion, while more than triple the time (50 hours) was required for compound **1** to achieve its maximum conversion, which is 89%. In addition, the % conversion of bpe to *rctt*-tpcb in compound **2** remained constant when UV irradiation time was doubled to 30 hours after its maximum conversion was achieved. After that, the % conversion started to decrease when UV irradiation time was pushed further to 50 hours as shown in **Table 1** and **Figure 40**.

The experiment of UV irradiating compound **2** for 50 hours was repeated several times to make sure that the decline in % conversion was not due to experimental errors in UV irradiation or other parts of the experiment. The decline in % conversion of bpe to *rctt*-tpcb in compound **2** when the sample UV irradiated for 50 hours is an indication that the long period of UV irradiation provides an excess of energy which caused the compound to start reverting back to the reactant (bpe) by disintegration of product (*rctt*-tpcb). This observation lead to the conclusion that compound **2** has a reversible photochemical property, where the photochemical [2+2]

cycloaddition reaction can be reversed in specific conditions. Such materials with reversibility property of the photochemical [2+2] cycloaddition reaction have been reported in the literature.[44] This type of materials have important applications in photo-switching, sensing and optical data storage.[45]

The reported photoreactive MOFs with reversible photochemical [2+2] cycloaddition reaction property have shown such behavior upon thermal treatment.[44] However, the prolong UV irradiation of **2** has triggered the reversible reaction without requiring any thermal treatment. This can be explained as thermal reversion due to heating the material by extended UV irradiation exposure long past the maximum conversion.

The difference in photochemical behavior between **1** and **2** can be directed to the difference in their lattice structures. The photochemical product of **2** is formed faster than **1** yet disintegrated back to bpe in contrast to **1**. These observations indicate that the photochemical product is less stable in **2** than it is in **1**. It can be due to the slight misalignment of bpe ligands within **2** (as it will be discussed in PXRD analysis section) which induces a slight strain on *rctt*-tpcb that allows it to undergo the reversible photochemical reaction. On the other hand, the long time needed for **1** to reach maximum conversion is due to requirement of several steps of large internal molecular motion (as it will be discussed in PXRD analysis section) before it can undergo the photochemical [2+2] cycloaddition reaction. It can be deduced that the photochemical product of **2** is more kinetically favored, while the photochemical product of **1** is thermodynamically favored.

4.1.2 Compound 4

4.1.2.1 Single Crystals Photodimerization

The photoreactivity of **4** was studied through monitoring the photochemical [2+2] cycloaddition reaction with ^{1}H-NMR spectroscopy. The MOF was produced in single crystals form by modified layering method.[41] The following figure **(Figure 41**) shows ^{1}H-NMR spectrum of these crystals before UV irradiation.

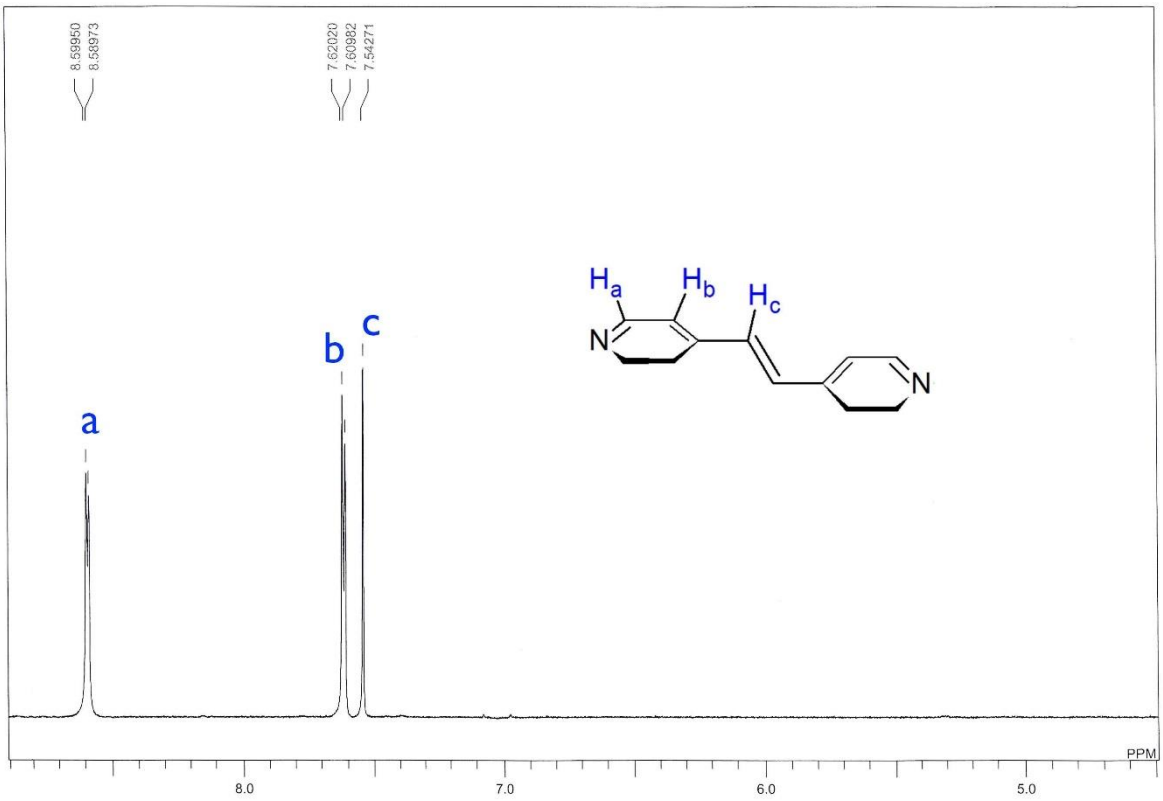

Figure 41: ^{1}H-NMR spectrum of **4** crystals before UV irradiation (DMSO-d_6).

Based on the reported structure (**Figure 18**), The maximum expected % conversion is about 67%. Therefore, the single crystals were UV irradiated for various time intervals; 5, 20 and 50 hours, to confirm the expected photochemical behavior of the MOF. The % conversion was calculated by integrating the relative peaks areas of bpe and *rctt*-tpcb in the obtained ^{1}H-NMR spectra as shown in **Figure 42-44**.

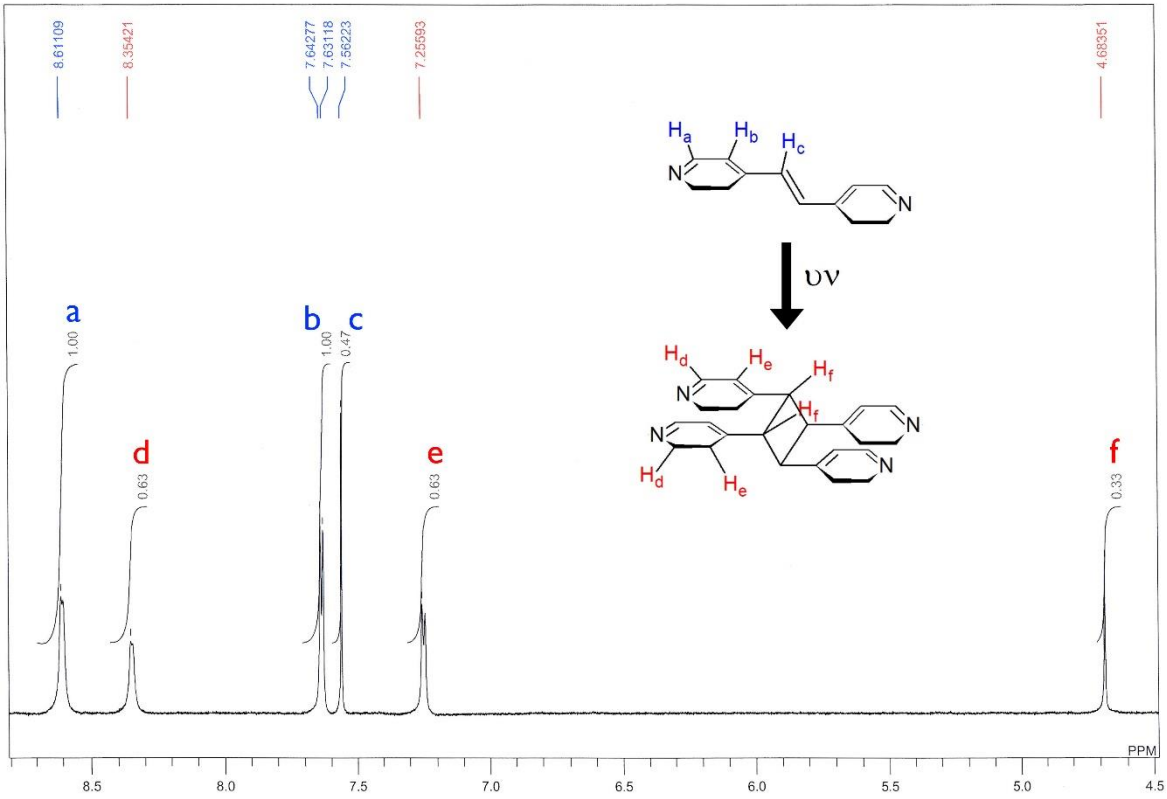

Figure 42: ^{1}H-NMR spectrum of **4** crystals after 5 hours of UV irradiation (DMSO-d_6).

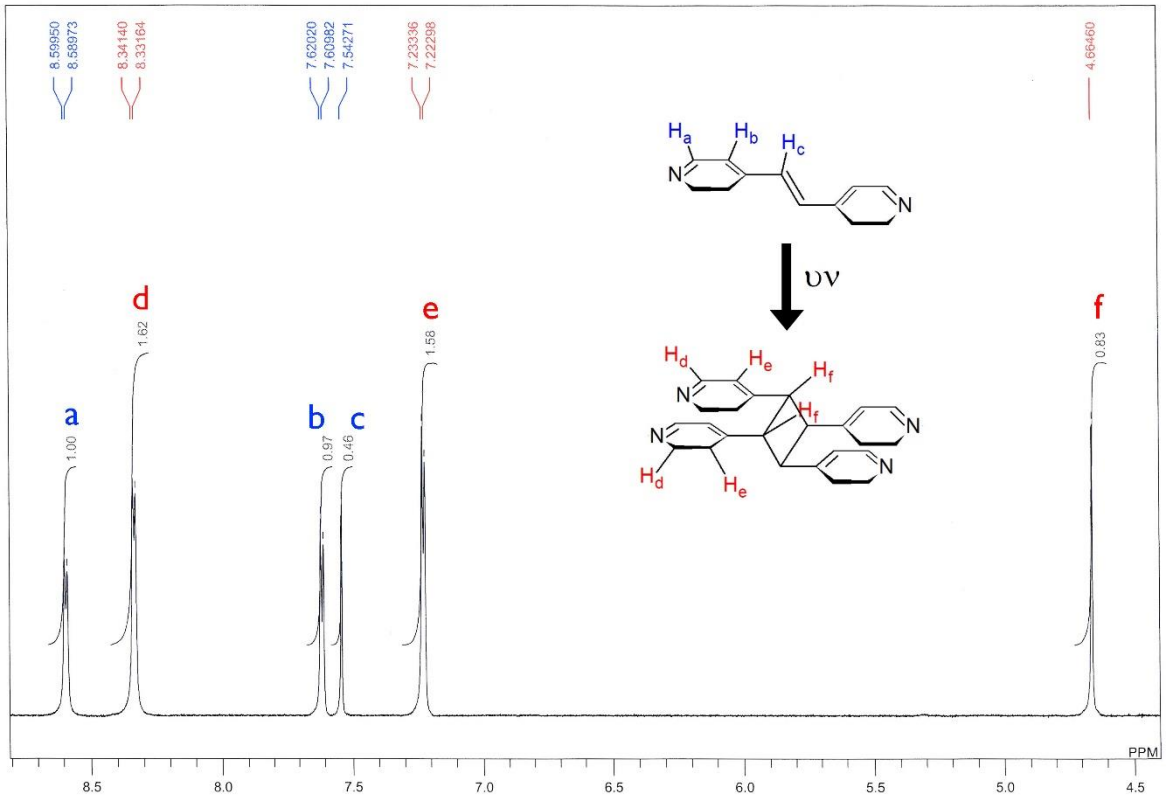

Figure 43: ^{1}H-NMR spectrum of **4** crystals after 20 hours of UV irradiation (DMSO-d_6).

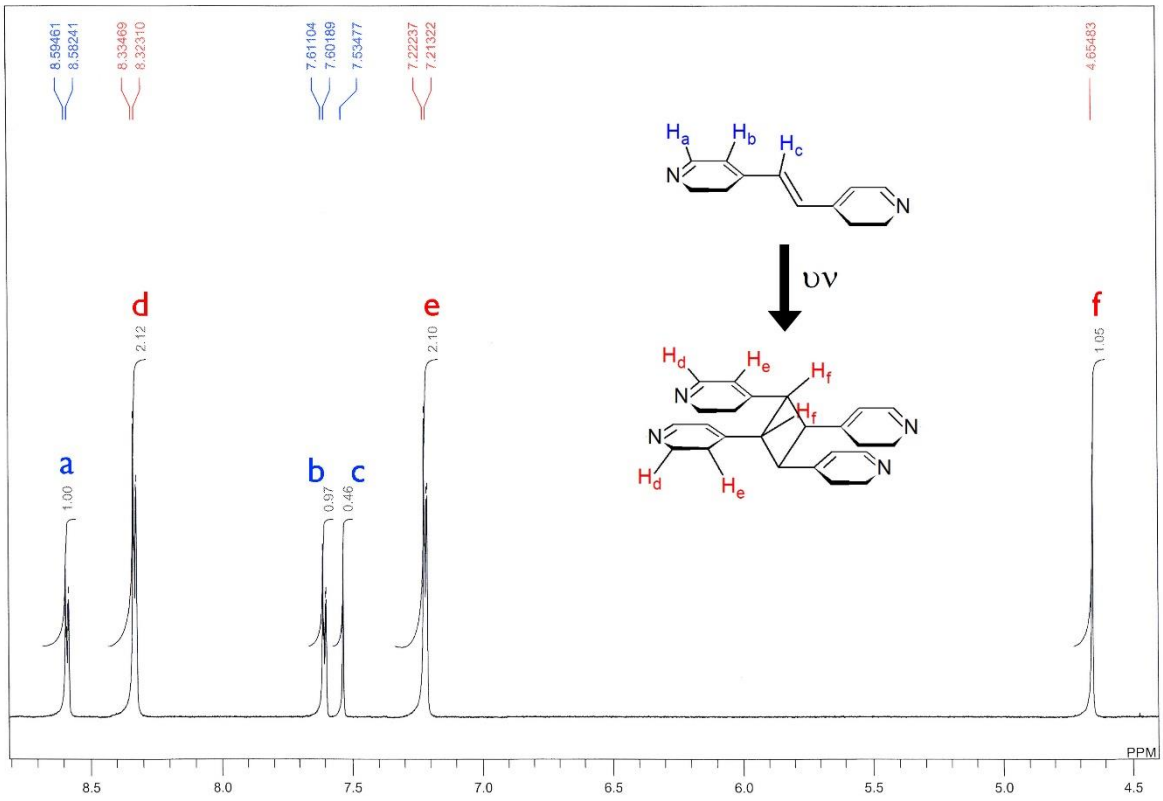

Figure 44: ^{1}H-NMR spectrum of **4** crystals after 50 hours of UV irradiation (DMSO-d_6).

The ^{1}H-NMR spectra (**Figure 42-44**) show a decrease in intensity of a, b and c signals, which belong to photochemically unreacted bpe, and appearance of d, e and f signals, which belong to the product of the photochemical [2+2] cycloaddition reaction; *rctt*-tpcb.

The % conversion of bpe to *rctt*-tpcb within the MOF was calculated for each obtained ^{1}H-NMR spectrum (**Figure 42-44**), and found to be about 40, 62 and 67% for 5, 20 and 50 hours of UV irradiation respectively. The maximum % conversion was found to be 67% as expected after 50 hours of UV irradiation of compound **4** (**Figure 44**). However, the bpe ligands within the MOF are not expected to undergo any further photodimerization by further prolonging UV irradiation time since the % conversion has increased only by 5% when the time of UV irradiation has been extended from 20 to 50 hours, which is more than double the time interval.

4.1.2.2 Grinded Samples Photodimerization

Based on the reported lattice structure (**Figure 18**), the maximum possible % conversion cannot exceed 67%. However, mechanical forces have been utilized to force partially photodimerizing systems to reach 100% conversion.[15] Several studies have shown that mechanical forces, such as grinding, accelerate the pedal-like motion of the system and force it to reach 100% conversion.[42] However, none of these studies have been about ladder-like structures. In order to study such possible effect on compound **4**, the produced crystals of the MOF were manually grinded for 10 minutes to a fine powder and its photoreactivity was explored.

The MOF ground samples were UV irradiated for various time intervals, namely 5, 10, 20, 30 and 50 hours, then ^{1}H-NMR spectra were recorded and % conversion was calculated for each spectrum. The following figures (**Figure 45-49**) show ^{1}H-NMR spectra of UV irradiated ground samples of **4** for 5, 10, 15, 30 and 50 hours, as well as the integrated peaks areas.

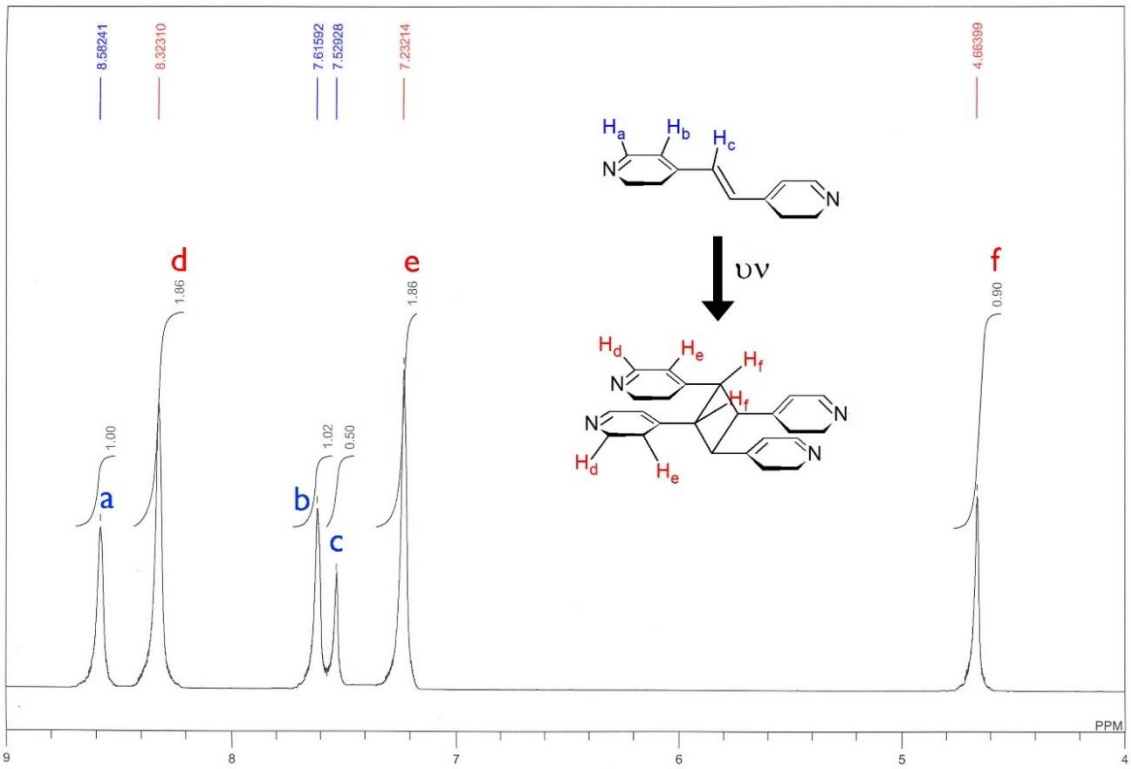

Figure 45: ^{1}H-NMR spectrum of ground crystals (powder sample) of **4** after 5 hours of UV irradiation (DMSO-d_6).

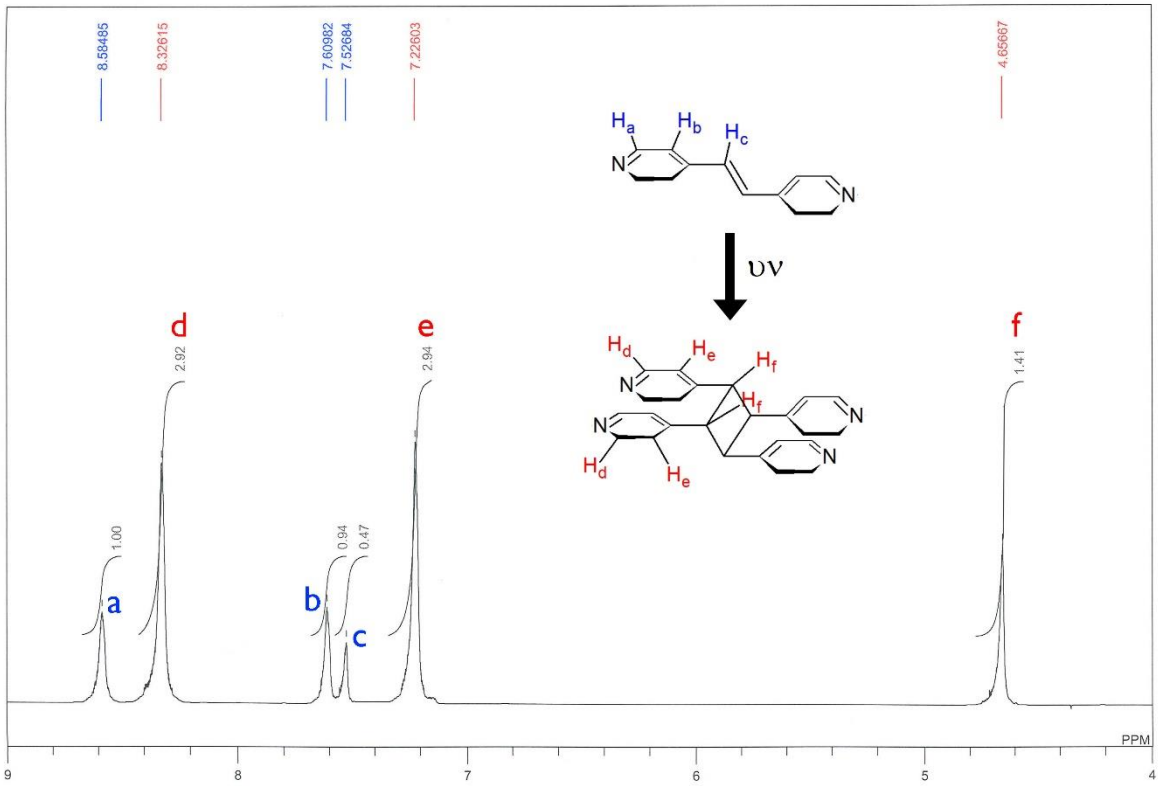

Figure 46: ^{1}H-NMR spectrum of ground crystals (powder sample) of **4** after 10 hours of UV irradiation (DMSO-d_6).

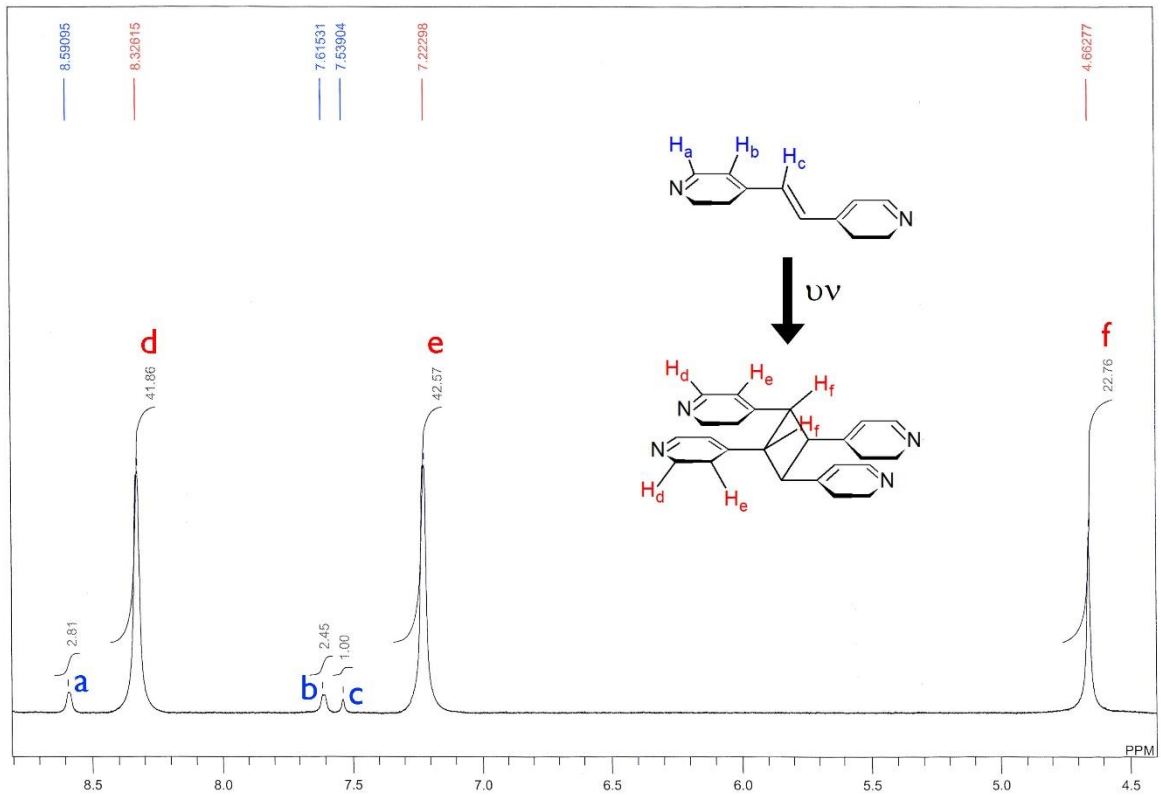

Figure 47: ^{1}H-NMR spectrum of ground crystals (powder sample) of **4** after 20 hours of UV irradiation (DMSO-d_6).

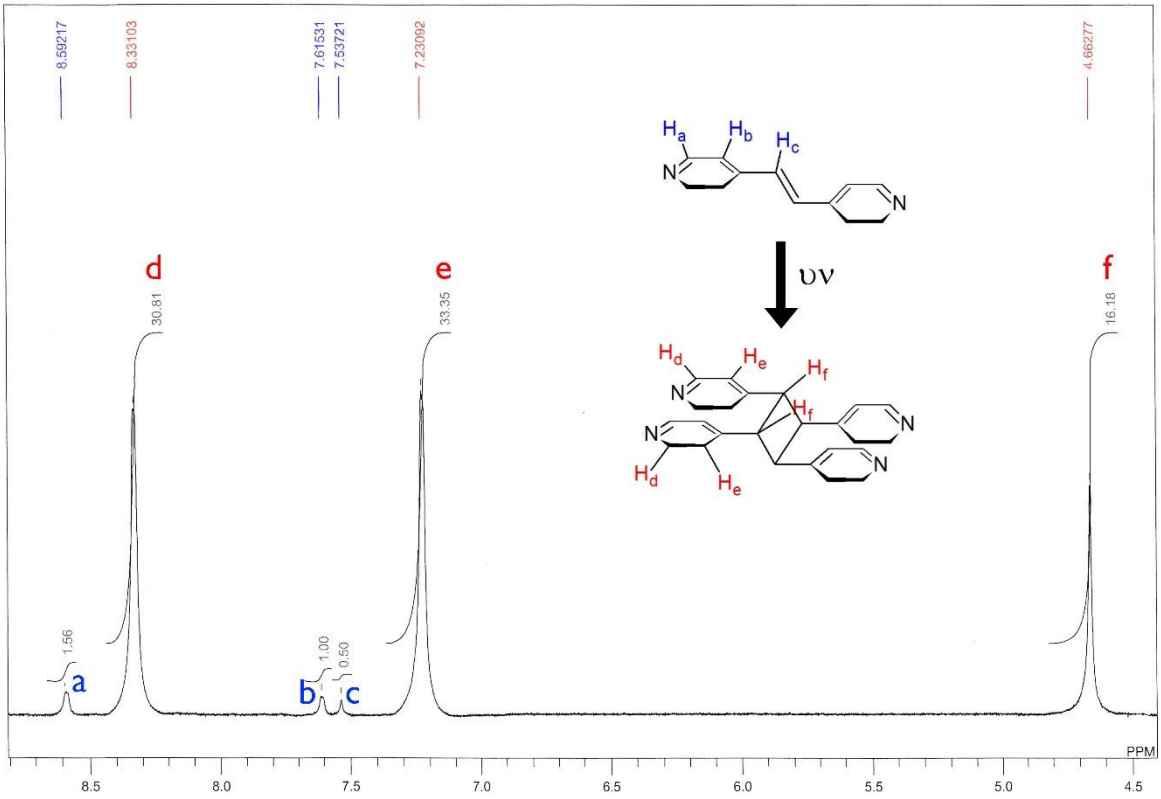

Figure 48: ^{1}H-NMR spectrum of ground crystals (powder sample) of **4** after 30 hours of UV irradiation (DMSO-d_6).

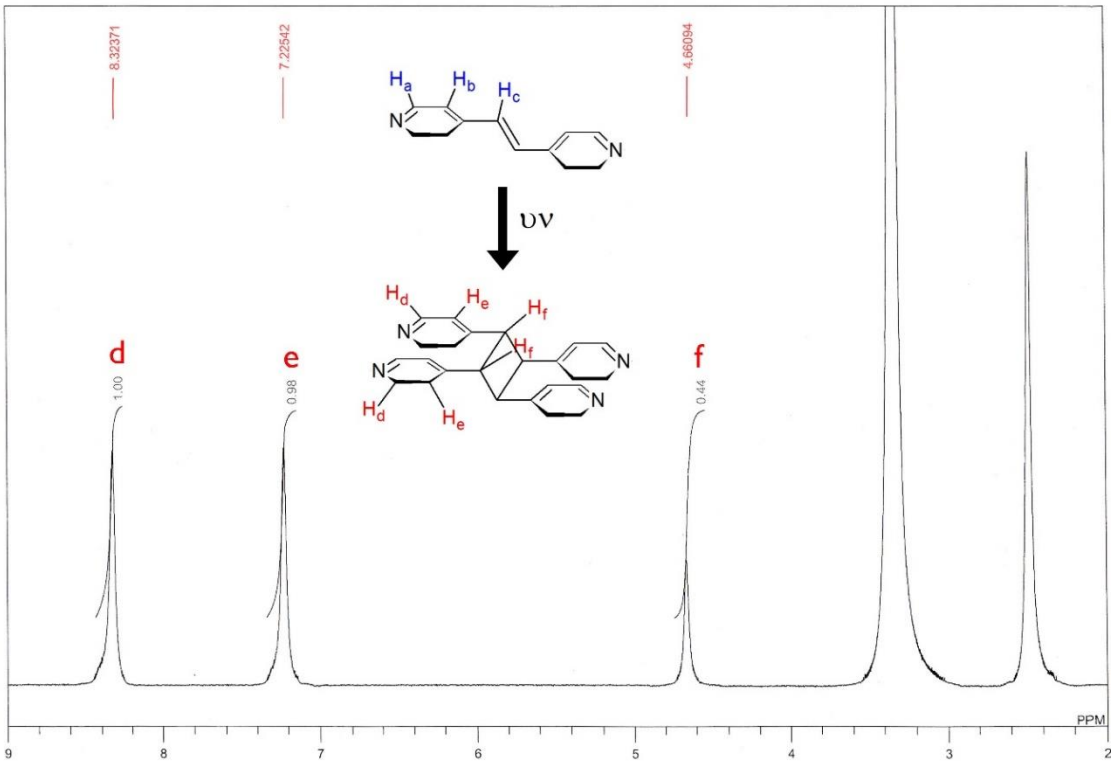

Figure 49: ^{1}H-NMR spectrum of ground crystals (powder sample) of **4** after 50 hours of UV irradiation (DMSO-d_6).

The % conversion of bpe to *rctt*-tpcb within the MOF was calculated for UV irradiated ground samples of **4** by integrating the relative peaks areas for both bpe and *rctt*-tpcb in these obtained ^{1}H-NMR spectra. The following table (**Table 2**) summarizes the % conversion of bpe to *rctt*-tpcb in each UV irradiated sample for both crystals and powder samples.

Table 2. Time of exposure and % conversion for single crystals and grinded samples of **4**.

Nature of the sample	Time of exposure, h	*rctt* isomer, %	Unreacted bpe, %	Bpe peaks total area	*rctt* isomer peaks total area	Total area of both
Single Crystal	0	0	100	6	0	6
	5	39.16	60.84	2.47	1.59	4.06
	20	62.38	37.62	2.43	4.03	6.46
	50	67.29	32.71	2.43	5	7.43
10 min. Grinding	0	0.0	100.0	6	0	6
	5	64.7	35.3	2.52	4.62	7.14
	10	75.1	24.9	2.41	7.27	9.68
	20	94.4	5.5	6.26	107.19	113.45
	30	97.0	3.0	2.5	80.34	82.84
	50	100.0	0.0	0	2.42	2.42

The obtained ^{1}H-NMR spectra (**Figure 45-49**) show that the crystal grinding has boosted the % conversion of the bpe ligands to *rctt*-tpcb within the MOF dramatically. After only 5 hours of UV irradiation the system has achieved almost 67% conversion, which is the maximum conversion of the crystals samples. Furthermore, the maximum obtained % conversion was found to be 100% after 50 hours of UV irradiation. The following figure (**Figure 50**) shows a comparison between the photochemical behavior between the crystals and grinded samples.

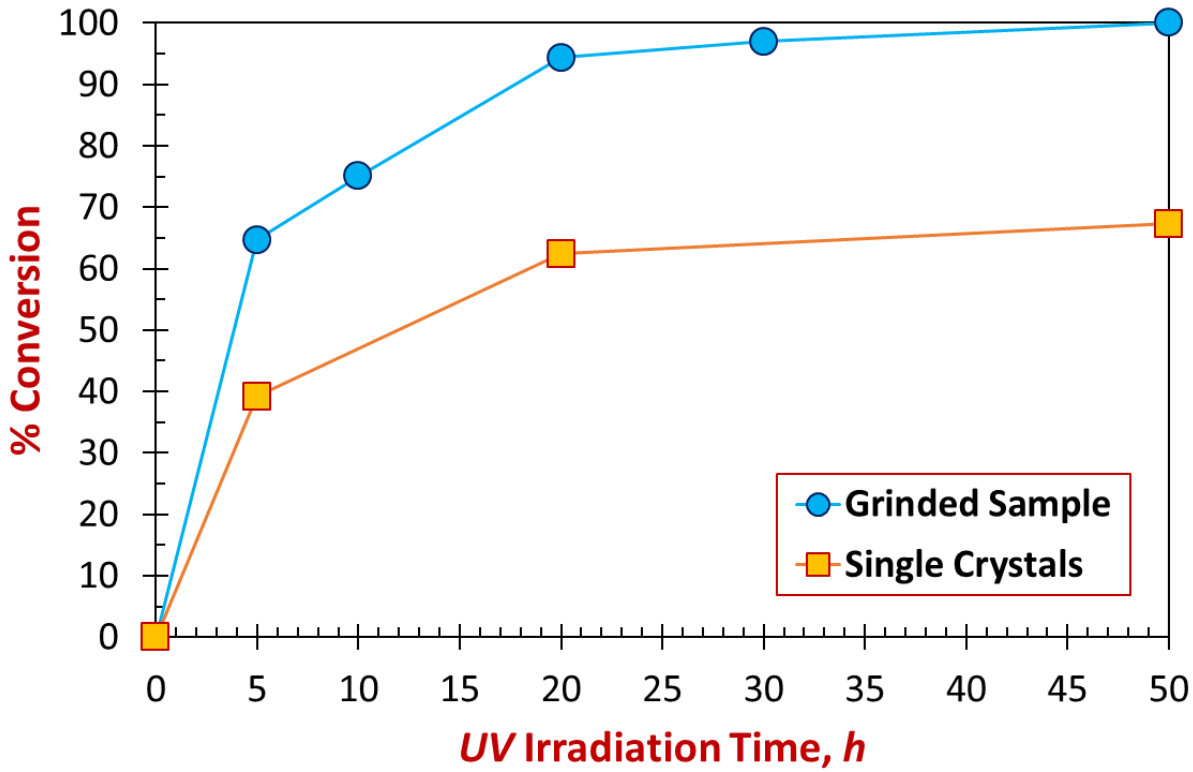

Figure 50: The % conversion of bpe to *rctt*-tpcb with respect to time in **4** for grinded (blue) and crystals (orange) samples.

This observed photochemical behavior is explained by large internal molecular movement within the lattice structure of the MOF due to grinding. The proposed mechanism is shown in the following figure (**Figure 51**).

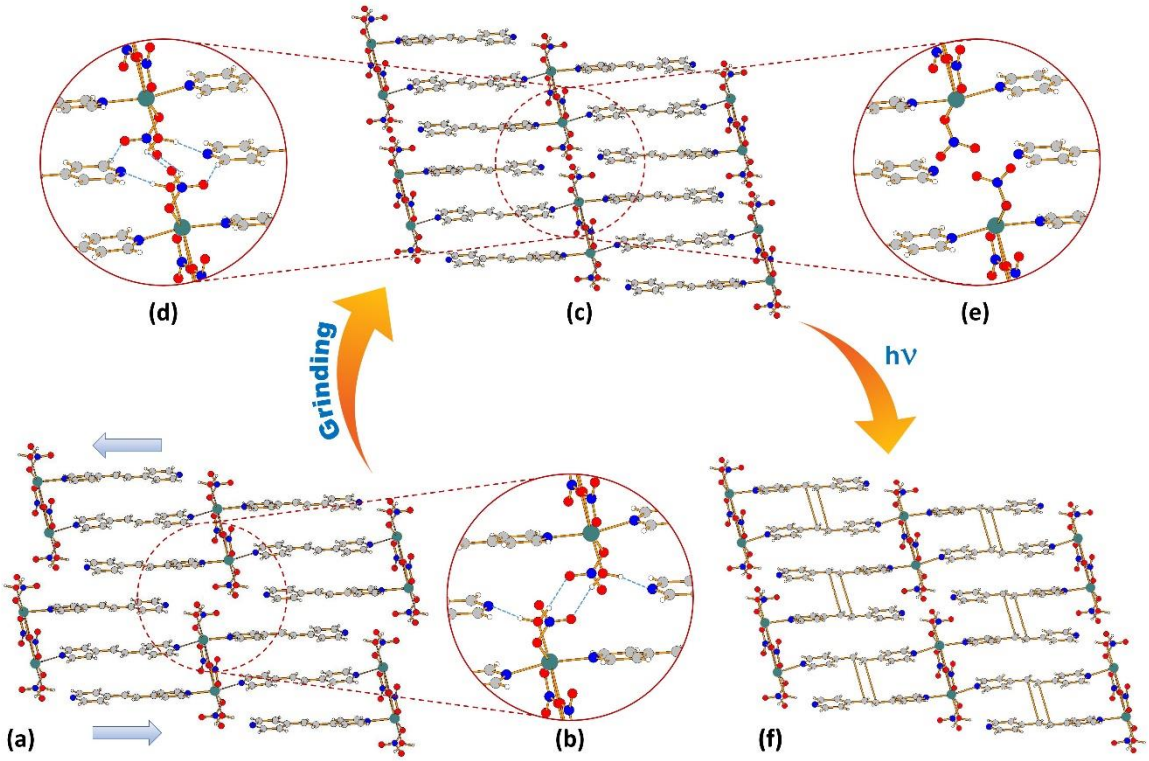

Figure 51: Proposed behavior due to grinding of dinuclear triple-strands-like one-dimensional ladder photoreactive cadmium-based MOF **4**.

The mechanism can be explained based on crystal structural analysis of 4.[41] The crystal structure of **4** contains adjacent slightly misaligned ladder structures held together by hydrogen bonding (**Figure 51b**). Each ladder structure contains sets of three aligned bpe held by strong coordination bonds through four Cd(II) centers, two from each side, and reinforced by π-π interaction between the aligned pyridyl rings, as shown in **Figure 18**.

The distance between each aligned pair of C=C double bonds in each set is 3.77 Å. It is well within the range where cyclobutane can be formed photochemically. Out of the three bpe in each set, only 2 can undergo photodimerization. This explains the 67% conversion for single crystals samples. On the other hand, the distance between a pair of C=C double bonds from adjacent ladder structures is 4.66 Å. Thus, a pair of C=C double bonds from adjacent ladder structures

within **4** cannot undergo photochemical reaction to form cyclobutane according to Schmidt's postulate.

The mechanical forces of grinding likely caused slightly misaligned ladder structures within **4** to move in opposite directions (**Figure 51a**) and align (**Figure 51c**). Thus, a structure with infinite number of bpe ligands parallelly and perfectly aligned will be produced due to these large internal molecular movements (**Figure 51c**). The distance between C=C double bonds from two adjacent ladder structures will be reduced to less than 4.2 Å, which allows photochemical [2+2] cycloaddition reaction to occur between the two adjacent ladder structures. Therefore, complete photodimerization (100% conversion) of all bpe ligands within **4** can be achieved (**Figure 51f**) as reported for similar ladder MOFs in the literature.[23]

The driving force for these large internal molecular movements is the formation of stronger molecular interactions. Initially, each of these ladder structures contain three aligned bpe repeatedly, which inherit π-π stacking that produce four π-π interactions in total for the three aligned bpe; one between each two pyridyl rings (**Figure 51a**). Moreover, each two ladder structures are held together by two hydrogen bonding (**Figure 51b**). The first one between a hydrogen atom from coordinated water molecule and an oxygen atom from coordinated nitrate of a neighbouring ladder structure, while the second one is the other way around. When crystals are grinded, adjacent ladder structures likely slide to opposite directions and alignment of six bpe ligands will occur, as shown in **Figure 51c**. Four new π-π interactions will then occur between the two-adjacent ladder structures, which is 20% increase in π-π interactions. These new interactions are partially the drive responsible for the internal molecular movement and lattice repacking. The newly formed packing has higher stability due to these interactions. However, the other part responsible for the stability of the newly formed repacking is the interactions between the terminal water and

nitrate ligands of each cadmium centre. There are two possible scenarios. The first one in which the hydrogen bonding will change upon the alignment of adjacent ladder structures, where the hydrogens of the terminal water ligands will form hydrogen bonding with two oxygens of the terminal nitrate ligands from adjacent ladder structure (**Figure 51d**). However, this possible scenario may require the rotation of the coordination bond of terminal water and change of its direction toward the metal centre of adjacent ladder. The other possible scenario is the loss of water molecule from the coordination sphere as shown in **Figure 51e**. Although it has been reported that loss of water has no effect on photoreactivity for other MOF structures,[26] that conclusion cannot be extended to other MOF structures due to the unique nature of each MOF structure. Thus, both scenarios are possible in our case, and can be confirmed by TGA since both coordinated and free water molecules in lattice structure have characteristic weight-lost temperature.

4.2 Structural Analysis

4.2.1 NMR Spectroscopy

The photochemical [2+2] cycloaddition reaction in the solid-state can be used as a tool to obtain structural information of the compounds **1-3**. It is an evidence that aligned C=C olefinic double bonds are actually present within the structures of these compounds. Furthermore, the % conversion of **1** and **2** indicates that these compounds might have infinite alignment of bpe ligands since they are matching the theoretical % conversion reported in the literature.[17]

4.2.2 Powder X-Ray Diffraction (PXRD)

The powder X-ray diffraction (PXRD) is an important technique for phase identification and structural investigation of crystalline materials.[46–49] The collected patterns were used for structural investigation of compounds (**1-3**) and structural confirmation of compound **4**. The following figures (**Figure 52** and **53**) show the obtained PXRD patterns of compounds (**1-3**).

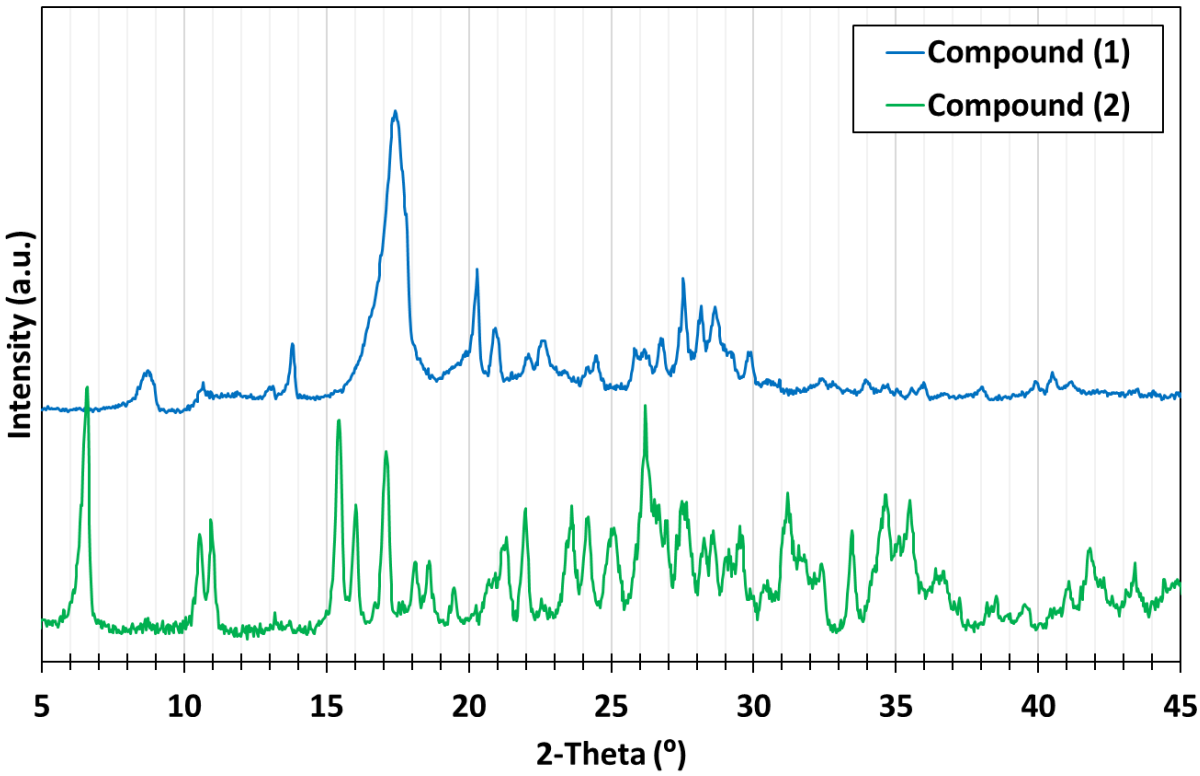

Figure 52: PXRD patterns of compounds **1** and **2**.

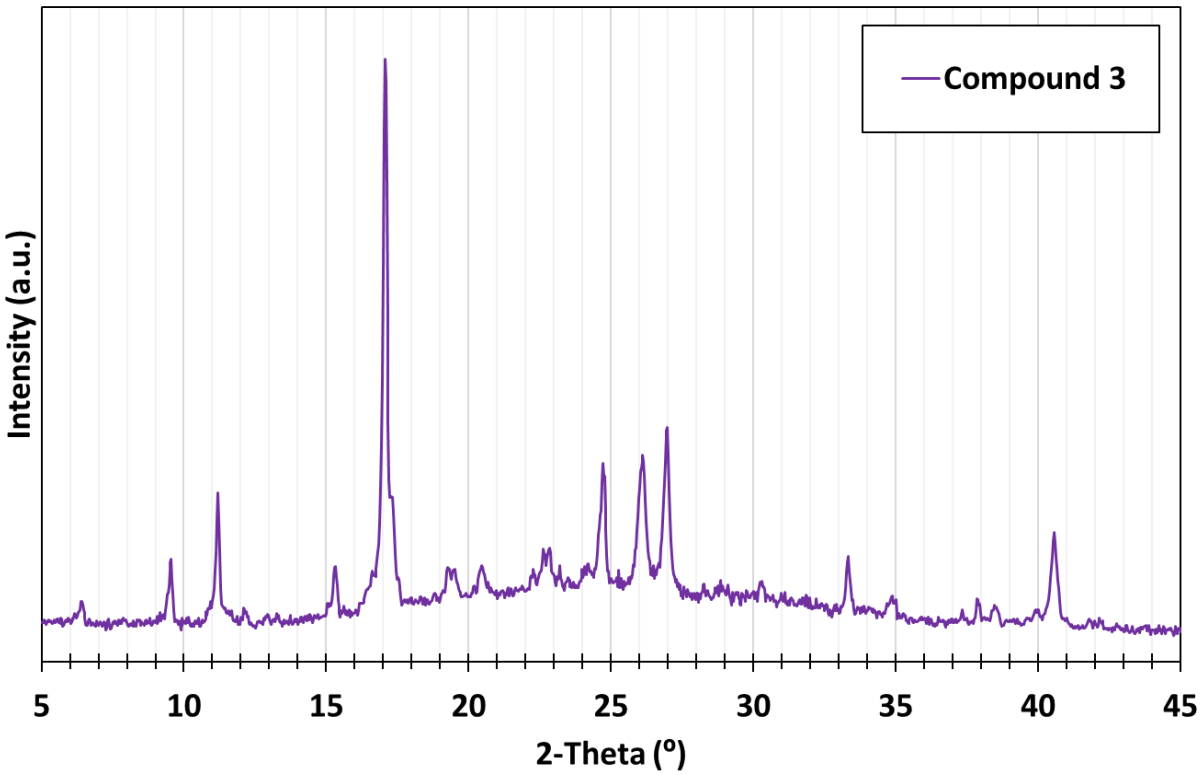

Figure 53: PXRD pattern of compound **3**.

Although the same stochiometric ratios of the metal ions and ligands were used during the synthesis process of compounds **1** and **2**, it is not expected for them to have the same structure due to the different coordination nature of Zn(II) and Pb(II). **Figure 52** shows that the collected patterns for each one of them is not matching the other, which verifies they have different structures.

Other structural information can also be deduced from collected PXRD patterns. The characteristic peak close to 5º (2θ) commonly appears for porous type materials. Furthermore, the two peaks around 10º (2θ) usually show for extended structures, such as (MOFs). The presence of these three peaks in **2** and **3** PXRD patterns (**Figure 52** and **53**) may indicate that these compounds are extended structures (MOFs) as well as porous materials. However, the dimensionality cannot be deduced from these PXRD patterns. The PXRD pattern for compound

1 shows only the presence of 10º (2θ) peaks. This observation leads to the conclusion that compound **1** may not porous but may have an extended structure.

Nevertheless, it was expected initially that compounds **1** or **2** might be isostructural to reported Mn(II)-based broken ladder-like 2D sheet MOF; $[Mn_2(\mu\text{-ox})_2(\mu\text{-bpe})(bpe)_2]_n$, shown in **Figure 17**.[35] However, the obtained PXRD patterns of compounds **1** and **2** (**Figure 52**) show that they are not isostructural to the former expected MOF. Furthermore, the presence of 5º (2θ) peak in the obtained PXRD pattern of **2** indicates that the compound is porous, while the reported Mn(II) MOF in **Figure 17** is not. Therefore, out of the two compounds (**1** and **2**) compound **1** is the only one with the possibility to be analogous to the expected Mn(II) MOF. However, it was found that the obtained PXRD pattern of compound **1** is not matching the calculated powder pattern of the expected broken ladder-like 2D sheet MOF in **Figure 17**.

The three obtained PXRD patterns of the compounds (**1-3**) have been compared with reported MOFs in the literature that contain the same ligands and found to be likely corelated to three different known MOF by comparison with their calculated powder patterns (**Figure 54-56**).[35,36]

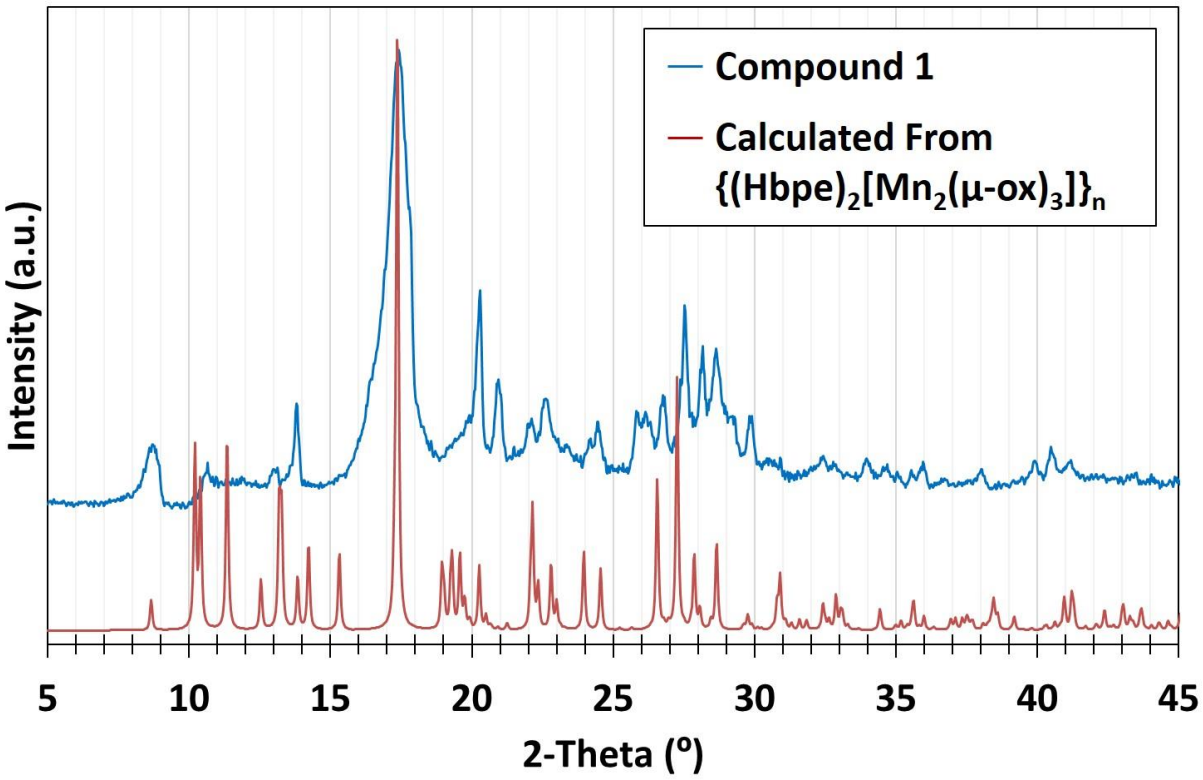

Figure 54: PXRD pattern of compound **1** (experimental) and $\{(Hbpe)_2[Mn_2(\mu\text{-}ox)_3]\}_n$ (calculated).[35]

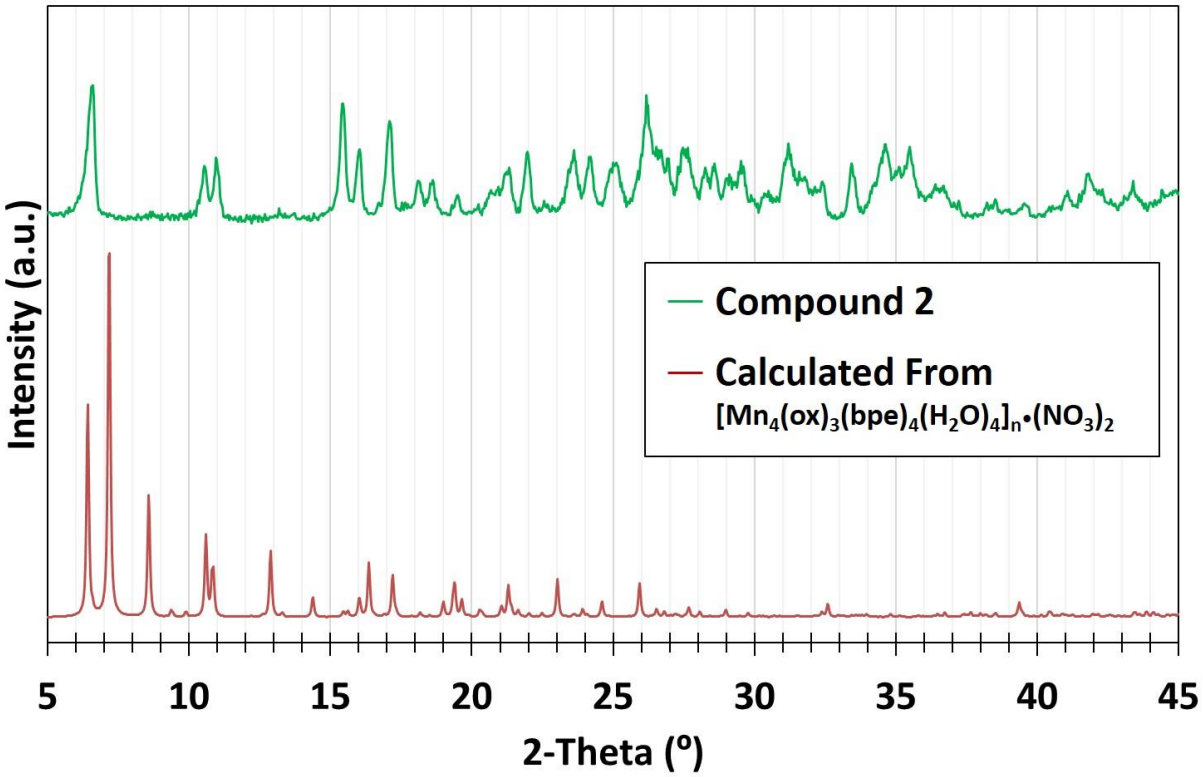

Figure 55: PXRD pattern of compound **2** (experimental) and $[Mn_4(ox)_3(bpe)_4(H_2O)_4]_n$ (calculated).[35]

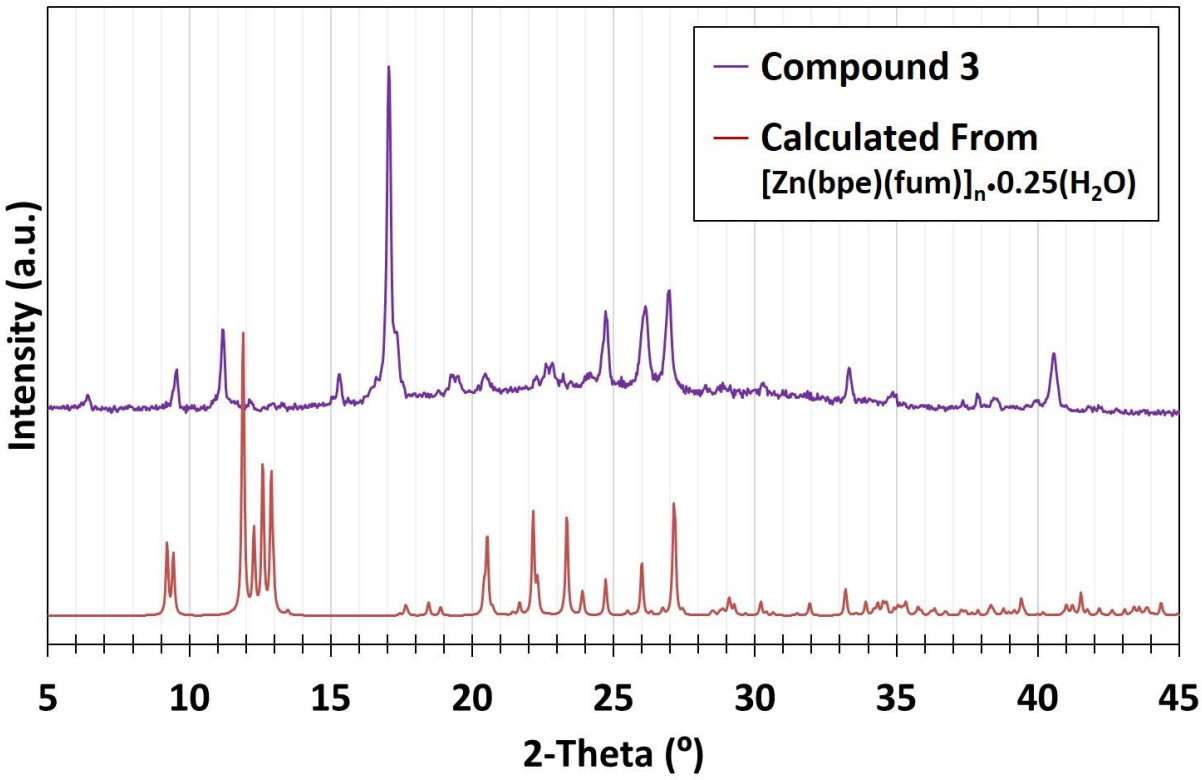

Figure 56: PXRD pattern of compound **3** (experimental) and $[Zn(bpe)(fum)]_n$ (calculated).[36]

The comparable PXRD pattern indicates that the lattice structure may be corelated. However, the difference in peaks intensity between experimental PXRD patterns and calculated one is due to the presence of different metal ion in synthesized compounds from calculated one. Therefore, compounds **1-3** might have similar structures these MOFs (**Figure 54-56**). Although many peaks are matching between synthesized compounds and calculated ones, the dissimilarities can be due to the difference in the orientation of the crystals within the powder sample.

4.2.2.1 Compound 1

The PXRD pattern of compound **1** has been found to be comparable to the calculated powder pattern of reported MOF, $\{(Hbpe)_2[Mn_2(\mu\text{-}ox)_3]\}_n$, as shown in **Figure 54**. The lattice structure of this MOF consists of alternating layers of free cationic bpe molecules and $[Mn_2(\mu\text{-}ox)_3]_n^{2-}$ 2D sheets (**Figure 57**).[35]

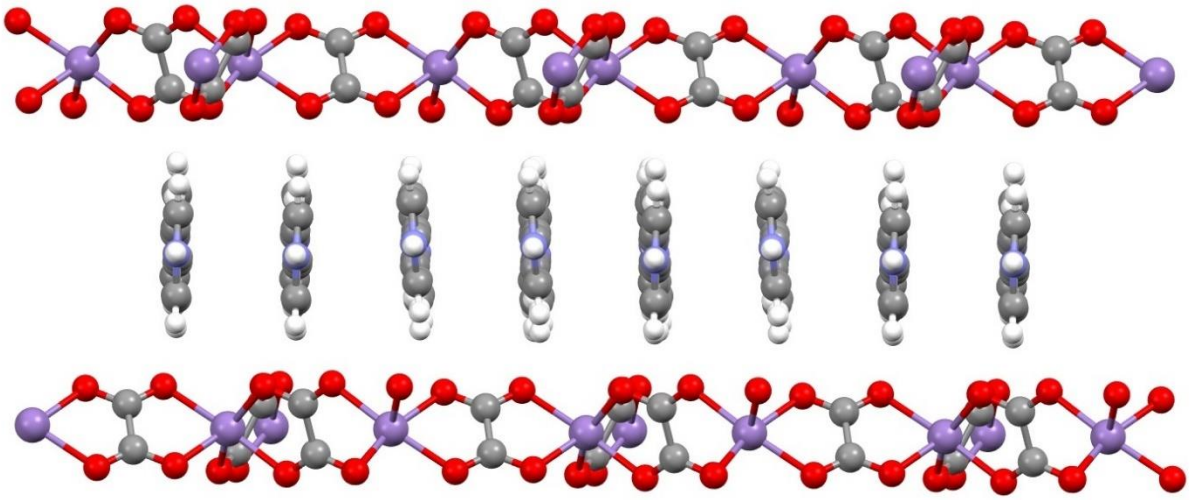

Figure 57: Free cationic bpe molecules held between two layers of $[Mn_2(\mu\text{-}ox)_3]_n^{2-}$.[35]

The $[Mn_2(\mu\text{-}ox)_3]_n^{2-}$ 2D sheets have honeycomb topology (**Figure 58**), while the free cationic bpe molecules are held together by hydrogen bonding and π-π interactions (**Figure 59**).

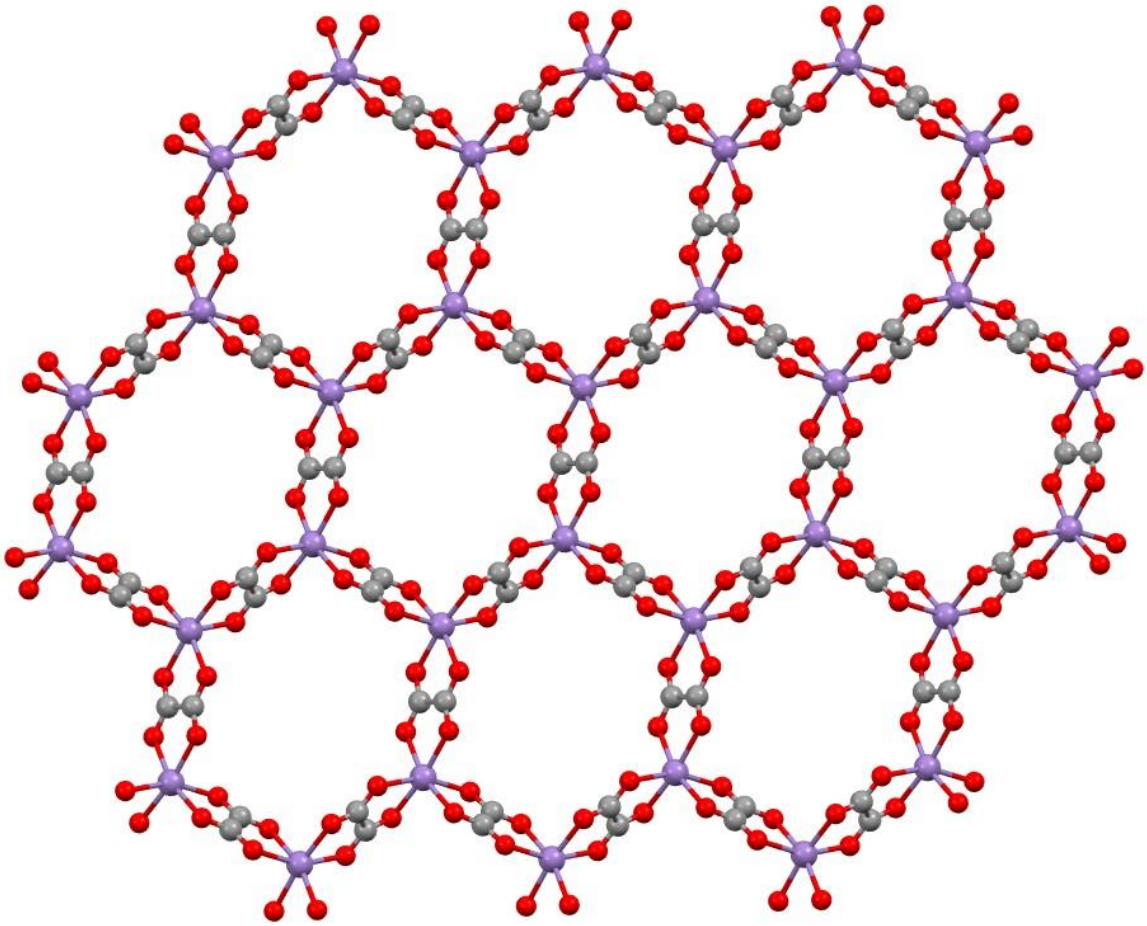

Figure 58: Lattice structure of $[Mn_2(\mu\text{-}ox)_3]_n^{2-}$ layers.[35]

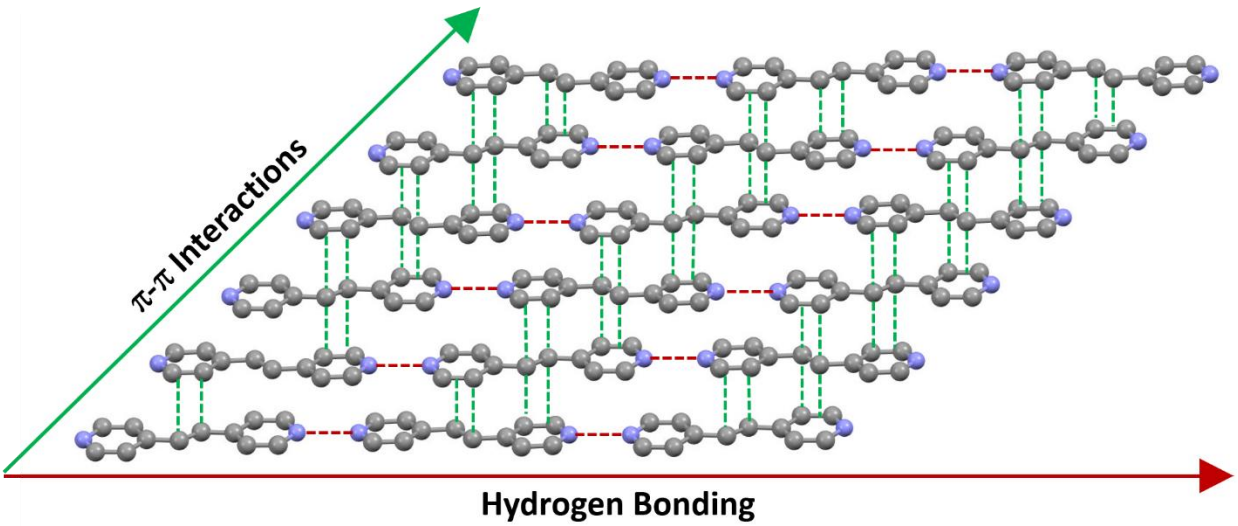

Figure 59: Free bpe molecules are held together by hydrogen bonding and π-π interactions.[35]

Although we are expecting **1** to have the similar lattice structure based on the comparable PXRD pattern (**Figure 54**), but these bpe molecules are not consistent with the Schmidt topochemical criteria for photochemical [2+2] cycloaddition reaction. They are not perfectly aligned and the distance between each pair of olefinic C=C double bonds is 4.769 Å, which is far away for the photochemical reaction to occur. In addition, the olefinic C=C double bonds are not aligned in parallel but criss-cross fashion.

Nevertheless, the photochemical study of compound **1** shows that it is photochemically active and can undergo photochemical [2+2] cycloaddition reaction. This leads to the conclusion that these bpe can either undergo large internal molecular motion due to UV irradiation to meet the right topochemical conditions for the photochemical reaction (**Figure 60**), or the actual alignment in **1** is not equal to the alignment of the Mn-MOF.

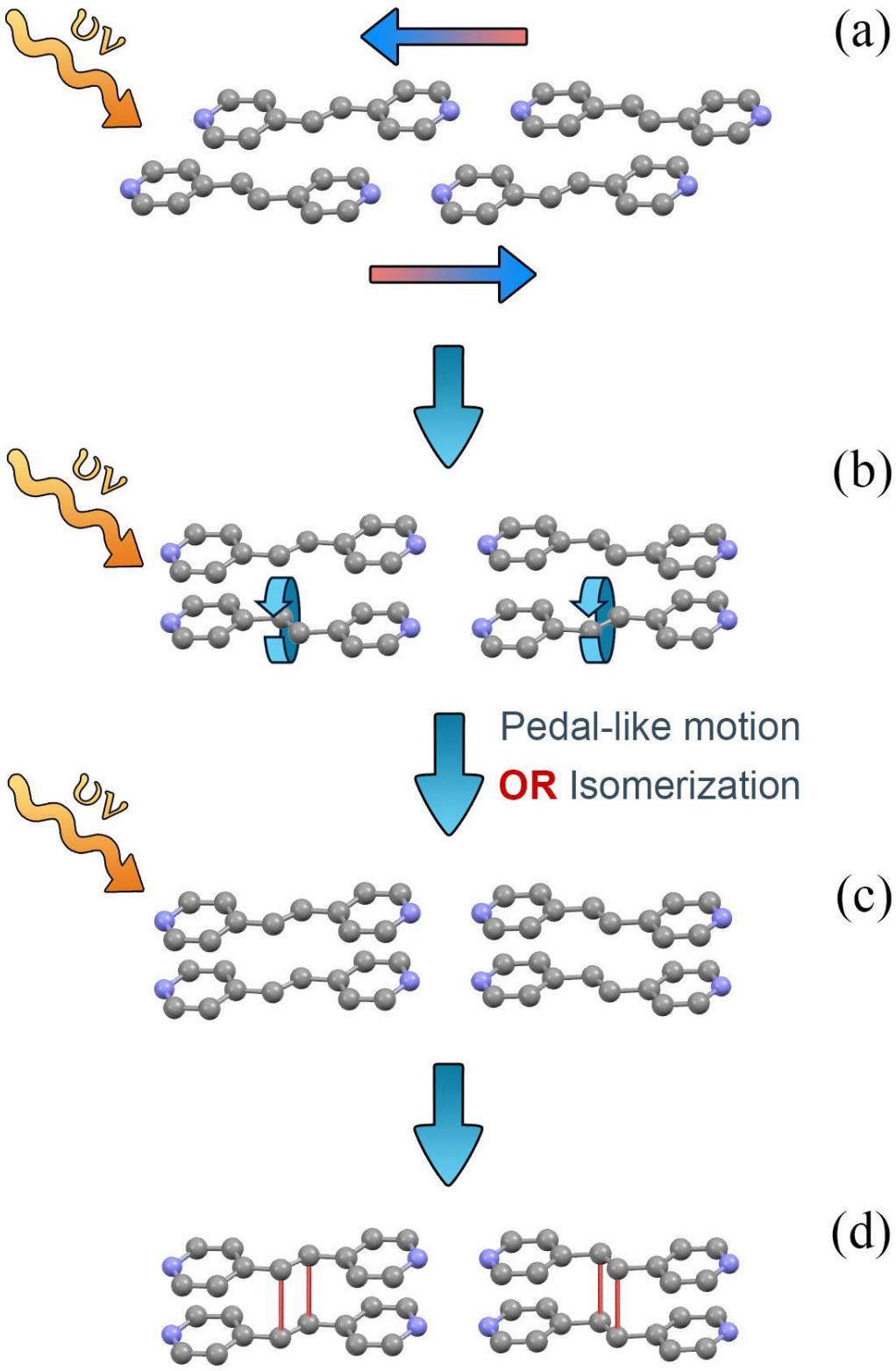

Figure 60: Free bpe molecules undergo large internal molecular motion to meet the right conditions for the photochemical [2+2] cycloaddition reaction in **1**.

Figure 60 shows a proposed mechanism for bpe molecules in compound **1** to undergo photochemical [2+2] cycloaddition reaction if bpe alignment assumed to be like that in Mn-MOF. Because these bpe molecules are free, they can move inside the lattice structure if enough energy is provided and void space is available. The UV irradiation provides the required energy for such behavior. Large internal molecular motion initiated by UV irradiation has been reported in the literature for variety of MOF structures (**Figure 15**).[23]

This proposed mechanism consists of several steps. In the first step, bpe molecules slides in opposite directions along the x-axis and aligns their pyridyl rings perfectly (**Figure 60a**). This step occurs due to increase in π-π interactions where two pyridyl rings and olefinic C=C double bonds contribute to reach thermodynamically more stable structure. In the second step, bpe molecules undergo *trans-trans* isomerization or pedal-like motion to form parallel alignment of the olefinic C=C double bonds (**Figure 60b**). The driving force of this step is initiation of photochemical process that causes the rotation of HOMO and LUMO orbitals of the two alkenes olefinic C=C double bonds to achieve preferred symmetry through suprafacial orientation. In the last step of the mechanism, the photochemical [2+2] cycloaddition reaction occurs and the formation of *rctt*-tpcb product is achieved (**Figure 60c** and **60d**).

4.2.2.2 Compound 2

The PXRD pattern of compound **2** has been found to comparable to the calculated powder pattern of reported MOF, $[Mn_4(ox)_3(bpe)_4(H_2O)_4]_n \cdot (NO_3)_2$, as shown in **Figure 55**. The compound is a three-dimensional framework with 1D pores. The lattice structure of this MOF consists of 2D sheets connected by bpe ligands to construct cationic 3D network; $[Mn_4(ox)_3(bpe)_4(H_2O)_4]_n^{2+}$. The repeating units of the MOF can be seen in **Figure 61**.[35]

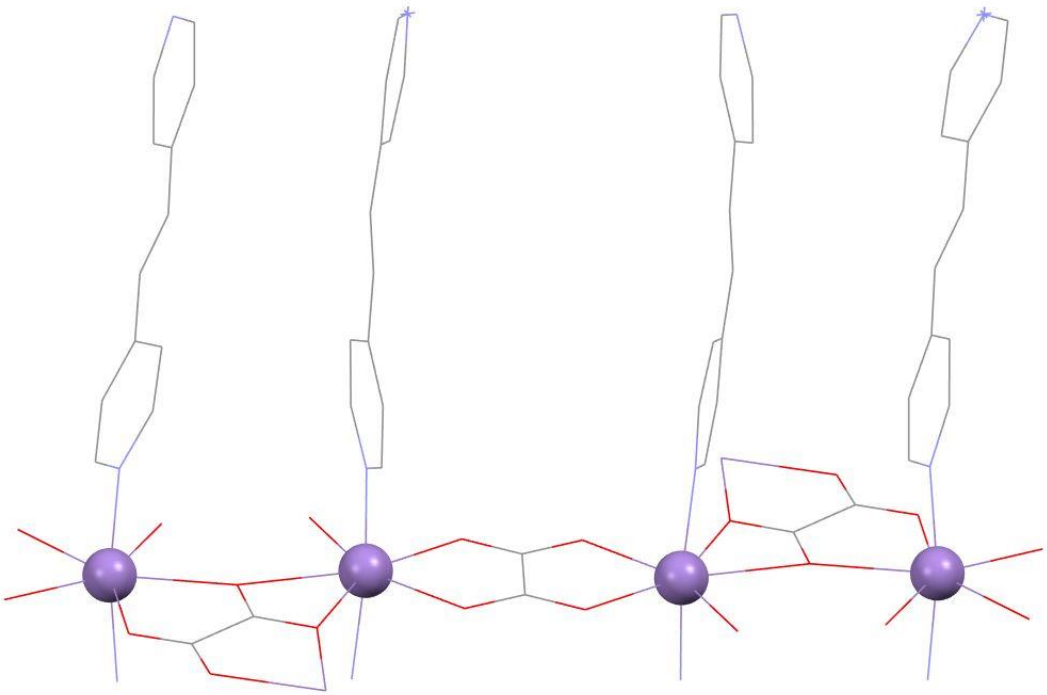

Figure 61: The repeating unit of $[Mn_4(ox)_3(bpe)_4(H_2O)_4]_n.(NO_3)_2$.[35]

Each repeating unit consists of four Mn(II) metal centers connected to each other through three oxalate ligands (**Figure 61**). The Mn(II) metal centers are hepta-coordinated in pentagonal bipyramidal geometry, with two bidentate oxalate ligands and one water molecule in equatorial orientations and two bpe ligands in axial positions (**Figure 61**). The repeating unit also has four bpe ligands, coordinated to axial positions in the four Mn(II) metal centers (**Figure 61**). The Mn(II) metal centers are connected through oxalate ligands to form 2D sheets; $[Mn_4(ox)_3(H_2O)_4]_n^{2+}$, as shown in **Figure 62**.[35]

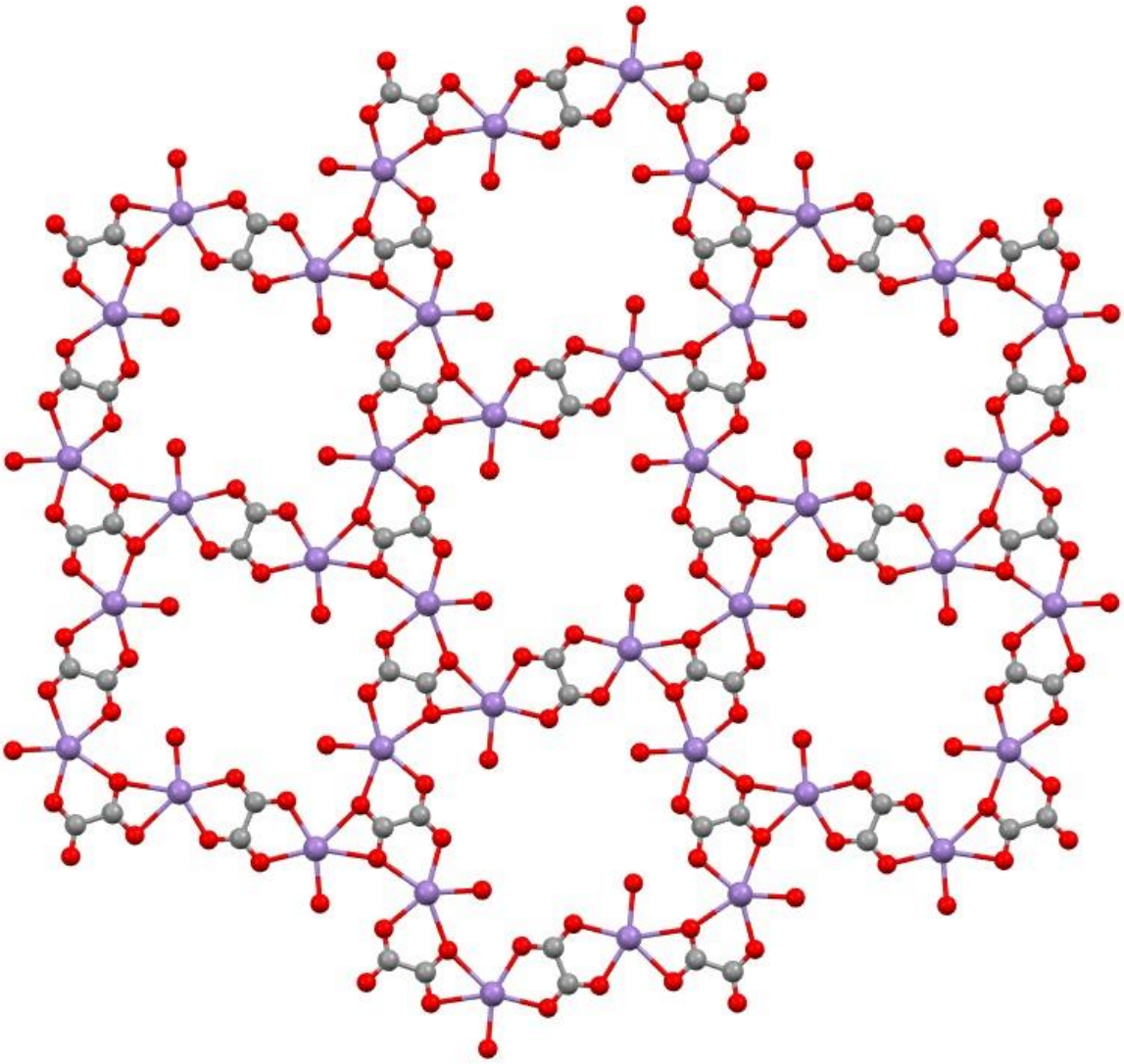

Figure 62: The topology of cationic 2D sheets.[35]

These 2D sheets contain hollow spaces formed by eight Mn(II) centers connected by eight oxalate ligands (**Figure 62**). Therefore, vacant channels are formed by the alignment of multiple sheets within the lattice structure (**Figure 63**) to construct the 1D pores within the MOF. Furthermore, four coordinated water molecules are directed inwards these hallow spaces, which renders the MOF hydrophilic.

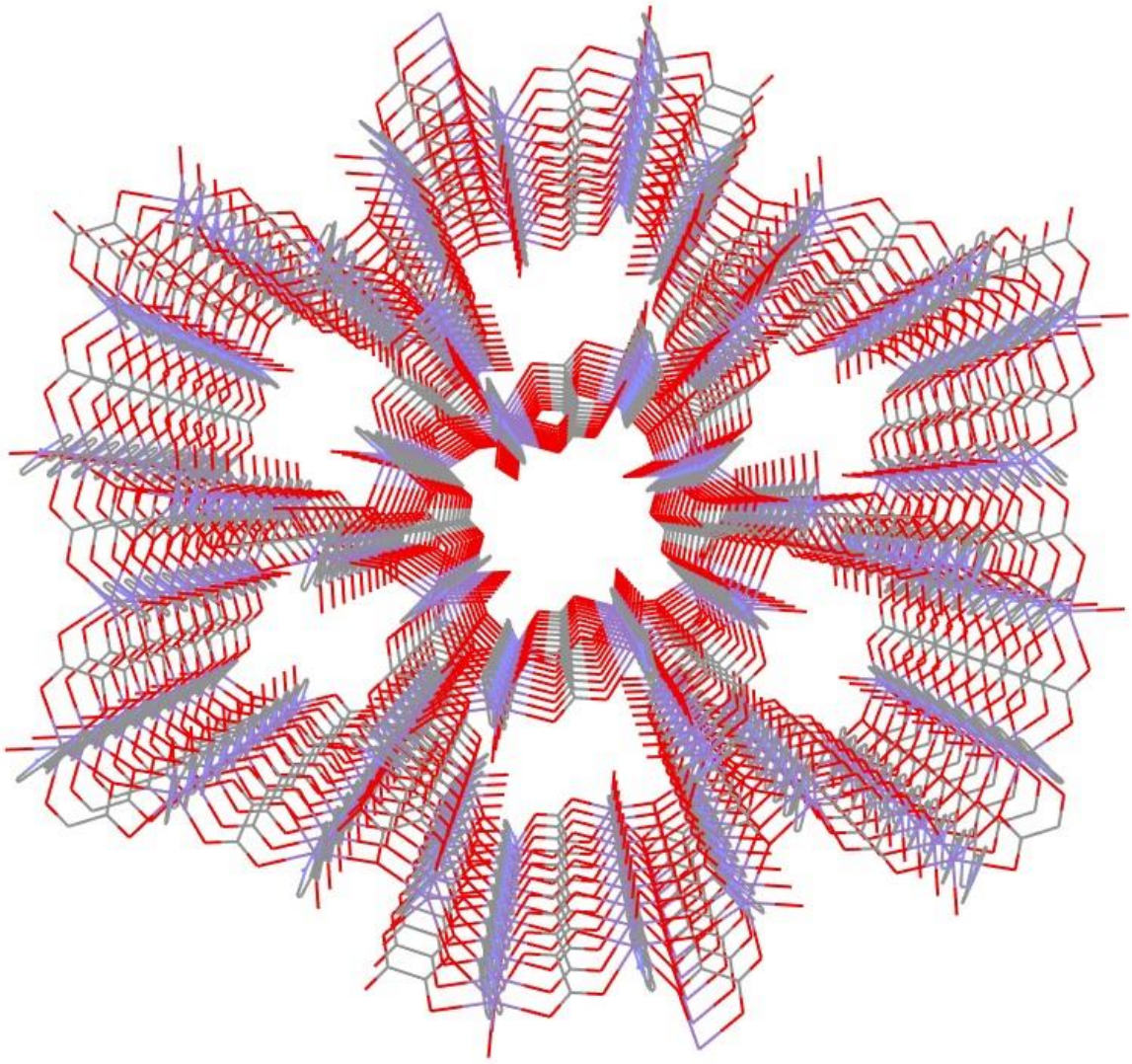

Figure 63: perspective channels view that construct 1D pores.[35]

Since **2** is expected to have the corelated lattice structure based on the comparable PXRD pattern shown in **Figure 55**, the most important attribute of this lattice structure for photochemical [2+2] cycloaddition reaction is bpe alignment. Bpe ligands are coordinated from both sides to two Mn(II) metal centers in axial position from two different 2D sheets and pillaring the layers of these sheets to form 3D framework (**Figure 64**).[35]

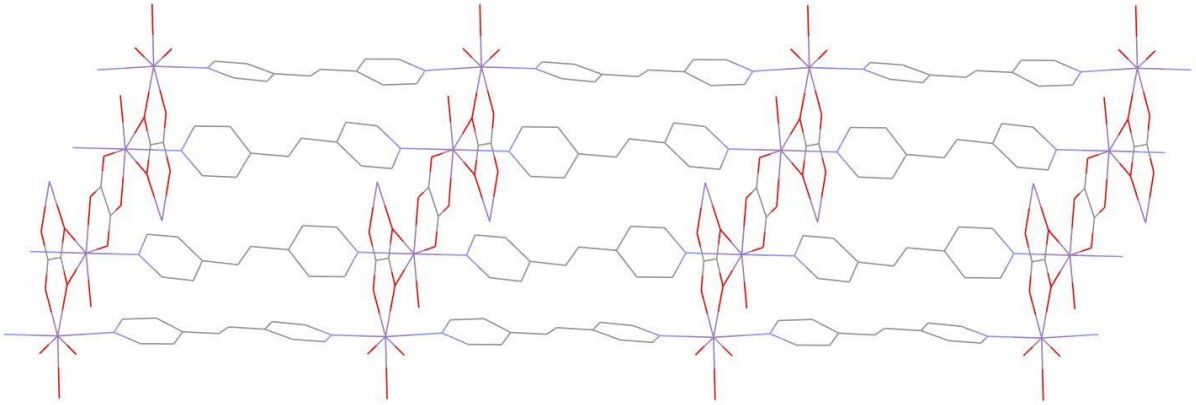

Figure 64: Bpe alignment within the lattice structure of Mn(II) compound.[35]

As it can be seen in **Figure 64**, each two bpe ligands coordinated to adjacent Mn(II) centers are aligned to each other with very slight misalignment in angle (**Figure 65**).

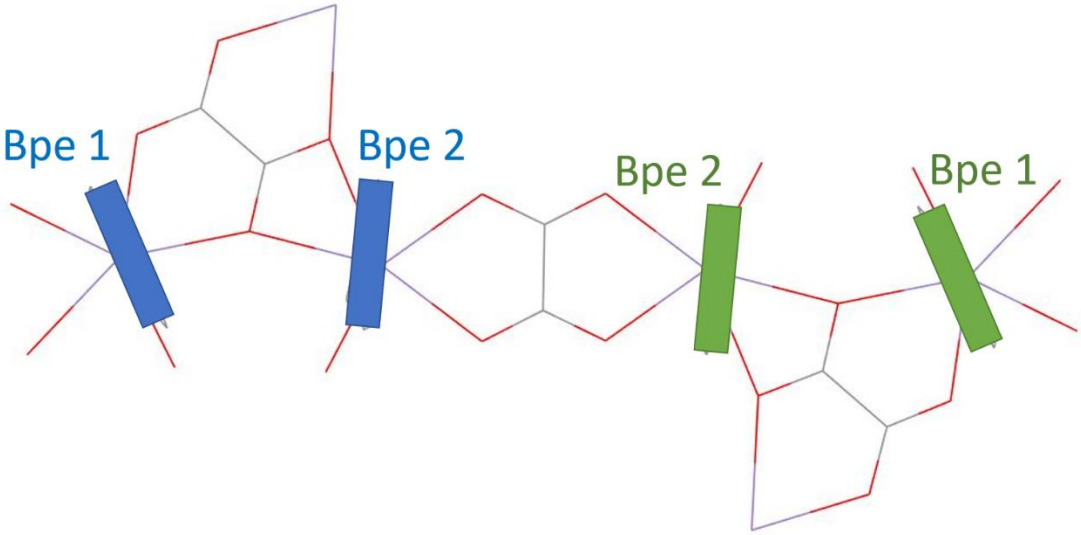

Figure 65: The disorientation of bpe alignment within the Mn(II) compound.[35]

This small misalignment can be overcome by rotation of the coordination bonds Mn-N. Therefore, it wouldn't prevent the photochemical [2+2] cycloaddition reaction from occurring. The distance between the centers of two olefinic C=C double bonds from aligned bpe ligands

was measured to be 3.995 Å, which is within the range where the photochemical [2+2] cycloaddition reaction can occur.

4.2.2.3 Compound 3

The PXRD pattern of compound **3** has been found to be comparable to the calculated powder pattern of reported MOF, $[Zn(bpe)(fum)]_n \cdot 0.25(H_2O)$, as shown in **Figure 56**. This compound is an interpenetrated 3D network that consists of 2D sheets pillared by bpe ligands that exhibit α-Po topology. The Zn(II) metal centers are penta-coordinated in trigonal bipyramidal geometry (**Figure 66**).[36] Each metal center is coordinated to two bpe in axial orientations and three fumarate ligands in equatorial orientations. However, the 2D sheets of this MOF have different topology from the one discussed in previous section as shown in **Figure 67**, and the connectivity of these sheets through bpe is shown in **Figure 68**.

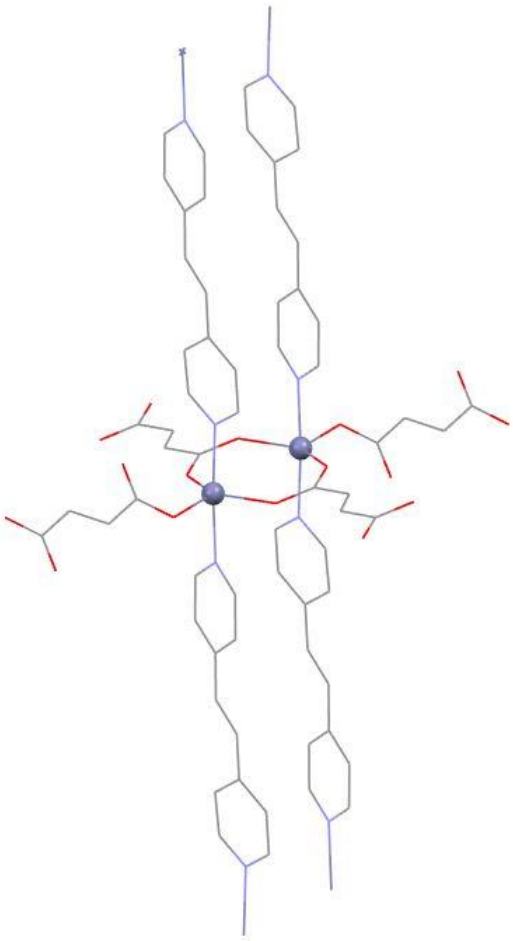

Figure 66: Ligands arrangement around Zn(II) centers within Zn(II) MOF.[36]

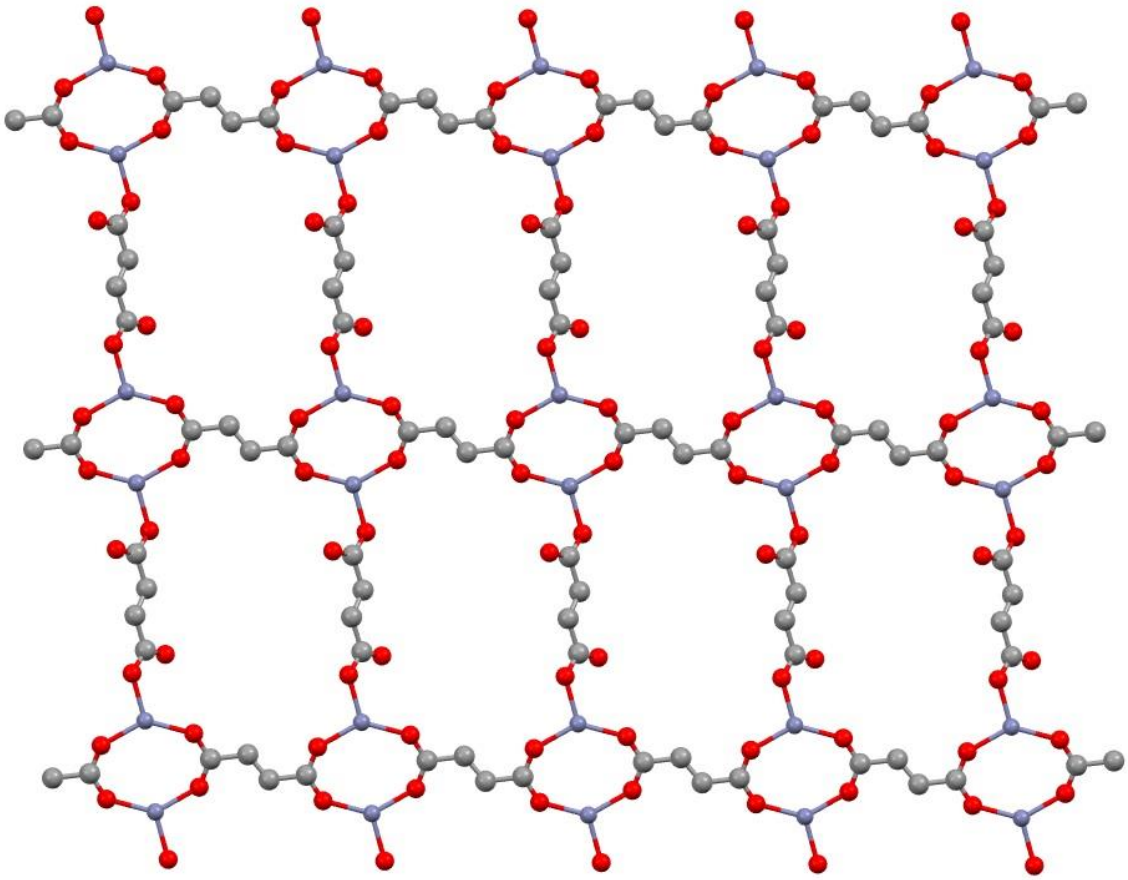

Figure 67: The topology of $[Zn(fum)]_n$ 2D sheets within the Zn(II) MOF.[36]

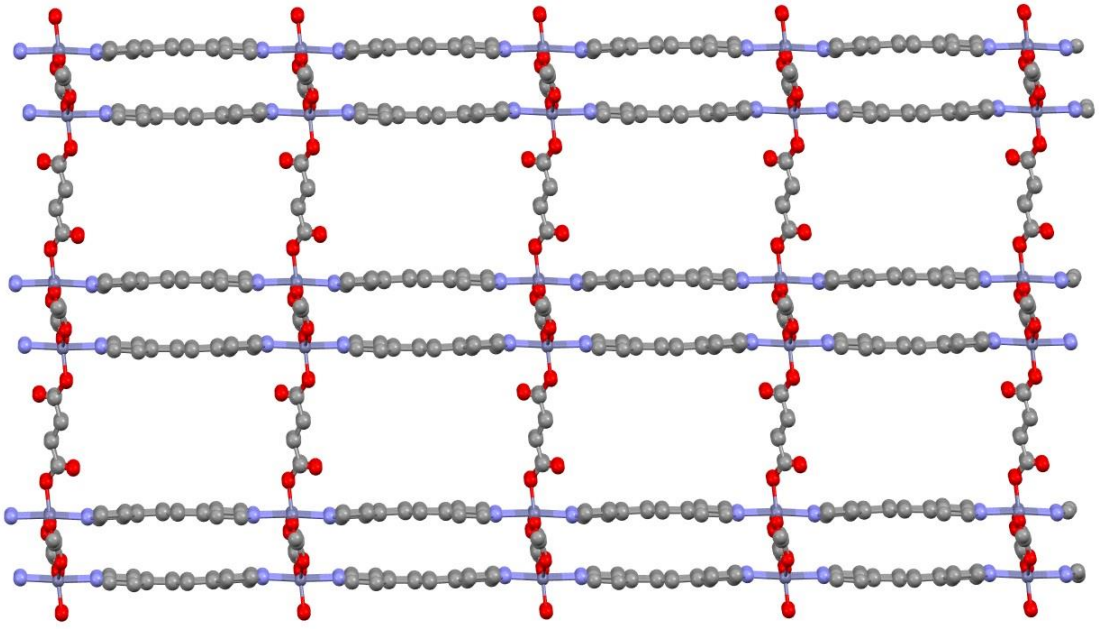

Figure 68: The connectivity of 2D sheets $[Zn(fum)]_n$ through bpe ligands within the Zn(II) MOF.[36]

The bpe ligands are coordinated through both nitrogen atoms to two Zn(II) centers from two different layers in the lattice structure (**Figure 68**). Each two bpe ligands are aligned to each other through coordination to adjacent Zn(II) metal centers (**Figure 66**). Every pair of olefinic C=C double bonds in adjacent bpe ligands within the MOF are parallelly aligned and have a distance of 3.992 Å, which will allow the photochemical [2+2] cycloaddition reaction to occur. Furthermore, since bpe ligands are distributed in pairs within the lattice structure, it is a valid reason for 100% conversion of bpe ligands to *rctt*-tpcb product due to the photochemical [2+2] cycloaddition reaction, which is consistent with the expectation of similar lattice structure of **3** to the Zn(II) MOF based on comparable PXRD pattern (**Figure 56**).

4.2.2.4 Compound 4

The collected PXRD pattern for compound **4** was found to be consistent with calculated pattern for the reported dinuclear triple-strands-like one-dimensional ladder photoreactive cadmium-based MOF, $[Cd(bpe)_{1.5}(NO_3)_2(H_2O)]_n$, as shown in the following figure (**Figure 69**).

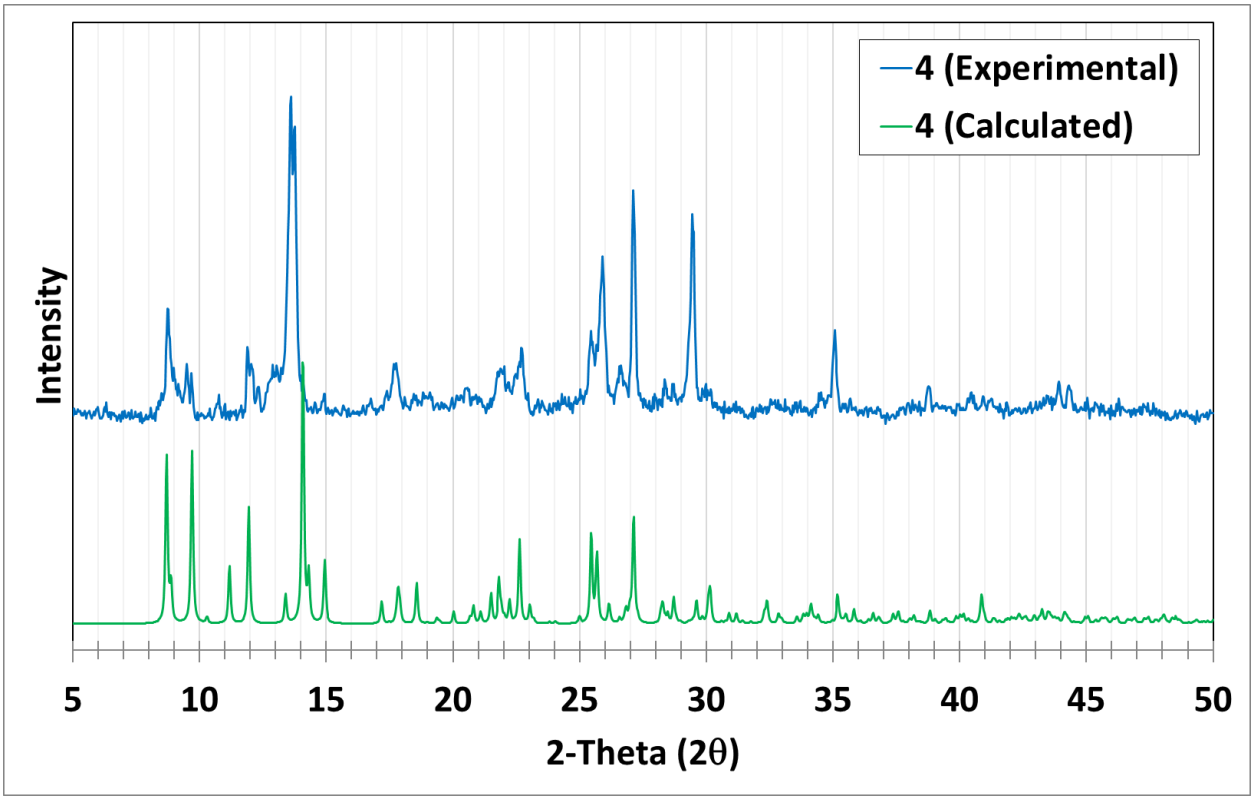

Figure 69: PXRD pattern of compound **4**; $[Cd(bpe)_{1.5}(NO_3)_2(H_2O)]_n$.[41]

The lattice structure is shown in **Figure 18** and its relation to the photoreactivity through the photochemical [2+2] cycloaddition reaction has been discussed in **Section 4.1.2** alongside with a proposed mechanism (**Figure 51**).

4.2.3 Elemental Analysis (CHN)

The elemental analysis (CHN) data were obtained for compounds **1-4** as shown in **Table 3**. The results were compared to calculated elemental analysis (CHN) of reported compounds that have their powder patterns compared with our synthesized compounds. However, one of the solvents in the chemical formula of **1** has been changed to matched experimental one instead of reported one because different solvents system has been used to synthesize these compounds. Dimethylformamide (DMF) has been used in compound **1** chemical formula instead of ethanol,

since DMF has been used in synthesis of **1** instead of ethanol, which is the reported solvent for the compared Mn(II) MOF.

Table 3. Elemental analysis (CHN) data before and after UV irradiation.

Compound	C %	H %	N %
$\{(Hbpe)_2[Zn_2(ox)_3]\}_n \cdot (H_2O) \cdot 2.2(DMF)$ **(1)** (Before UV irradiation)	46.45	3.79	10.73
$\{(Hbpe)_2[Zn_2(ox)_3]\}_n \cdot (H_2O) \cdot 2.2(DMF)$ **(1)** (Calculated)	46.76	4.22	9.24
$\{(Hbpe)_2[Zn_2(ox)_3]\}_n \cdot (H_2O) \cdot 2.2(DMF)$ **(1)** (after UV irradiation)	46.10	2.6	11.7
$[Pb_4(ox)_3(bpe)_4(H_2O)_4]_n \cdot (NO_3)_2$ **(2)** (before UV irradiation)	30.35	0.99	7.11
$[Pb_4(ox)_3(bpe)_4(H_2O)_4]_n \cdot (NO_3)_2$ **(2)** (Calculated)	30.28	2.26	7.85
$[Pb_4(ox)_3(bpe)_4(H_2O)_4]_n \cdot (NO_3)_2$ **(2)** (after UV irradiation)	25.49	0.73	7.62
$[Pb(bpe)(fum)]_n \cdot 0.25(H_2O)$ **(3)** (before UV irradiation)	56.09	3.28	8.44
$[Pb(bpe)(fum)]_n \cdot 0.25(H_2O)$ **(3)** (Calculated)	38.17	2.4	5.56
$[Pb(bpe)(fum)]_n \cdot 0.25(H_2O)$ **(3)** (after UV irradiation)	60.69	3.14	9.41
$[Cd(bpe)_{1.5}(NO_3)_2(H_2O)]_n$ **(4)** (Found)	40.9	3.34	13.06
$[Cd(bpe)_{1.5}(NO_3)_2(H_2O)]_n$ **(4)** (Calculated)	40.96	3.25	13.27

Apart from compound **4**, which has been successfully reproduced with experimental elemental analysis results that matching the calculated ones with a maximum difference of 0.05%, all others have maximum difference less than 1.5% either in hydrogen, such as **2**, or hydrogen and nitrogen such as **1**. The mentioned difference is present due to defects in the MOF structure, as well as the none constant chemical species in the edge of an infinite MOF structure.

The slight change between before and after UV irradiation can be explained by the change in water or solvent content due to UV irradiation. However, the change in compound **3** is not small. The sample was UV irradiated for 50 hours for elemental analysis (CHN), while it reaches full conversion after only 5 hours of UV irradiation. It is possible that the long period of UV

irradiation has change some structural features within the lattice structure, such as loss of coordinated ligand. However, the true reason behind the change in elemental % cannot be determined without proper and deep study of the lattice structure with single crystal XRD.

4.2.4 Thermogravimetric Analysis (TGA)

The thermogravimetric analysis (TGA) is an essential technique for both organic and inorganic materials. It can be used to obtain various type of information about the chemical compounds. All TGA experiments were conducted in inert nitrogen atmosphere.

4.2.4.1 Compounds 1-3

TGA technique was used here to confirm obtained structural information about compounds **1-3**. The following figures (**Figure 70-72**) show obtained TGA thermograms for compounds **1-3**.

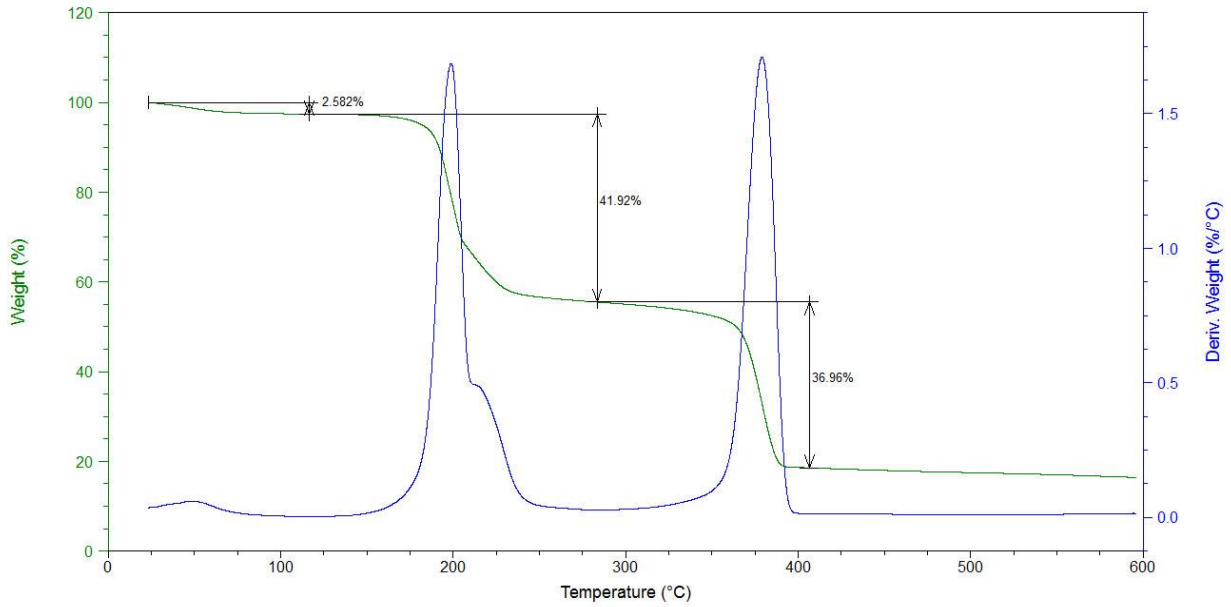

Figure 70: TGA of compound **1**.

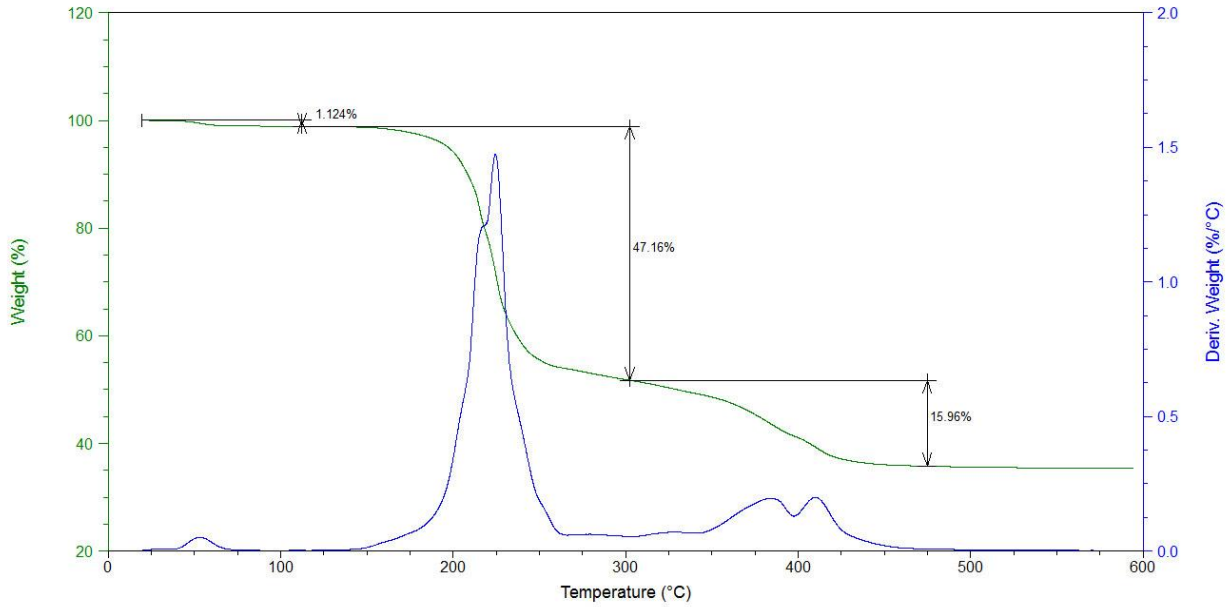

Figure 71: TGA of compound **2**.

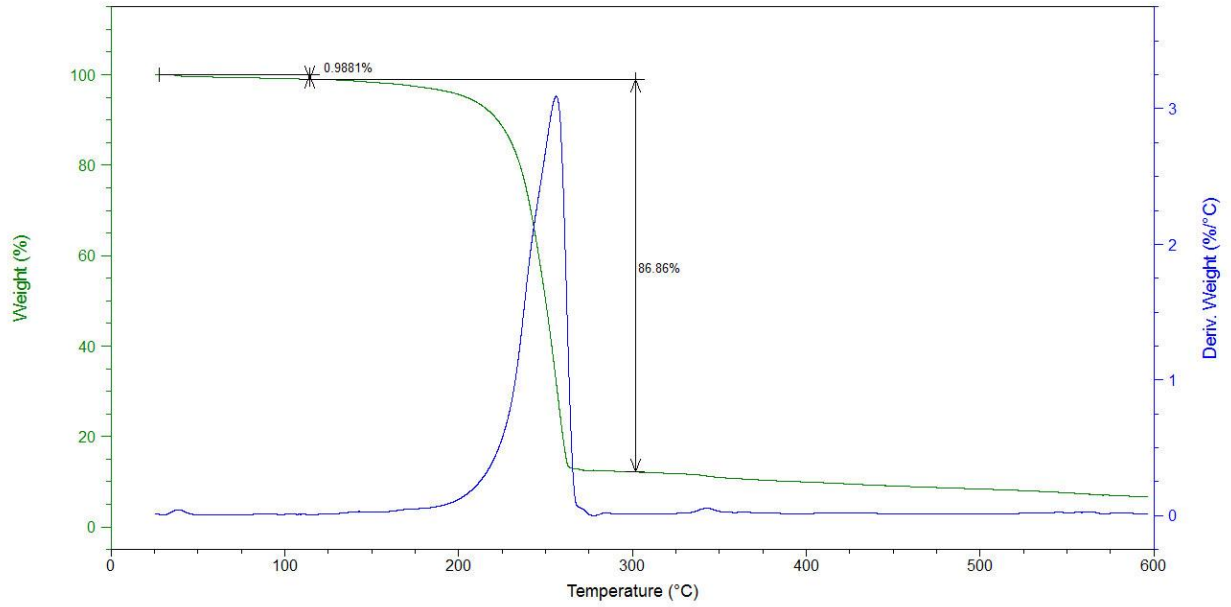

Figure 72: TGA of compound **3**.

The presence of two steps in the thermal decomposition for compounds **1** (**Figure 70**) indicates the presence of two different types of bonded chemical species within the lattice structure. These chemical species are bpe, which decompose in the first step, and oxalate, which decompose in the second step due to higher strength of Zn-O bond. Furthermore, the 2.5% loss in weight % at around 100 ^{0}C corresponds to one water molecule predicted by elemental analysis.

The situation is more complicated for compound **2** because the thermogram shows several changes in the slope during the thermal decay of the compound (**Figure 71**). These slope changes indicate inequivalent stability of chemical species within the lattice structure as well as complexity in the MOF structure. The first step in **Figure 71** thermogram belongs to four bpe and three oxalate ligands. The second step is for various decomposition steps for Pb and the residue is three PbO_2.

Compound **3** TGA thermogram (**Figure 72**) hides even more information since some MOF structures with 3D pores show integration of all chemical species decomposition on one large step. However, the 1% loss of water can be seen in low temperature, which is also matched with reported TGA for analogous Zn(II) MOF.[36]

4.2.4.2 Compound 4

Thermogravimetric analysis (TGA) experiments were conducted to investigate the behavior of water molecules during grinding and its impact on the photoreactivity in compound **4**. A total of six TGA experiments were conducted on 3 samples, each before and after UV irradiation. These three samples are single crystals, 10 and 20 minutes grinded samples. The following figures (**Figure 73-78**) show the obtained TGA thermograms for each sample before and after UV irradiation.

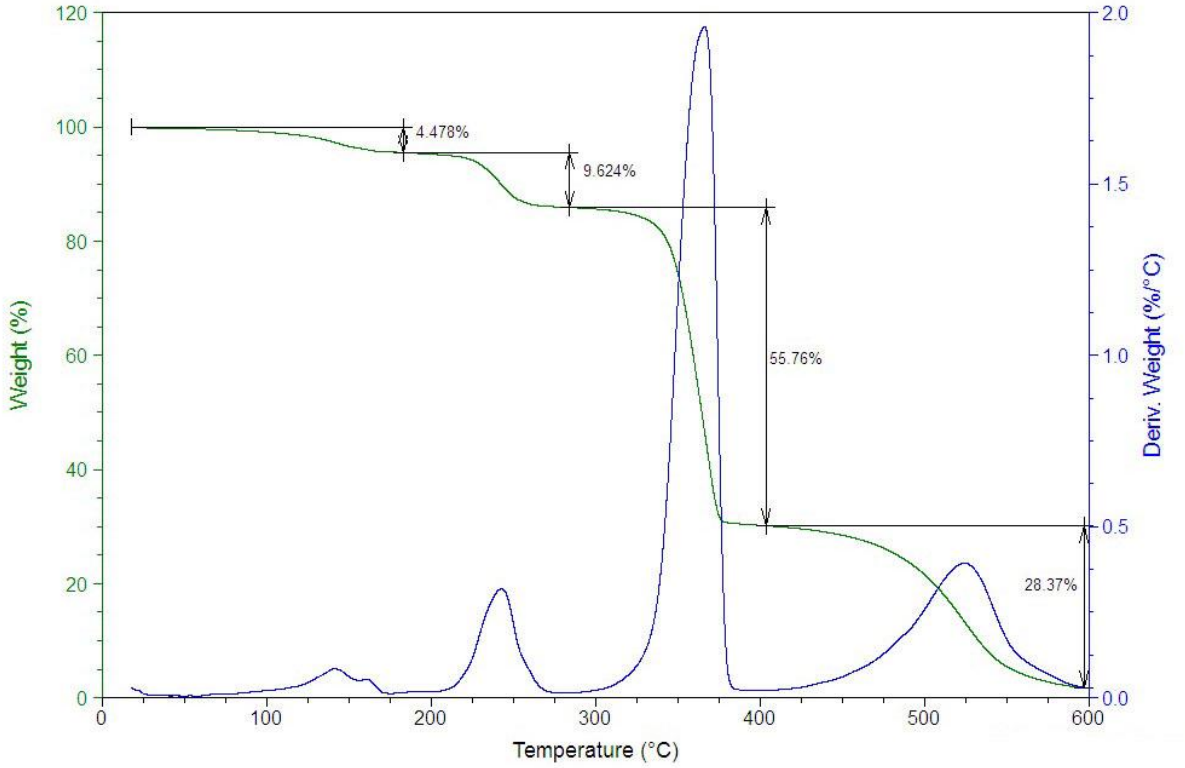

Figure 73: TGA of single crystals sample of compound **4** before UV irradiation.

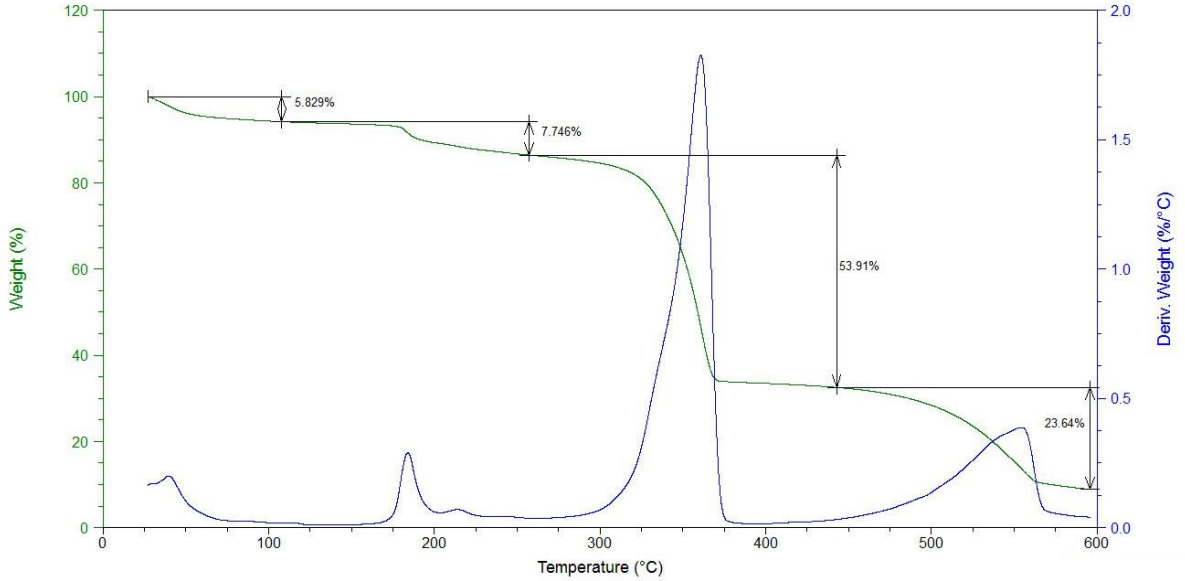

Figure 74: TGA of 10 minutes grinded crystals sample of compound **4** before UV irradiation.

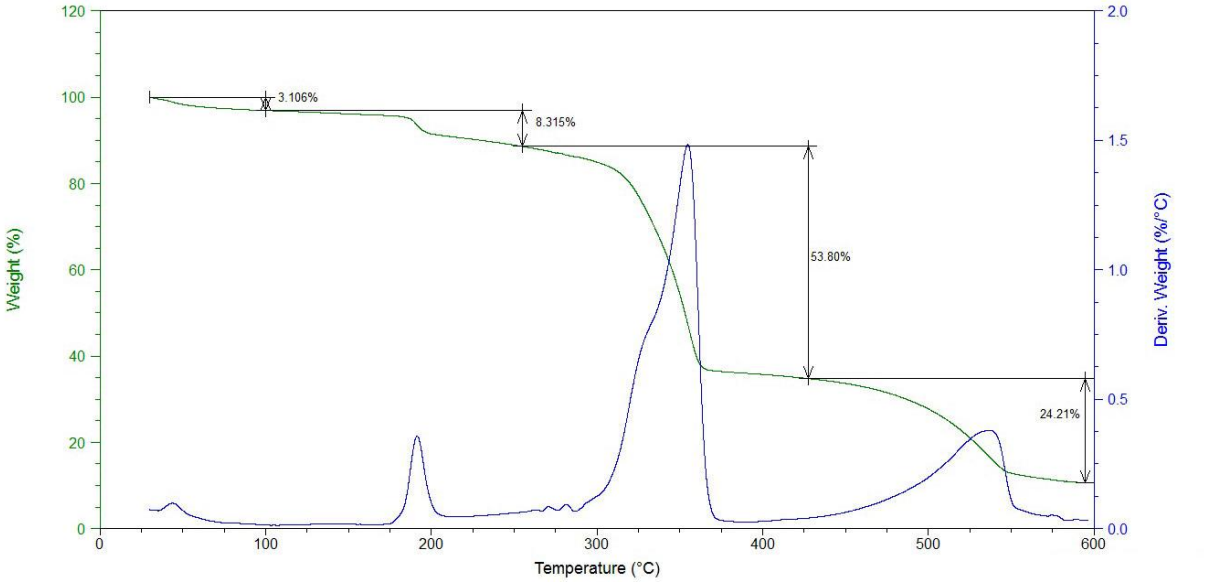

Figure 75: TGA of 20 minutes grinded crystals sample of compound **4** before UV irradiation.

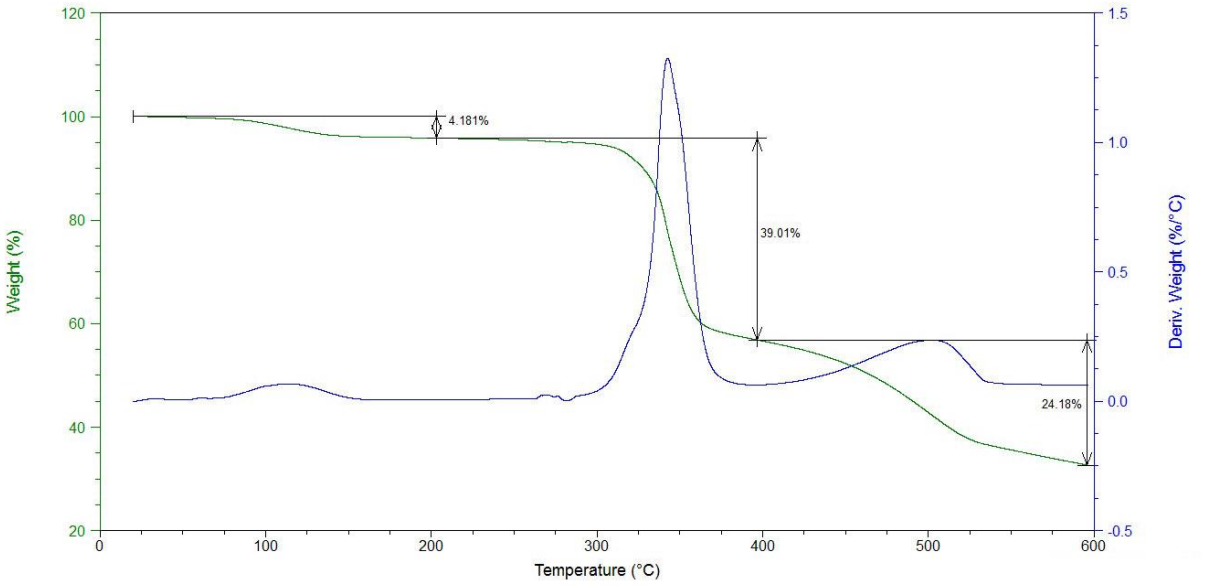

Figure 76: TGA of single crystals sample of compound **4** after 50 hours of UV irradiation.

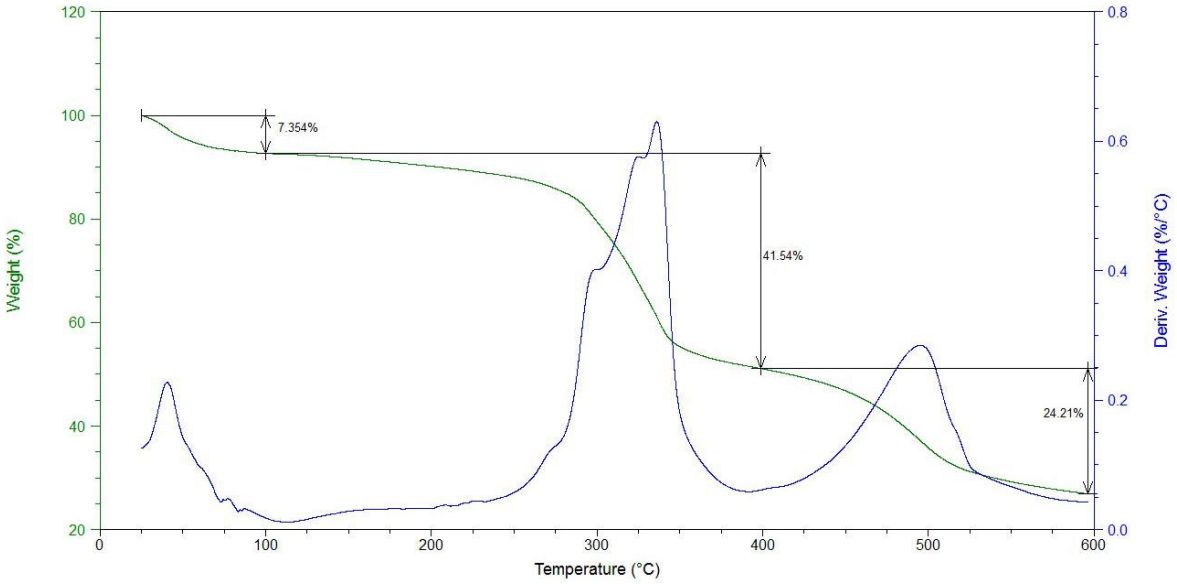

Figure 77: TGA of 10 minutes grinded crystals sample of compound **4** after 50 hours of UV irradiation.

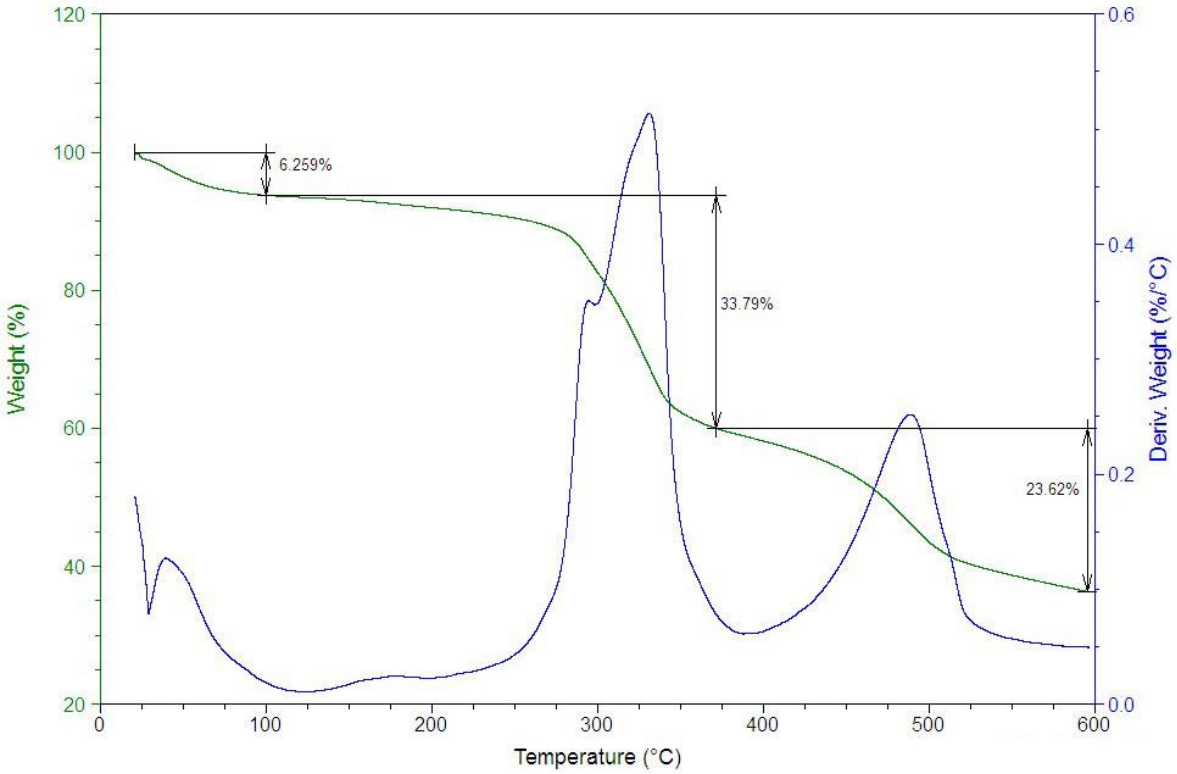

Figure 78: TGA of 20 minutes grinded crystals sample of compound **4** after 50 hours of UV irradiation.

The following table **(Table 4**) shows a summary of % weight loss of water molecules obtained from TGA thermograms (**Figure 73-78**).

Table 4. % Weight loss of H_2O molecules in **4** from TGA.

Compound **4***	% Wt. Loss
Single Crystals	4.48
Single Crystals (UV Irradiated)	4.18
10 min. Grinded Crystals	5.83
10 min. Grinded Crystals (UV Irradiated)	7.35
20 min. Grinded Crystals	3.11
20 min. Grinded Crystals (UV Irradiated)	6.23

* Expected weight loss for one water molecule is 3.41%

Although the expected weight loss for one water molecule in **4** is 3.41%, **Table 4** shows 25% higher values in single crystals than the theoretically calculated values. It can be due to absorption of water molecules from air. Ground crystals show even higher values, which is due to higher surface area. UV irradiated samples have higher values of water % weight loss due to long exposure to atmosphere while irradiating for 50 hours in photoreactor.

The following figures (**Figure 79** and **80**) show compiled obtained TGA thermograms before and after UV irradiation for the three samples.

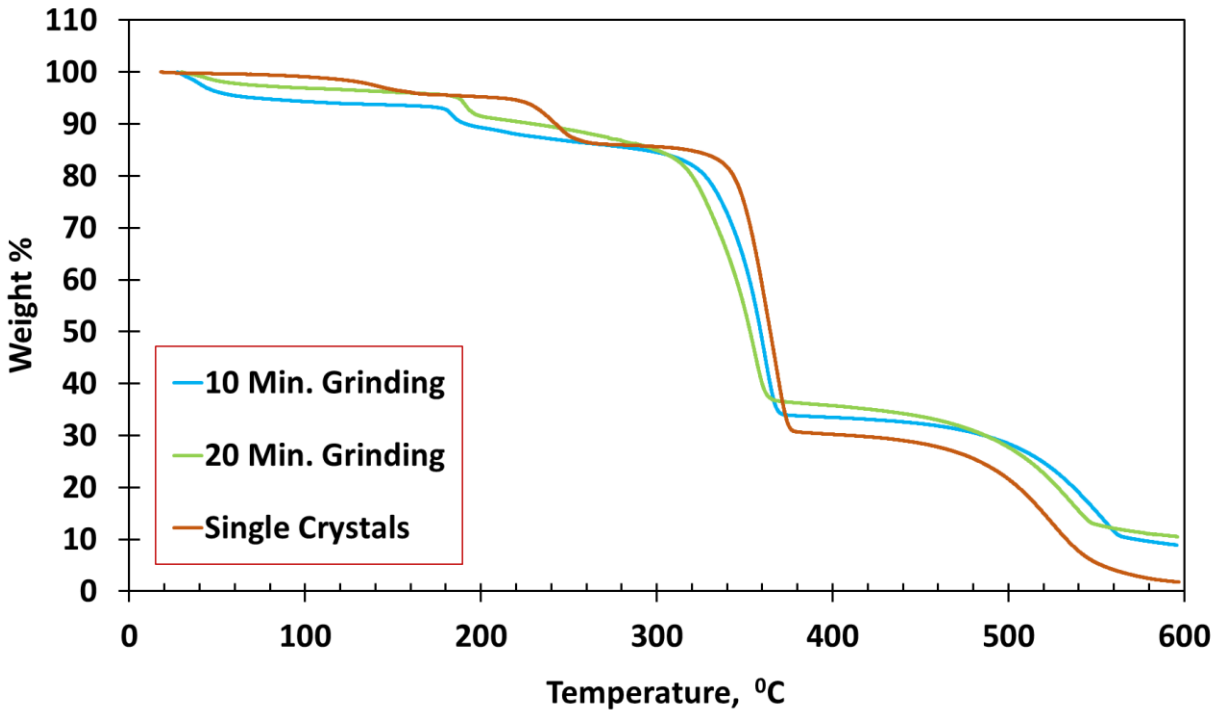

Figure 79: Compiled TGA thermograms of single crystals, 10 and 20 minutes grinded samples of compound **4** before UV irradiation.

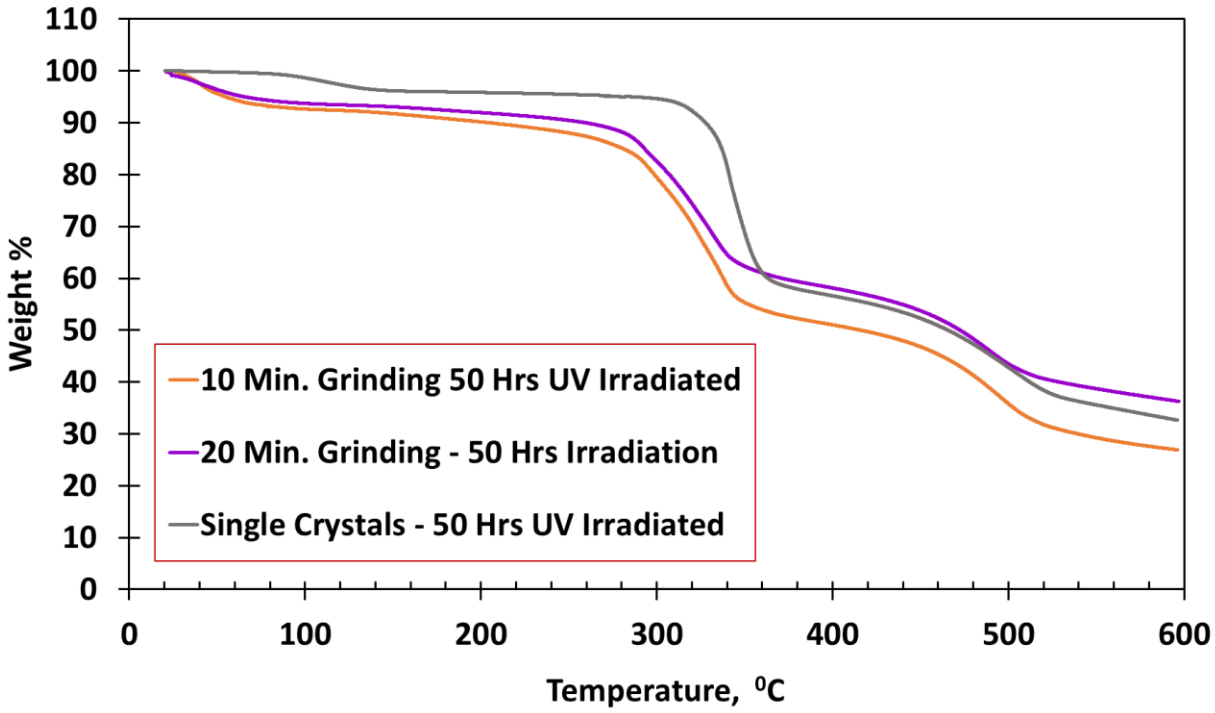

Figure 80: Compiled TGA thermograms of single crystals, 10 and 20 minutes grinded samples of compound **4** after 50 hours of UV irradiation.

The thermogravimetric analysis data was compiled in **Figure 79** and **80**. The graphs show that there is not much difference between 10 and 20 minutes grinding samples as their TGA curve is almost identical. they also show that the temperature of water molecules loss has not changed between pre- and post-irradiation samples. However, loss of water molecules of single crystals is above 110 ^{0}C, while It is near 50 ^{0}C for ground crystal samples.

The change in water loss temperature between single and ground crystals indicates these water molecules are coordinated in single crystals, while they are uncoordinated (free water molecules) within the lattice structure of ground crystal samples. These observations show that grinding caused the coordinated water molecules to break free from the coordination sphere. The change in water molecules bonding and arrangement within the lattice structure has caused photoreactivity to increase. It is well known that these mechanical approaches enhance the reactivity due to increase in surface area, as well as formation of crystal defects.[50]

4.2.5 FT-IR Spectroscopy

The FT-IR is a typical technique to identify structural features of inorganic materials. The shift of FT-IR spectra signals, as well as their appearance or disappearance can be interpreted in terms of coordination of the ligands to the metal ions. The FT-IR spectra were taken to investigate the coordination of organic linkers through its carboxylic acid peaks, as well as other characteristic bands. The following figures **(Figures 81-88)** show the FT-IR spectra of each compound (**1-4**) before and after UV irradiation:

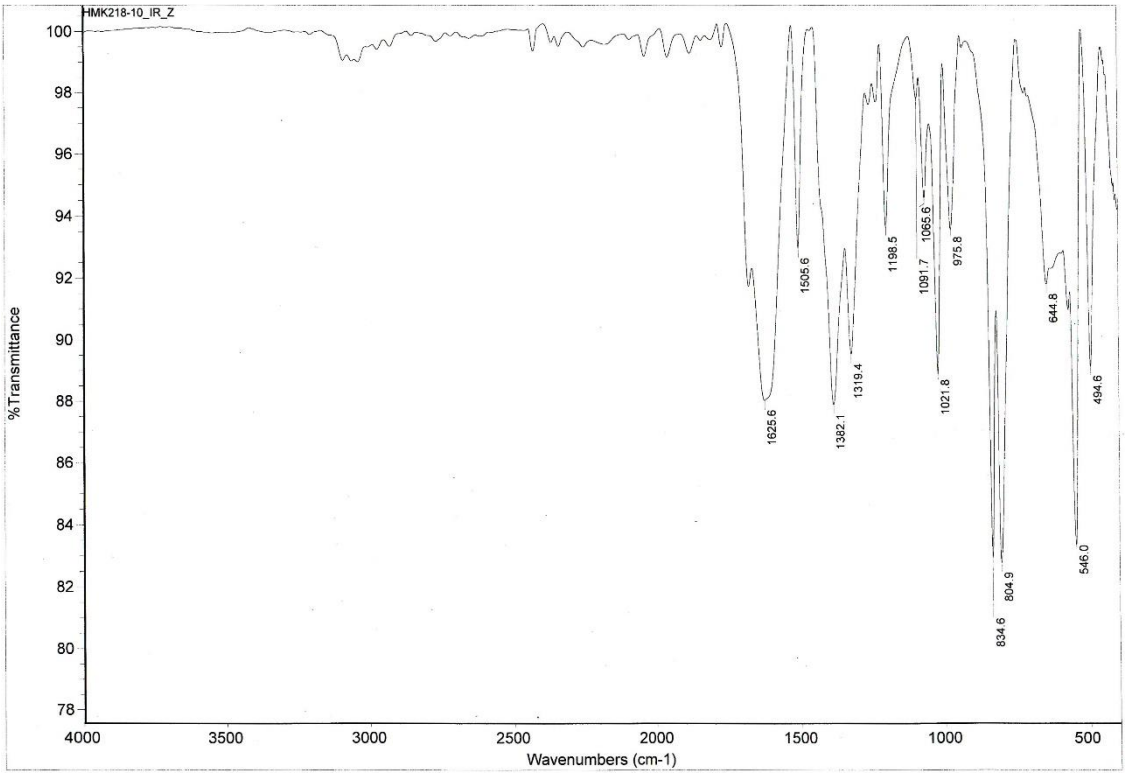

Figure 81: FT-IR spectrum of **1** before UV irradiation.

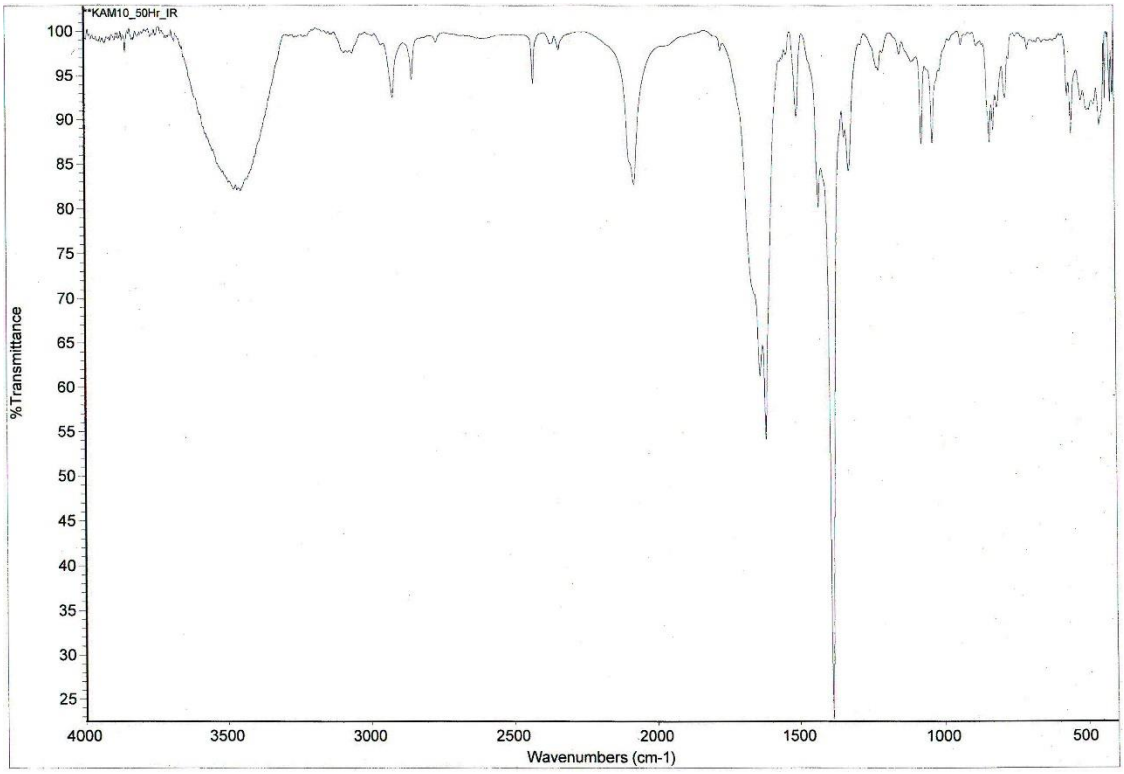

Figure 82: FT-IR spectrum of **1** after 50 hours of UV irradiation.

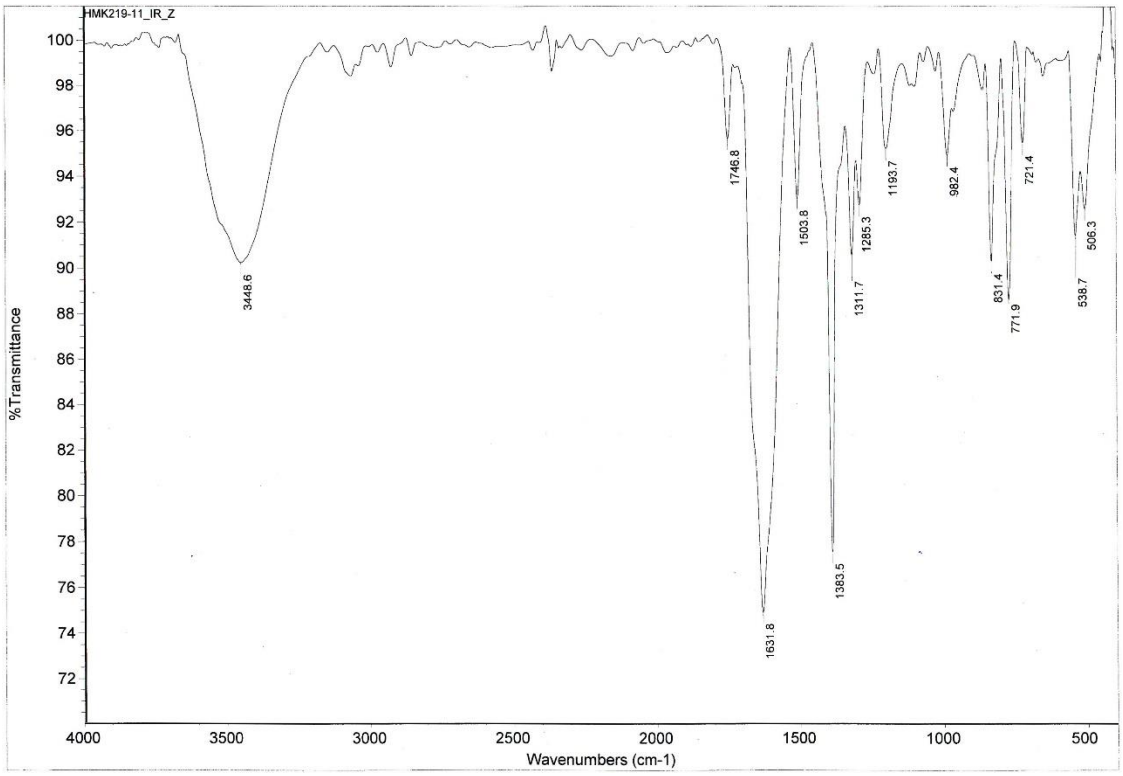

Figure 83: FT-IR spectrum of **2** before UV irradiation.

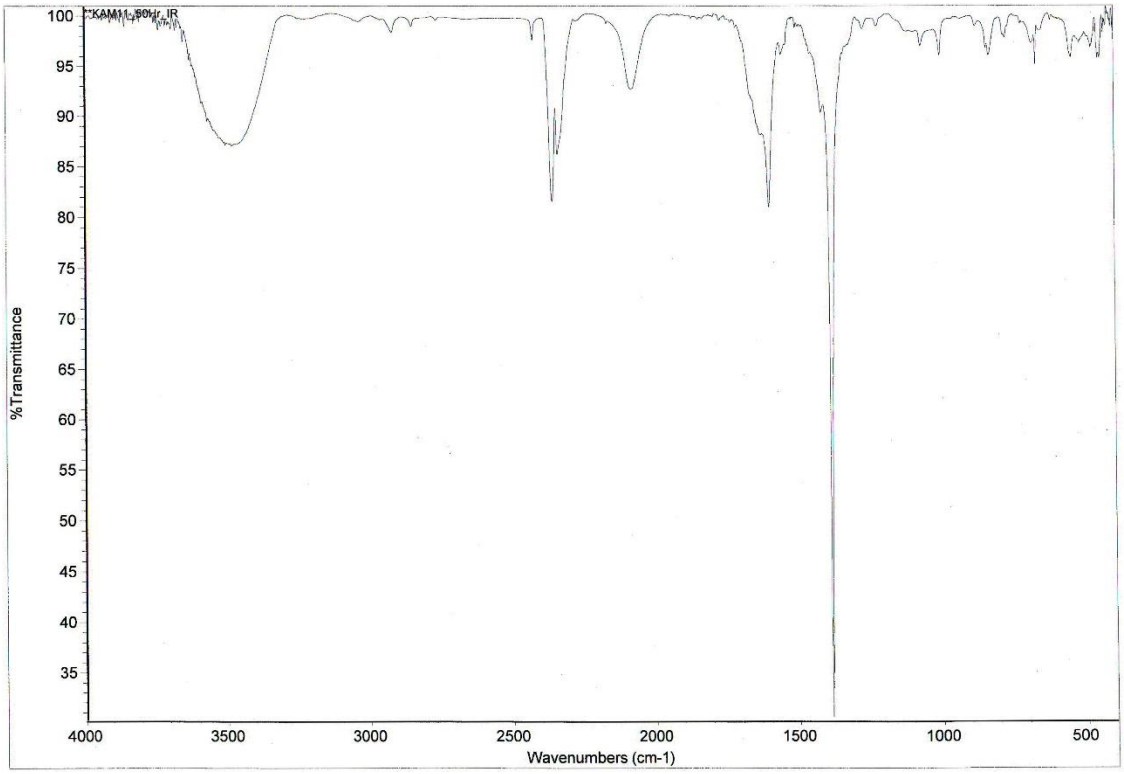

Figure 84: FT-IR spectrum of **2** after 50 hours of UV irradiation.

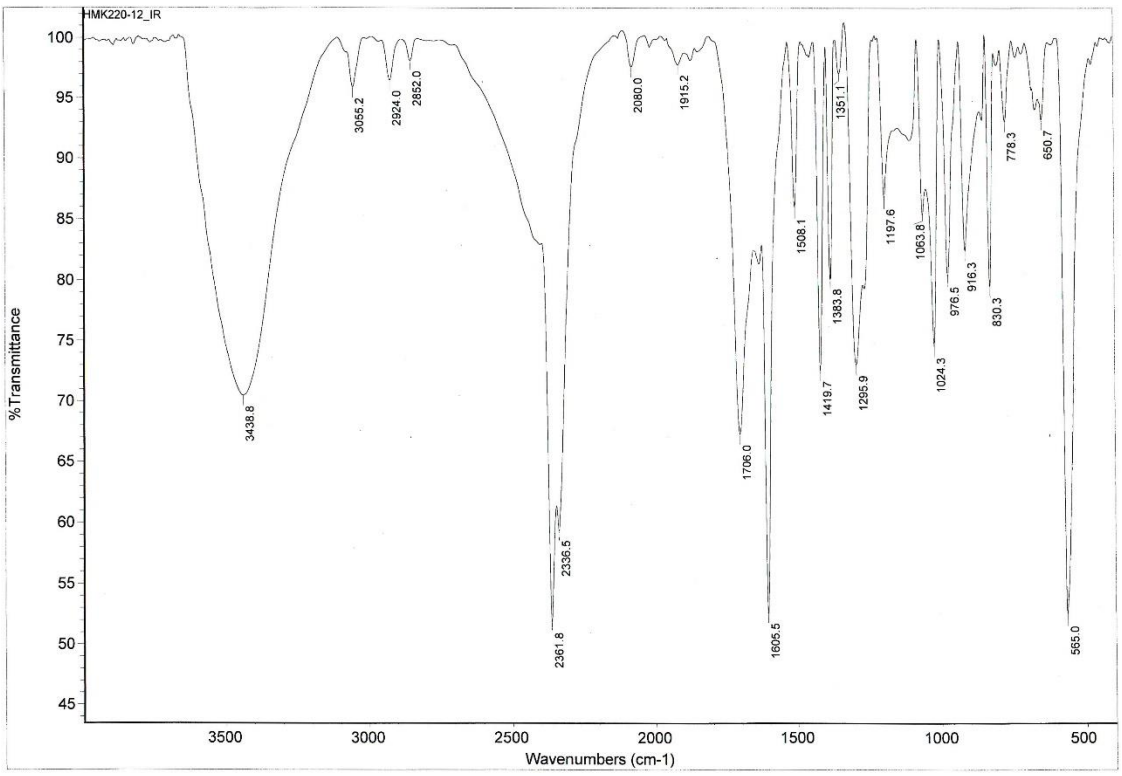

Figure 85: FT-IR spectrum of **3** before UV irradiation.

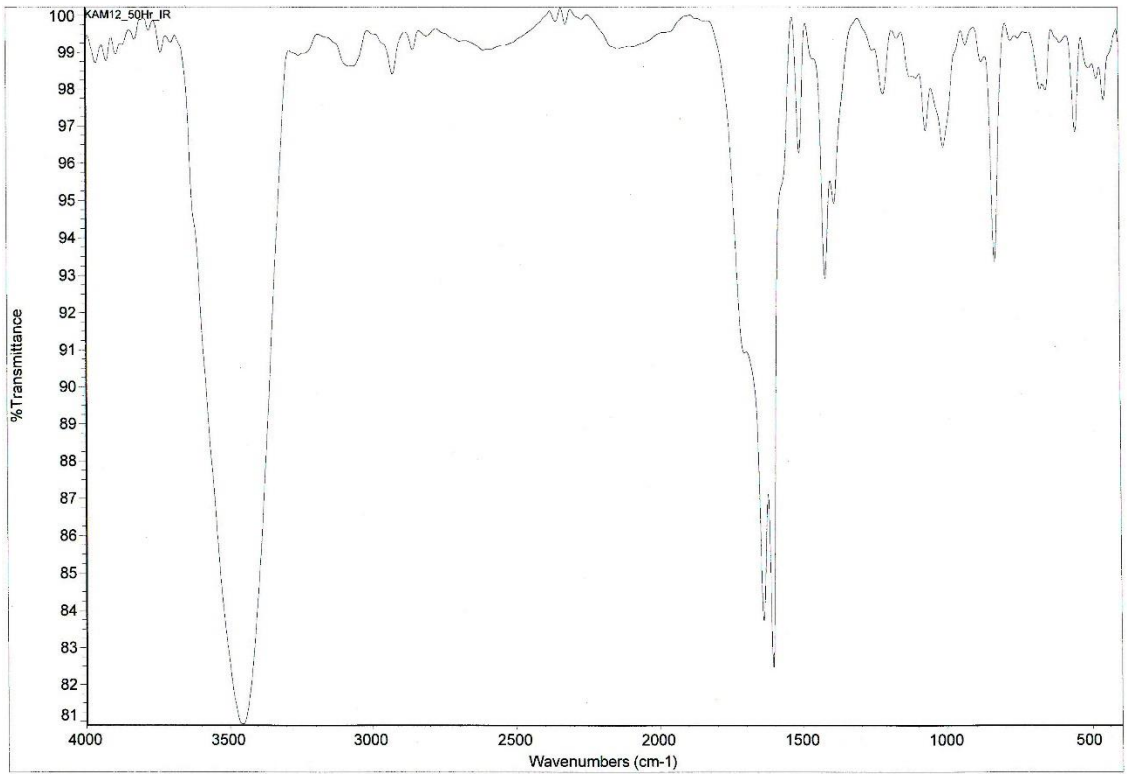

Figure 86: FT-IR spectrum of **3** after 50 hours of UV irradiation.

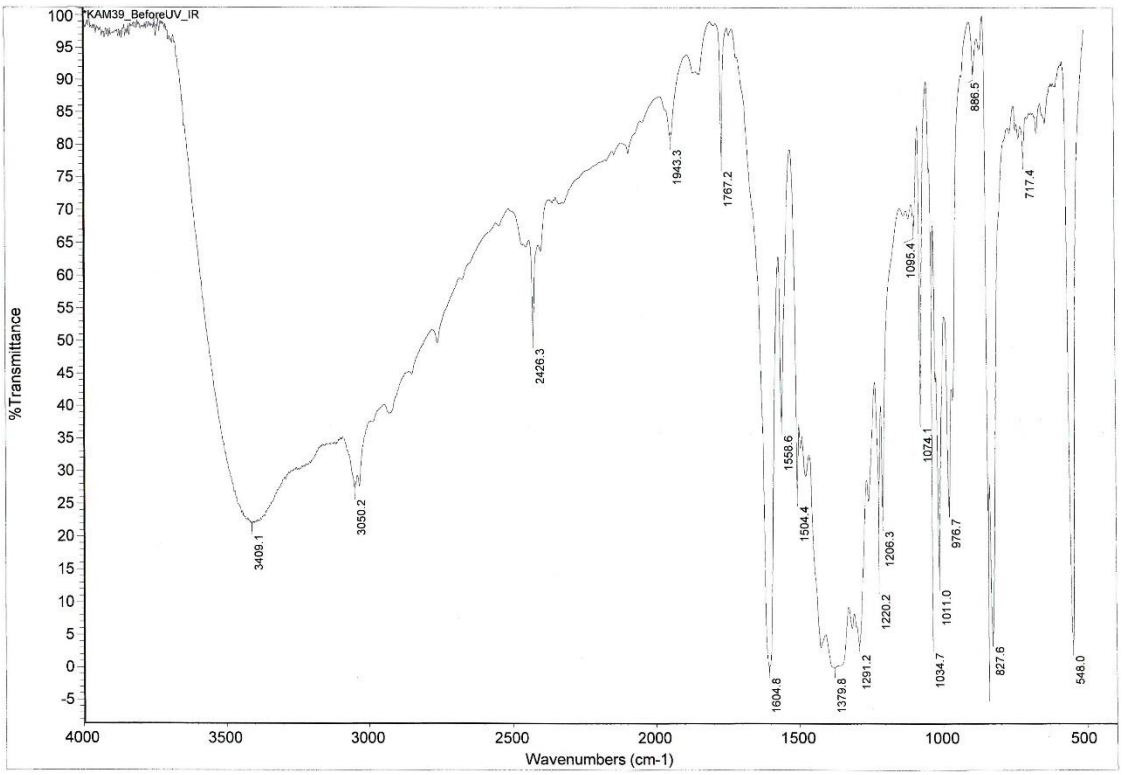

Figure 87: FT-IR spectrum of **4** before UV irradiation.

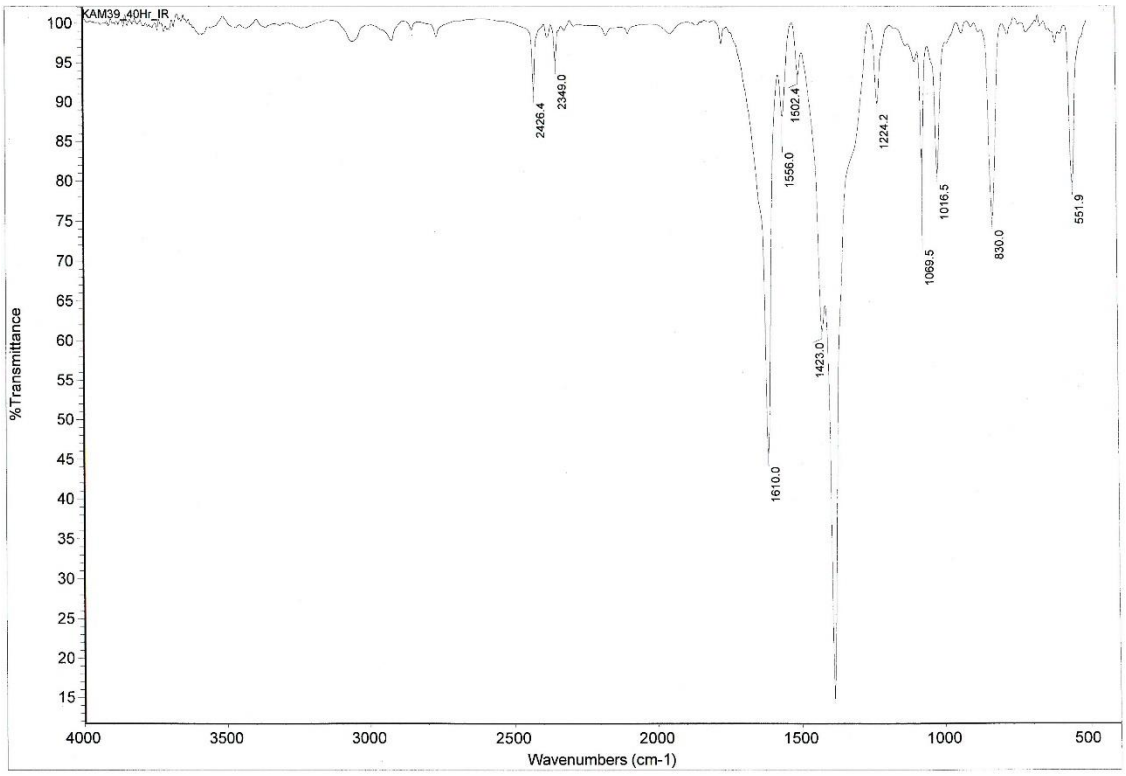

Figure 88: FT-IR spectrum of **4** after 40 hours of UV irradiation.

The disappearance of carboxylic acid O-H stretching frequency of oxalic or fumaric acid, a broad and strong peak from 2500-3300 cm^{-1}, in before UV irradiation FT-IR spectra for the four compounds **(Figures 81, 83, 85** and **87)** is a result of deprotonation of carboxylic acid functional groups that leads to coordination of the oxygen atoms to the metal ion in the MOF.

Although Zn-N stretching vibration can be observed below 500 cm^{-1},[51] Zn-O stretching also can be observed in the same region.[52] The precise location of the signals can vary depending on the electronic environment as well as the morphology of the compound.[52] Two signals can be observed at 494.6 and 546.0 cm^{-1} in the spectrum of compound **1** before UV irradiation **(Figure 81)**. These bands were assigned to O-Zn-O symmetrical and asymmetrical stretching vibrations. Conversely, Pb-O and Pb-N stretching bands for compounds **2** and **3** cannot be seen in **Figure 83** and **85** as their stretching frequencies are 272 and 213 cm^{-1} respectively.[53] Although compounds **1**-**3** have not been reported previously in the literature, the FT-IR spectrum of compound **4 (Figures 87)** is matching with the reported one.[41]

The photochemical [2+2] cycloaddition reaction forms cyclobutane derivative, which lead to the disappearance of alkene C-H stretching (slightly above 3000 cm^{-1} wavelength) from after UV irradiation spectra. However, it cannot be observed clearly due to interference of alkene C-H stretching bands with the hydrogens of the rings of bpe. Moreover, the appearance of alkane C-H stretching (slightly before 3000 cm^{-1} wavelength) due to the photochemical [2+2] cycloaddition reaction is barely visible, but it can be seen for spectra of compounds **1**, **2** and **4**. Depending on alkene C=C stretching is not practical due to presence of aromatic C=C stretching in the same region, which makes it difficult to distinguish between the two bands.

The broad peak observed around 3500 cm^{-1} in the spectra **(Figures 82-87)** is due to presence of water molecules within the lattice structure of compounds **1-4**, as well as absorption of moisture

from the air. However, the presence of hydrogen bonding might also contribute to the appearance of this broad peak.

It was proposed that **1** contains DMF solvent molecules in previous CHN analysis section. This claim can be confirmed through the presence of characteristic signals in the FT-IR spectrum. The main functional groups of DMF that can be identified through FT-IR are sp^3 C-H stretching vibrations from methyl groups, carbonyl and C-N stretching bands. Although sp^3 C-H stretching bands near 3000 cm^{-1} can be seen in **Figure 81** and **82**, they are relatively weak. However, the carbonyl band is strong and can be seen clearly at 1625 cm^{-1} in **Figure 81**.[54] The C-N stretching band of amide appears near 1400 cm^{-1}.[54] It can be assigned to the medium-intensity peak at 1382.1 cm^{-1} in **Figure 81**.

The presence of NO_3^- anion in **2** and **4** also can be investigated through identification of characteristic signals in FT-IR spectra of the two compounds. NO_3^- anions presence can be identified by 2 characteristic peaks range between 800-860 and 1340-1410 cm^{-1}.[55] These characteristic signals can be seen at 831.4 and 1383.5 in **Figure 83** for **2**, which is consistent with the proposed formula in the previous elemental analysis section. However, they are less apparent after UV irradiation (**Figure 84**). These two peaks also can be identified for **4** before and after UV irradiation (**Figure 87** and **88**) at around 830 and 1380 cm^{-1}, which also confirm the successful synthesis of targeted compound.

CHAPTER 5
CONCLUSION AND RECOMMENDATIONS

5.1 Conclusion

Four photoreactive MOFs (**1-4**) were successfully synthesized to undergo photochemical [2+2] cycloaddition reaction in the solid-state using bpe, ox and fum as spacer ligands with Zn(II), Pb(II) and Cd(II) as metals ion nodes. The synthesized compounds **1-3** are unreported in the literature, and were characterized *via* FT-IR, ^{1}H-NMR, PXRD, Elemental Analysis and TGA.

The lattice structures of these compounds were investigated by comparing experimental powder patterns with calculated ones from reported known MOFs in the literature. The elemental analysis and TGA results are consistent with the proposed structures based on comparable powder patterns.

Based on comparable powder patterns, photodimerizable lattice structures have been proposed. The proposed structure of compound **1** is expected to have free misaligned bpe ligands which can undergo large internal molecular motion to overcome this misalignment. A mechanism consists of three steps; sliding, isomerization and bonds formation, were proposed to explain such observation. Compound **2** and **3** proposed structures are expected to be 3D frameworks and consist of 2D sheets with different topologies pillared by bpe ligands in different manners.

The photoreactivity of these compounds were studied through monitoring the photochemical [2+2] cycloaddition reaction using ^{1}H-NMR spectroscopy. These studies were carried out on the compounds before and after *UV* irradiation for a variety of time durations (5, 10, 15, 30, and 50 hours). About 90% conversions of bpe ligands within compounds **1-2** have photochemically

reacted to yield *rctt*-tpcb after 50 hours of UV irradiation for **1** and 15 hours for **2**, while 100% conversion were achieved after only 5 hours of UV irradiation for **3**. Compound **2** was found to be able to undergo reversible photochemical [2+2] cycloaddition reaction which can find its way to important applications in photo-switching, sensing and optical data recording.

A reported MOF **4** was successfully reproduced and its photoreactivity has been successfully boosted by initiation of large internal molecular movement through grinding. The initiation of large internal molecular movement by grinding in this type of ladder MOF has not been reported before. The yield of the photochemical [2+2] cycloaddition reaction upon 50 hours of UV irradiation of single crystals was found to be 67% conversion of bpe to *rctt*-tpcb. However, when single crystals were grinded into a powder form and UV irradiated for 50 hours the yield has been increased to 100% conversion of bpe to *rctt*-tpcb.

The TGA study showed that water molecules were lost from the coordination sphere and became free water molecules within the crystal lattice due to grinding. The change of water molecules arrangement inside the crystal lattice structure due to grinding has allowed the ladder structures to get very close to each other for the photochemical [2+2] cycloaddition reaction to occur. This type of photoactive materials may find potential applications in sensors, optical switches and in photolithography. The current investigation has significant impact in the fields of crystal engineering, organic photochemistry and materials science.

5.2 Recommendations

The results of this research can be improved by applying the following recommendations.

Recommendation I

There are many reported MOFs, complexes and organic salts in the literature that contain aligned olefinic double bonds of bpe ligands that can undergo the photochemical [2+2] cycloaddition reaction, however their photoreactivity has not been studied yet.

Recommendation II

The obtained compounds **1** and **2** may be porous materials. These materials can be further studied for their porosity and surface area for gas storage applications.

Recommendation III

Crystalizing compounds **1-3** and obtaining single crystals would make a huge impact on the presented research work.

Recommendation IV

The photoluminescence (PL) of these compounds can be studied further and that will unravel materials for sensors applications.

References:

(1) Li, J.-R.; Sculley, J.; Zhou, H.-C. Metal–Organic Frameworks for Separations. *Chem. Rev.* **2012**, *112* (2), 869–932.

(2) Furukawa, H.; Cordova, K. E.; O'Keeffe, M.; Yaghi, O. M. The Chemistry and Applications of Metal-Organic Frameworks. *Science* **2013**, *341* (6149), 1230444.

(3) Batten, S. R.; Champness, N. R.; Chen, X.-M.; Garcia-Martinez, J.; Kitagawa, S.; Öhrström, L.; O'Keeffe, M.; Paik Suh, M.; Reedijk, J. Terminology of Metal–organic Frameworks and Coordination Polymers (IUPAC Recommendations 2013). *Pure Appl. Chem.* **2013**, *85* (8).

(4) Wang, Z. Design of Metal-Organic Framework Materials Based upon Inorganic Clusters and Polycarboxylates, 2006.

(5) Zhou, H. C.; Long, J. R.; Yaghi, O. M. Introduction to Metal-Organic Frameworks. *Chemical Reviews*. 2012, pp 673–674.

(6) Alshammari, A.; Jiang, Z.; Cordova, K. E. Metal Organic Frameworks as Emerging Photocatalysts. In *Semiconductor Photocatalysis - Materials, Mechanisms and Applications*; InTech, 2016.

(7) Lu, W.; Wei, Z.; Gu, Z.-Y.; Liu, T.-F.; Park, J.; Park, J.; Tian, J.; Zhang, M.; Zhang, Q.; Gentle III, T.; et al. Tuning the Structure and Function of Metal–organic Frameworks via Linker Design. *Chem. Soc. Rev.* **2014**, *43* (16), 5561–5593.

(8) Allendorf, M. D.; Stavila, V. Crystal Engineering, Structure–function Relationships, and the Future of Metal–organic Frameworks. *CrystEngComm* **2015**, *17* (2), 229–246.

(9) Gui, B.; Meng, X.; Xu, H.; Wang, C. Postsynthetic Modification of Metal-Organic Frameworks through Click Chemistry. *Chinese Journal of Chemistry*. 2016, pp 186–190.

(10) MacGillivray, L. R. *Metal-Organic Frameworks : Design and Application*; John Wiley & Sons, 2010.

(11) Burrows, A. D. Metal-Organic Frameworks: Postsynthetic Modification. In *Encyclopedia of Inorganic and Bioinorganic Chemistry*; John Wiley & Sons, Ltd: Chichester, UK,

2014; pp 1–24.

(12) Cohen, S. M. Postsynthetic Methods for the Functionalization of Metal-Organic Frameworks. *Chemical Reviews*. 2012, pp 970–1000.

(13) Kim, M.; Cahill, J. F.; Fei, H.; Prather, K. A.; Cohen, S. M. Postsynthetic Ligand and Cation Exchange in Robust Metal-Organic Frameworks. *J. Am. Chem. Soc.* **2012**, *134* (43), 18082–18088.

(14) Hu, Y.-Q.; Li, M.-Q.; Li, T.; Wang, Y.-Y.; Zheng, Z.; Zheng, Y.-Z. An Alkali-Ion Insertion Approach to Structurally Transform Metal–organic Frameworks. *CrystEngComm* **2016**, *18* (40), 7680–7684.

(15) Nagarathinam, M.; Peedikakkal, A. M. P.; Vittal, J. J. Stacking of Double Bonds for Photochemical [2+2] Cycloaddition Reactions in the Solid State. *Chem. Commun.* **2008**, No. 42, 5277.

(16) Hazra, A.; Bonakala, S.; Bejagam, K. K.; Balasubramanian, S.; Maji, T. K. Host-Guest [2+2] Cycloaddition Reaction: Postsynthetic Modulation of CO2 Selectivity and Magnetic Properties in a Bimodal Metal-Organic Framework. *Chem. - A Eur. J.* **2016**, *22* (23), 7792–7799.

(17) Chanthapally, A.; Vittal, J. J. Metal-Organic Frameworks: Photoreactive Frameworks. *Encycl. Inorg. Bioinorg. Chem.* **2014**, 1–23.

(18) Carey, F. A.; Sundberg, R. J. Concerted Pericyclic Reactions. In *Advanced Organic Chemistry*; Springer US: Boston, MA, 2007; pp 833–892.

(19) Ajay Kumar, K. Comprehensive Review on Huisgen's Cycloaddition Reactions. *International Journal of ChemTech Research*. 2013, pp 3032–3050.

(20) Pericyclic Reactions: Electrocyclizations, Cycloadditions and Sigmatropic Rearrangements http://ictwiki.iitk.ac.in/wiki/index.php/Pericyclic_Reactions_Electrocyclizations,_Cycloadditions_and_Sigmatropic_Rearrangements (accessed Dec 5, 2017).

(21) Matthew Todd. Cycloadditions https://openwetware.org/wiki/Todd:Chem3x11_ToddL13 (accessed May 7, 2018).

(22) Schmidt, G. M. J. 385. Topochemistry. Part III. The Crystal Chemistry of Some Trans-Cinnamic Acids. *J. Chem. Soc.* **1964**, *0* (0), 2014.

(23) Kole, G. K.; Peedikakkal, A. M. P.; Toh, B. M. F.; Vittal, J. J. Solid-State Structural Transformations and Photoreactivity of 1D-Ladder Coordination Polymers of PbII. *Chem. - A Eur. J.* **2013**, *19* (12), 3962–3968.

(24) Lyndon, R.; Konstas, K.; Ladewig, B. P.; Southon, P. D.; Kepert, P. C. J.; Hill, M. R. Dynamic Photo-Switching in Metal-Organic Frameworks as a Route to Low-Energy Carbon Dioxide Capture and Release. *Angew. Chemie - Int. Ed.* **2013**, *52* (13), 3695–3698.

(25) Yanai, N.; Uemura, T.; Inoue, M.; Matsuda, R.; Fukushima, T.; Tsujimoto, M.; Isoda, S.; Kitagawa, S. Guest-to-Host Transmission of Structural Changes for Stimuli-Responsive Adsorption Property. *J. Am. Chem. Soc.* **2012**, *134* (10), 4501–4504.

(26) Peedikakkal, A. M. P. Solid-State Photochemical [2+2] Cycloaddition Reaction of Hydrogen-Bonded Zn(II) Metal Complex Containing Several Parallel C=C Bonds. *J. Chem. Sci.* **2017**, *129* (2), 239–247.

(27) Peedikakkal, A. M. P.; Vittal, J. J. Solid-State Photochemical Behavior of a Triple-Stranded Ladder Coordination Polymer. *Inorg. Chem.* **2010**, *49* (1), 10–12.

(28) Ni, L. T.; Nagarathinam, M.; Vittal, J. J. Topochemical Photodimerization in the Coordination Polymer [{(CF 3CO2)(μ-O2CCH3)Zn} 2(μ-bpe)2]n through Single-Crystal to Single-Crystal Transformation. *Angew. Chemie - Int. Ed.* **2005**, *44* (15), 2237–2241.

(29) Peedikakkal, A. M. P.; Koh, L. L.; Vittal, J. J. Photodimerization of a 1D Hydrogen-Bonded Zwitter-Ionic Lead(<scp>ii</scp>) Complex and Its Isomerization in Solution. *Chem. Commun.* **2008**, No. 4, 441–443.

(30) Nagarathinam, M.; Vittal, J. J. Anisotropic Movements of Coordination Polymers upon Desolvation: Solid-State Transformation of a Linear 1D Coordination Polymer to a Ladderlike Structure. *Angew. Chemie - Int. Ed.* **2006**, *45* (26), 4337–4341.

(31) Paul, A. K.; Karthik, R.; Natarajan, S. Synthesis, Structure, Photochemical [2 + 2] Cycloaddition, Transformation, and Photocatalytic Studies in a Family of Inorganic-

Organic Hybrid Cadmium Thiosulfate Compounds. *Cryst. Growth Des.* **2011**, *11* (12), 5741–5749.

(32) Chanthapally, A.; Oh, W. T.; Vittal, J. J. [2 + 2] Cycloaddition Reaction as a Tool to Monitor the Formation of Thermodynamically Stable Ladder Coordination Polymers. *CrystEngComm* **2013**, *15* (45), 9324.

(33) Ou, Y. C.; Zhi, D. S.; Liu, W. T.; Ni, Z. P.; Tong, M. L. Single-Crystal-to-Single-Crystal Transformation from 1 D Staggered-Sculls Chains to 3 D NbO-Type Metal-Organic Framework through [2+2] Photodimerization. *Chem. - A Eur. J.* **2012**, *18* (24), 7357–7361.

(34) García-Couceiro, U.; Castillo, O.; Luque, A.; García-Terán, J. P.; Beobide, G.; Román, P. Rational Design of 2D Magnetic Metal-Organic Coordination Polymers Assembled from Oxalato and Dipyridyl Spacers. *Cryst. Growth Des.* **2006**, *6* (8), 1839–1847.

(35) García-Couceiro, U.; Castillo, O.; Cepeda, J.; Lanchas, M.; Luque, A.; Pérez-Yáñez, S.; Román, P.; Vallejo-Sánchez, D. Influence of the Synthetic Conditions on the Structural Diversity of Extended Manganese-Oxalato-1,2-bis(4-Pyridyl)ethylene Systems. *Inorg. Chem.* **2010**, *49* (24), 11346–11361.

(36) Mir, M. H.; Koh, L. L.; Tan, G. K.; Vittal, J. J. Single-Crystal to Single-Crystal Photochemical Structural Transformations of Interpenetrated 3D Coordination Polymers by [2+2] Cycloaddition Reactions. *Angew. Chemie - Int. Ed.* **2010**, *49* (2), 390–393.

(37) Michaelides, A.; Skoulika, S.; Siskos, M. G. Designed Self-Assembly of a Reactive Metal–organic Framework with Quasi α-Po Topology. *CrystEngComm* **2008**, *10* (7), 817.

(38) Friščić, T.; Fábián, L. Mechanochemical Conversion of a Metal Oxide into Coordination Polymers and Porous Frameworks Using Liquid-Assisted Grinding (LAG). *CrystEngComm* **2009**, *11* (5), 743.

(39) Kishida, K.; Horike, S.; Watanabe, Y.; Tahara, M.; Inubushi, Y.; Kitagawa, S. Structural Optimization of Interpenetrated Pillared-Layer Coordination Polymers for Ethylene/ethane Separation. *Chem. - An Asian J.* **2014**, *9* (6), 1643–1647.

(40) Xu, J.-Y.; Hurtado, E. J.; Lobkovsky, E. B.; Chen, B. Poly[(μ 2 - Trans -Di-4-

Pyridylethylene-κ 2 N : N ′)(μ 2 -Fumarato-κ 2 O : O ′)zinc(II)]. *Acta Crystallogr. Sect. E Struct. Reports Online* **2007**, *63* (8), m2205–m2205.

(41) Dong, Y.-B.; Layland, R. C.; Smith, M. D.; Pschirer, N. G.; Bunz, U. H. F.; zur Loye, H.-C. Syntheses and Characterizations of One-Dimensional Coordination Polymers Generated from Cadmium Nitrate and Bipyridine Ligands. *Inorg. Chem.* **1999**, *38* (13), 3056–3060.

(42) Peedikakkal, A. M. P.; Vittal, J. J. Solid-State Photochemical [2+2] Cycloaddition in a Hydrogen-Bonded Metal Complex Containing Several Parallel and Crisscross C=C Bonds. *Chem. - A Eur. J.* **2008**, *14* (17), 5329–5334.

(43) Kroll, L. Solid Sample FTIR: Preparation and Use http://faculty.taylor.edu/lrkroll/CHE311Web/FTIRSolidsInstructions.html (accessed Dec 9, 2017).

(44) Kole, G. K.; Kojima, T.; Kawano, M.; Vittal, J. J. Reversible Single-Crystal-to-Single-Crystal Photochemical Formation and Thermal Cleavage of a Cyclobutane Ring. *Angew. Chemie - Int. Ed.* **2014**, *53* (8), 2143–2146.

(45) Medishetty, R.; Park, I.-H.; Lee, S. S.; Vittal, J. J. Solid-State Polymerisation via [2+2] Cycloaddition Reaction Involving Coordination Polymers. *Chem. Commun.* **2016**, *52* (21), 3989–4001.

(46) Chung, F. H. Quantitative Interpretation of X-Ray Diffraction Patterns of Mixtures. III. Simultaneous Determination of a Set of Reference Intensities. *J. Appl. Crystallogr.* **1975**, *8* (1), 17–19.

(47) Klug, H. P. (Harold P.; Alexander, L. E. (Leroy E. *X-Ray Diffraction Procedures for Polycrystalline and Amorphous Materials*; John Wiley & Sons, 1974.

(48) O'Connor, B. H.; Li, D. Y.; Sitepu, H. Strategies for Preferred Orientation Corrections in X-Ray Powder Diffraction Using Line Intensity Ratios. In *Advances in X-Ray Analysis*; Springer US: Boston, MA, 1991; pp 409–415.

(49) Sitepu, H.; O'Connor, B. H.; Li, D. Comparative Evaluation of the March and Generalized Spherical Harmonic Preferred Orientation Models Using X-Ray Diffraction Data for

Molybdite and Calcite Powders. *J. Appl. Crystallogr.* **2005**, *38* (1), 158–167.

(50) Boldyrev, V. V. Mechanochemical Modification and Synthesis of Drugs. *J. Mater. Sci.* **2004**, *39* (16–17), 5117–5120.

(51) Tapia-Benavides, A. R.; Tlahuextl, M.; Tlahuext, H.; Galán-Vidala, C. Synthesis of Zn Compounds Derived from 1H-Benzimidazol-2-Ylmethanamine. *Arkivoc* **2008**, *2008* (5), 172–186.

(52) Zamiri, R.; Rebelo, A.; Zamiri, G.; Adnani, A.; Kuashal, A.; Belsley, M. S.; Ferreira, J. M. F. Far-Infrared Optical Constants of ZnO and ZnO/Ag Nanostructures. *RSC Adv.* **2014**, *4* (40), 20902–20908.

(53) *Spectroscopic Properties of Inorganic and Organometallic Compounds*; Davidson, G., Ebsworth, E. A. V, Eds.; Spectroscopic Properties of Inorganic and Organometallic Compounds; Royal Society of Chemistry: Cambridge, 1982; Vol. 15.

(54) Silverstein, R. M. (Robert M.; Webster, F. X.; Kiemle, D. J.; Bryce, D. L. (David L. *Spectrometric Identification of Organic Compounds*, 8th ed.; Wiley, 2014.

(55) Stuart, B. H. *Infrared Spectroscopy : Fundamentals and Applications*; Wiley, 2004.

Vitae

Name	:	Hasan Ali Al-Mohsin
Nationality	:	Saudi
Date of Birth	:	22/2/1984
Postal Address	:	P.O. Box 1745, Sayhat 31972, Saudi Arabia
Resident Address	:	6604 Yanbu – An Nur, Sayhat 32452 – 3363, Eastern Province – Saudi Arabia
Contacts	:	Mobile # +966 503 815 321
	:	E-Mail: hasan.almohsin@outlook.com

Academic Background

2015-2018	M.Sc. in Chemistry at King Fahd University of Petroleum and Minerals
2010-2014	B.Sc. in Industrial Chemistry at King Fahd University of Petroleum and Minerals

Academic Research Experience

2015-2018	Synthesis, characterization and photochemistry of some metal-organic frameworks.
2014	Kinetic studies for reacting some biological ligands with potential anti-cancer complexes.

Awards

1 My research about 'boosting photoreactivity of a metal-organic framework through grinding' won **3rd place** at 9th Students Scientific Conference at KFUPM, **2018**.

2 My research about 'kinetic studies of reactions between some biological ligands and potential anti-cancer complexes' won **4th place** at 6th Students Scientific Conference at Jeddah, **2015**.

Manuscripts

1 Omer, K. H.; Seliman, A. A. A.; **Al-Mohsin, H**. A.; Kawde, A.-N.; Altaf, M.; Wazeer, M. I. M.; Ahmad, S.; Musa, M. M.; Isab, A. A. Study of the Interaction of Some Potential Anticancer Gold(III) Complexes with Biologically Important Thiols Using NMR, UV-Vis, and Electrochemistry. *Int. J. Chem. Kinet.* **2017**, *49* (6), 387–397. (Published)

2 **Al-Mohsin, H.** A.; Peedikakkal, A. M. P. Solid-State Photochemical [2+2] Cycloaddition Reaction of 1D Cd(II) Hydrogen-Bonded Triple-Stranded-like Ladder Coordination Polymer. *RCS Adv*. **2018**. (to be submitted)

3 **Al-Mohsin, H.** A.; Peedikakkal, A. M. P. Synthesis and Solid-State Photochemical [2+2] Cycloaddition Reaction of MOFs Containing 4,4′-bipyridyl-ethylene. J. Chem. Sci. **2018**. (under preparation)

4 **Al-Mohsin, H.** A.; Peedikakkal, A. M. P. LAG Synthesis and Photoluminescence Study of Pb(II)-based Coordination Polymers Assembled from 4,4'-bipyridine Ligand. **2018**. (under preparation)

Conferences

1 **Al-Mohsin, H.** A.; Peedikakkal, A. M. P. Large Internal Molecular Motion in 1D Cd(II) Ladder Metal-Organic Frameworks via Solid-state Photochemical [2+2] Cycloaddition Reaction. In *9th Students Scientific Conference* at KFUPM, Dhahran, Saudi Arabia, May 1-2, **2018**.

2 **Al-Mohsin, H.** A.; Peedikakkal, A. M. P. Design and Synthesis of Metal-Organic Frameworks for Photochemical [2+2] Cycloaddition Reaction in the Solid-state. In *8th Students Scientific Conference* at KFUPM, Dhahran, Saudi Arabia, Oct. 4-5, **2017**.

3 **Al-Mohsin, H.** A.; Isab, A. A. NMR and kinetic studies of the interaction of the anti-cancer complexes [Au(*cis*-DACH)Cl_2]Cl and [Au(*cis*-DACH)$_2$]Cl_3 with penicillamine. In *6th Students Scientific Conference*, Jeddah, Saudi Arabia, March 30 - April 2, **2015**.